Technical Report
RAL-TR-2004-039

CCLRC

Electronic Properties of materials observed in X-ray diffraction

S W Lovesey E Balcar K S Knight J Fernandez-Rodriguez

20 January 2005

Council for the Central Laboratory of the Research Councils

Library and Information Services
CCLRC Rutherford Appleton Laboratory
Chilton Didcot
Oxfordshire OX11 0QX
UK
Tel: +44 (0)1235 445384
Fax: +44 (0)1235 446403
Email: library@rl.ac.uk

CCLRC reports are available online at:
http://www.clrc.ac.uk/Activity/ACTIVITY=Publications;SECTION=225;

ISSN 1358-6254

Electronic properties of materials observed in x-ray diffraction

S.W. Lovesey [a], E. Balcar [b], K.S. Knight [c] and J. Fernández Rodríguez [d]

[a] *Diamond Light Source Ltd. and the ISIS Facility, RAL, Oxfordshire OX11 0QX, England, UK and RIKEN Harima Institute, SPring-8, Hyogo 679-5148, Japan*

[b] *Vienna University of Technology, Atominstitut, Stadionallee 2, A1020, Vienna, Austria*

[c] *ISIS Facility, RAL, Oxfordshire OX11 0QX, England, UK and Department of Mineralogy, The Natural History Museum, London SW7 5BD, UK*

[d] *Departamento de Física, Universidad de Oviedo, E-33007 Oviedo, Spain*

Abstract

The few electrons in valence states of a material participate in many of its physical properties, including both structural and transport properties. In the diffraction of x-rays, or neutrons, valence electrons can lead to weak Bragg reflections that are extremely sensitive signatures of their charge and magnetic degrees of freedom. In this regard, diffraction instruments supplied with x-rays from a synchrotron source are particularly useful because the brightness, tuneability and polarization of the x-rays are all helpful in making valuable observations. The data obtained from Bragg diffraction can be analyzed on the basis of an atomic model, which has the virtue that it can be used as a common platform for the analysis of x-ray and neutron diffraction and, in addition, the analysis of observations made with x-ray absorption, NMR, EPR, muon and Mössbauer spectroscopies. We present the salient features for the calculation of structure factors based on an atomic model and applied to the analysis of Bragg diffraction by non-magnetic and magnetic materials, with an emphasis on resonant x-ray Bragg diffraction. In addition we discuss the complementary observation of dichroic signals.

The survey of available analytical tools is complemented by a series of worked examples demonstrating the application of the formalism to different materials with different crystal structures and resonant ions: dysprosium borocarbide (DyB_2C_2), vanadium sesquioxide (V_2O_3), gadolinium tetraboride (GdB_4), chromium sesquioxide (Cr_2O_3), haematite and perovskite-type manganites.

Key words:
PACS: 78.70.Ck, 61.10.Dp, 33.55.Ad

1 Introduction

X-ray and neutron diffraction are mainstays of many aspects of the science of materials [1,2]. The contribution from x-ray diffraction to the subject has recently been enhanced by diffraction instruments at synchrotron sources where they are supplied with x-rays that are very bright, highly polarized and tuneable in energy [3]. All these attributes are a help when it comes to measuring weak reflections in a diffraction pattern due to the relatively few electrons in valence states which possess angular anisotropy and, possibly, a magnetic moment. The importance of observations made by analyzing the weak reflections can hardly be exaggerated, for the electrons in question participate in a host of physical properties, including, covalency, superconductivity, magnetoresistance, ferro- and pyroelectricity, structural phase transitions and all manner of magnetic phenomena [4–8].

A successful framework for analyzing the weak features in a diffraction pattern gathered on a spatially ordered material is based on an atomic, or localized, electron model. The corresponding structure factor for diffraction, F, is a sum of contributions from participating ions weighted by the standard spatial phase-factors. If all contributions are the same, F is simply the sum of the phase factors and F is different from zero at the space-group allowed Bragg reflections admitted by extinction rules or crystallographic systematic absence conditions. The additional, weak reflections we have mentioned occur when ions in the unit cell are not equivalent on account of a lack of translational symmetry in their environments. The symmetry elements of F must include the symmetry elements of the space-group of the crystal, whereas a bulk physical property is constrained by the point-group of the crystal only. Ordering of the valence states or an ordering of magnetic moments will break the translational symmetry. For example, a simple antiferromagnetic motif of moments leads to reflections not indexed by the chemical unit cell.

Atomic models have a long and distinguished life in the interpretation of both neutron and Thomson scattering measurements. One of the attractive features of these models is that the atomic quantities, such as spin and orbital magnetic moments and orbital quadrupole moments, can be probed by various experimental techniques. Hence, atomic models provide a common platform for the analysis of observations made in diffraction experiments and NMR, EPR, muon spin-rotation and Mössbauer spectroscopies. To this list of observations that can be analyzed on the basis of atomic models one can add x-ray Bragg diffraction in which the intensity of a reflection is increased by tuning the x-ray energy to an atomic resonance, although the suitability of an atomic model needs to be tested case by case. Resonance enhancement increases the visibility of certain features in a diffraction pattern and it provides an element selectivity [9,10]. Intensities can be sensitive to polarization in the primary and

secondary x-ray beams and this sensitivity is another useful aspect of resonant Bragg diffraction. The wavelength of the x-rays is determined by the energy of the resonance event being exploited and very often the wavelength is too long to satisfy the Bragg condition at more than two, or three, reflections. In the best cases, resonant Bragg diffraction provides a sensitivity at the level of a small fraction of an electron, and data gathered can be used with confidence to infer the wavefunction of the valence state which accepts the photo-ejected core electron.

We review observations made by analyzing diffraction measurements in terms of an atomic model, with some emphasis on x-ray resonant Bragg diffraction. Most of the necessary atomic calculations are already available in published literature, and our goal is to gather them in a coherent format in one place. We add to these calculations one required to describe parity-breaking contributions to scattering. In absorption experiments these contributions can give rise to natural circular and magnetochiral dichroism.

The analysis of observations made with absorption spectroscopies has received a lot of attention, and significant developments have been made with atomic models and multiple-scattering models [11]. Magnetic circular dichroism is a powerful technique by which to investigate magnetocrystalline anisotropy in a variety of materials, including, chemically ordered alloys and artificially layered structures. Absorption spectroscopies and resonant x-ray Bragg diffraction are just two sides of one coin, for both are related to the scattering amplitude. However, in principle there is more useful information to be got from diffraction than there is from dichroism because dichroism is a bulk, or global, property. Put another way, dichroism is described by the structure factor F evaluated at zero Bragg angle (forward scattering) and for this condition the symmetry elements of F must include the symmetry elements of the point group of the crystal (Neumann's principle), i.e. one of the 32 crystal classes. The full F, required for diffraction at a non-trivial Bragg reflection, depends on the relative position of the symmetry elements and translations associated with glide planes and screw axes in the unit cell because the spatial phase-factors are not all equal. Diffraction, therefore, is constrained by elements of symmetry in one of the 230 different space groups. Similar reasoning applies when the discussion of dichroic signals and diffraction is extended to magnetic crystals.

Besides resonant x-ray Bragg diffraction and dichroic signals, we consider the Thomson scattering and magnetic scattering of x-rays with high energies, away from atomic resonances. The magnetic scattering of x-rays and the magnetic scattering of neutrons have many features in common, and it is for this reason that we also include a brief survey of magnetic neutron scattering.

The Compton scattering of x-rays is spatially incoherent and inelastic, and

it provides information on the spin magnetization. This information nicely complements measurements of the spin and orbital magnetization by x-ray Bragg diffraction. However, Compton scattering, necessarily, is sensitive to bulk properties of the target sample, and in this respect it is the same as x-ray absorption spectroscopies that we have discussed earlier on. In particular, studies of magnetic properties are limited to ferro- or ferrimagnets, where the net magnetic moments are non-zero.

Our notation for x-ray scattering follows that used in references [12,13]. We refer the reader to these articles for some background material, such as the description of states of partial polarization and the Stokes parameters.

2 Thomson scattering by spatially ordered materials

2.1 Unit-cell structure factor

It is customary to develop the x-ray scattering length in powers of $E/m_{\rm e}c^2$ where E is the primary energy and the rest mass energy of an electron $m_{\rm e}c^2 = 0.511$ MeV. The first term in the development is proportional to the spatial Fourier transform of the electron charge density and it is responsible for the Thomson scattering of x-rays. (The development referred to is provided in references [14,15] and it is summarized in equation (8.17) in reference [13].)

Let $\mathbf{k}$ denote the difference between the primary $\mathbf{q}$ and secondary $\mathbf{q}'$ wavevectors with $\mathbf{k} = \mathbf{q} - \mathbf{q}'$. The corresponding polarization vectors are $\boldsymbol{\varepsilon}$ and $\boldsymbol{\varepsilon}'$ and they satisfy $\mathbf{q} \cdot \boldsymbol{\varepsilon} = \mathbf{q}' \cdot \boldsymbol{\varepsilon}' = 0$. Writing $r_{\rm e} = \alpha^2 a_0 = 0.282 \times 10^{-12}$ cm for the classical radius of the electron, the Thomson contribution to the x-ray scattering length per unit cell is $-r_{\rm e}(\boldsymbol{\varepsilon}' \cdot \boldsymbol{\varepsilon}) F_c(\mathbf{k})$ where $F_c(\mathbf{k})$ is the appropriate unit-cell structure factor. Here, we attach a subscript c to denote the charge density.

In an atomic model, $F_c(\mathbf{k})$ is a sum over every ion in the unit cell that contributes to scattering. A site in the unit cell is labelled by its position $\mathbf{d}$. We then have,

$$F_c(\mathbf{k}) = \sum_{\mathbf{d}} {\rm e}^{{\rm i}\mathbf{k}\cdot\mathbf{d}} \langle \sum_j {\rm e}^{{\rm i}\mathbf{k}\cdot\mathbf{R}_j} \rangle_{\mathbf{d}} \ , \tag{1}$$

where angular brackets denote the mean value, or time-average value, of the enclosed quantity and the j-sum is over the positions $\mathbf{R}_j$ of the electrons associated with the site $\mathbf{d}$. The quantity $\langle \sum_j {\rm e}^{{\rm i}\mathbf{k}\cdot\mathbf{R}_j} \rangle$ is often called an atomic form factor and it is equal to the number of electrons when $\mathbf{k} = 0$. If there

Table 1
Parity-even multipoles

Rank K	Name= 2^K
$K = 1$	Dipole
$K = 2$	Quadrupole
$K = 3$	Octupole
$K = 4$	Hexadecapole
$K = 5$	Triakontadipole
$K = 6$	Hexacontatetrapole

is translational symmetry between the sites in the cell, $F_c(\mathbf{k})$ is simply proportional to the sum of the spatial phase factors $e^{i\mathbf{k}\cdot\mathbf{d}}$ and the sum is different from zero for $\mathbf{k} = \boldsymbol{\tau}(hkl)$ where the Miller indices hkl label a space-group allowed reflection. Additional, weak reflections may arise because some ions in the unit cell are not equivalent on account of a lack of translational symmetry in their environments.

To describe the contribution to $F_c(\mathbf{k})$ made by such ions we introduce an atomic tensor $\langle T_Q^K \rangle_c$ for each ion [16–18]. Here the positive integer K is the rank of the spherical tensor and the projection Q can take $(2K + 1)$ integer values that satisfy $-K \leq Q \leq K$. An atomic tensor is also called a multipole moment and they are named by the Greek word for the number 2^K. For completeness, and because not all authors use our naming rule, Table 1 contains the names of multipoles $K = 1$ to $K = 6$.

An actual definition of $\langle T_Q^K \rangle_c$ follows by separating the angular dependence of $\mathbf{k}$ and $\mathbf{R}_j$ in $e^{i\mathbf{k}\cdot\mathbf{R}_j}$ which is accomplished with the identity,

$$e^{i\mathbf{k}\cdot\mathbf{R}_j} = 4\pi \sum_{KQ} i^K j_K(kR_j)\{Y_Q^K(\hat{\mathbf{k}})\}^* Y_Q^K(\hat{\mathbf{R}}_j) \ . \tag{2}$$

Here, $\hat{\mathbf{k}} = \mathbf{k}/k$ and $\hat{\mathbf{R}}_j = \mathbf{R}_j/R_j$ are unit vectors, $j_K(kR_j)$ is a spherical Bessel function and $Y_Q^K(\hat{\mathbf{k}}) = (-1)^Q\{Y_{-Q}^K(\hat{\mathbf{k}})\}^*$ is a spherical harmonic. Our definition of a spherical harmonic is a standard one. An alternative definition $i^K Y_Q^K(\hat{\mathbf{k}})$ has the appealing property that its complex conjugate and the function differing in the sign of Q have a relation that is the same as that between a spinor and its time-reversed state (see appendix C). Using (2), we write the mean value of $e^{i\mathbf{k}\cdot\mathbf{R}_j}$ which is required in the structure factor as,

$$\langle \sum_j e^{i\mathbf{k}\cdot\mathbf{R}_j} \rangle = (4\pi)^{1/2} \sum_{KQ} i^K \langle j_K \rangle (-1)^Q Y_{-Q}^K(\hat{\mathbf{k}}) \langle T_Q^K \rangle_c \ , \tag{3}$$

with,

$$\langle T_Q^K \rangle_c = (4\pi)^{1/2} \sum_j \langle Y_Q^K(\hat{\mathbf{R}}_j) \rangle \ , \tag{4}$$

and the reduced matrix element for T_Q^K is found in equation (16). In equation (3), $\langle j_K(k) \rangle$ is the integral of a spherical Bessel function of order K weighted by the radial density of the valence wavefunction and $\langle j_K(0) \rangle = 0$ for $K > 0$. The atomic tensor $\langle T_Q^K \rangle_c$ evaluated for $K = Q = 0$ is equal to the number of valence electrons. Weak Bragg reflections arise from tensors with rank $K > 0$. We have written the right-hand side of (3) as a scalar product of two tensors of equal rank; if $\mathbf{A}$ and $\mathbf{B}$ are vector quantities (tensors of rank 1) their scalar product $\mathbf{A} \cdot \mathbf{B} = A_x B_x + A_y B_y + A_z B_z$ written in terms of spherical components, $A_{+1} = -(A_x + \mathrm{i}A_y)/\sqrt{2}$, $A_0 = A_z$ and $A_{-1} = (A_x - \mathrm{i}A_y)/\sqrt{2}$ and similar expressions for B_Q, is $\mathbf{A} \cdot \mathbf{B} = \sum_Q (-1)^Q A_{-Q} B_Q$.

After inserting (3) in (1), the Thomson structure factor may be written as,

$$F_c(\mathbf{k}) = (4\pi)^{1/2} \sum_{KQ} \mathrm{i}^K \langle j_K \rangle (-1)^Q Y_{-Q}^K(\hat{\mathbf{k}}) \Psi_Q^K \ , \tag{5}$$

where,

$$\Psi_Q^K = \sum_{\mathbf{d}} \mathrm{e}^{\mathrm{i}\mathbf{k}\cdot\mathbf{d}} \langle T_Q^K \rangle_{c,\mathbf{d}} \ . \tag{6}$$

We assume that $\langle j_K \rangle$ is the same for each ion that contributes to the weak Bragg reflection in question, for which $\Psi_0^0 = 0$. Note that $F_c(\mathbf{k})$ is a scalar product of a tensor $Y_Q^K(\hat{\mathbf{k}})$ associated with the x-rays and a tensor Ψ_Q^K associated with the electrons. This feature of the structure factor will appear again and again in scattering processes, including resonant x-ray diffraction. The x-ray factor $\mathrm{i}^K Y_Q^K(\hat{\mathbf{k}})$ in (5) satisfies $\mathrm{i}^K Y_{-Q}^K(\hat{\mathbf{k}}) = (-1)^{K+Q} [\mathrm{i}^K Y_Q^K(\hat{\mathbf{k}})]^*$ and a similar relation holds for x-ray factors in resonant x-ray diffraction, as we shall see later in Tables 3, 4, and 5.

2.2 Application to DyB_2C_2

As an example of the type of scattering under discussion in this section let us consider diffraction by a crystal of Dysprosium borocarbide (DyB_2C_2). On lowering the temperature through T = 24.7 K the material undergoes a continuous structural phase-transition in which there is a buckling of B and C rings of ions normal to the crystal c-axis. The transition reduces the crystal symmetry to $P4_2/mnm$, down from the crystal symmetry P4/mbm [19]. The

change in symmetry is accompanied by doubling the unit cell along the c-axis, and a reduction in symmetry of the sites occupied by Dy ions to 2/m (C_{2h}) from 4/m (C_{4h}). Various aspects of the crystal structure are illustrated in Fig. 1.

When it comes to calculating Ψ_Q^K, we apply to $\langle T_Q^K\rangle_{c,\mathbf{d}}$ the symmetry operators that relate the four Dy sites in the unit cell of $P4_2/mnm$. The ions are at sites 4(c) with symmetry 2/m and the diad parallel to the c-axis. The ions are at sites with positions $\mathbf{d} = (0,0,0)$, $(\frac{1}{2}a, \frac{1}{2}b, 0)$, $(0,0,c)$ and $(\frac{1}{2}a, \frac{1}{2}b, c)$ and we label them 1, 2, 3 and 4, respectively, as in Fig. 1. Note we have translated the unit cell origin by the vector $\mathbf{b}/2$ from the standard origin in International Tables for Crystallography [6]. Ions 1 and 3 are related by a rotation of $\pi/2$ about the c-axis and, thus, $\langle T_Q^K\rangle_{c,3} = \mathrm{e}^{\mathrm{i}Q\pi/2}\langle T_Q^K\rangle_{c,1}$. This relation is one of several that are discussed in appendix B. Sites 2 and 4 are also related by a rotation of $\pi/2$ about the c-axis, and sites 1 and 2 by reflection in a plane normal to the direction $[\frac{1}{2}a, \frac{1}{2}b, 0]$. To implement this symmetry we invoke the identity between reflection in a plane and the product of inversion ($x \longrightarrow -x, y \longrightarrow -y, z \longrightarrow -z$) and rotation by π about an axis normal to the reflection plane. The atomic tensor $\langle T_Q^K\rangle_c$ is changed by inversion of the coordinate system to $(-1)^K\langle T_Q^K\rangle_c$ and such a tensor is called a true (or polar) tensor. For Thomson scattering by equivalent electrons in a single atomic-shell K is always an even integer and associated atomic tensors are parity-even, c.f. section 2.3. In consequence, under reflection in a plane normal to $[\frac{1}{2}a, \frac{1}{2}b, 0]$ the tensor $\langle T_Q^K\rangle_c$ is effectively rotated by π about $[\frac{1}{2}a, \frac{1}{2}b, 0]$ and one finds that $\langle T_Q^K\rangle_{c,2} = (-1)^K\mathrm{e}^{\mathrm{i}Q\pi/2}\langle T_{-Q}^K\rangle_{c,1}$. Using the foregoing expressions for tensors at sites 2, 3 and 4 in terms of $\langle T_Q^K\rangle_{c,1}$ in Ψ_Q^K the latter reduces to [20,21],

$$\Psi_Q^K = \langle T_Q^K\rangle_{c,1}\{1 + \nu_Q\mathrm{e}^{\mathbf{i}\mathbf{k}\cdot\mathbf{d}_3}\} + (-1)^K\nu_Q\langle T_{-Q}^K\rangle_{c,1}\{\mathrm{e}^{\mathbf{i}\mathbf{k}\cdot\mathbf{d}_2} + \nu_Q\mathrm{e}^{\mathbf{i}\mathbf{k}\cdot\mathbf{d}_4}\} \ , \qquad (7)$$

where $\nu_Q = \mathrm{e}^{\mathrm{i}Q\pi/2}$.

We consider two classes of space-group forbidden reflections hkl which we label (a) and (b). The corresponding spatial phase factors are:

(a) $h + k$ =odd, $l = (2n+1)/2$,

$\mathrm{e}^{\mathbf{i}\mathbf{k}\cdot\mathbf{d}_2} = \mathrm{e}^{\mathbf{i}\mathbf{k}\cdot\mathbf{d}_3} = -1 \quad , \quad \mathrm{e}^{\mathbf{i}\mathbf{k}\cdot\mathbf{d}_4} = +1 \quad .$

(b) $h + k$ =even, $l = (2n+1)/2$,

$\mathrm{e}^{\mathbf{i}\mathbf{k}\cdot\mathbf{d}_2} = +1 \quad , \quad \mathrm{e}^{\mathbf{i}\mathbf{k}\cdot\mathbf{d}_3} = \mathrm{e}^{\mathbf{i}\mathbf{k}\cdot\mathbf{d}_4} = -1 \quad .$

We find,

$$\Psi_Q^K(\mathrm{a}) = (1 - \nu_Q)\{\langle T_Q^K\rangle_{c,1} - (-1)^K\nu_Q\langle T_{-Q}^K\rangle_{c,1}\} \ , \qquad (8)$$

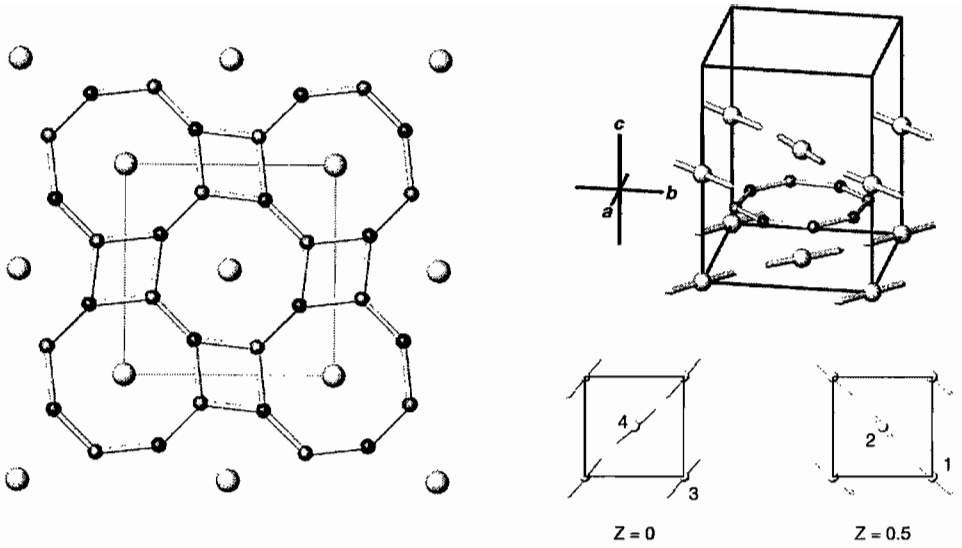

Fig. 1. Low temperature structure of DyB_2C_2 [19,20]. In the left-hand panel the c-axis is normal to the plane of the diagram which contains the Dy ions represented by large shaded circles. The right-hand panel illustrates the configuration of Dy magnetic moments.

and,

$$\Psi_Q^K(\mathrm{b}) = (1-\nu_Q)\{\langle T_Q^K\rangle_{c,1} + (-1)^K \nu_Q \langle T_{-Q}^K\rangle_{c,1}\} \ , \tag{9}$$

and the common prefactor guarantees $\Psi_0^K(\mathrm{a}) = \Psi_0^K(\mathrm{b}) = 0$, a result, that is a signature of space-group forbidden reflections.

There are more selection rules on K and Q that are derived from Ψ_Q^K. First, for Thomson scattering K is an even integer, as we mentioned, and the maximum $K = 2l$ when l is the angular momentum of the valence shell occupied by the equivalent electrons. In our example, the valence shell is expected to be formed by the Dy 4f state and $l = 3$. Thus, the possible Ψ_Q^K are Ψ_Q^2, Ψ_Q^4 and Ψ_Q^6 which, respectively, are linear combinations of quadrupoles, hexadecapoles and hexacontatetrapoles of the Dy 4f valence state. The contributions they make to $F_c(\mathbf{k})$ are weighted by $\langle j_2\rangle$, $\langle j_4\rangle$ and $\langle j_6\rangle$ which vanish as $k = |\mathbf{k}|$ goes to zero, and the magnitude of $\langle j_2\rangle$ is much larger than the magnitudes of both $\langle j_4\rangle$ and $\langle j_6\rangle$. Secondly, the diad parallel to the c-axis requires that $\langle T_Q^K\rangle_{c,1}$ is unchanged by a rotation by π about the c-axis, i.e. $\langle T_Q^K\rangle_{c,1} = \mathrm{e}^{\mathrm{i}Q\pi}\langle T_Q^K\rangle_{c,1}$. The non-trivial condition is that Q be an even integer $Q = \pm 2, \pm 4, \ldots$ However, a necessary condition for scattering is $\nu_Q = \mathrm{e}^{\mathrm{i}Q\pi/2} = -1$, and hence the allowed $Q = \pm 2, \pm 6 \ldots$ Notice that, in the room temperature structure P4/mbm, there is no Thomson scattering because Dysprosium ions occupy sites with a tetrad parallel to the c-axis and this rotation symmetry restricts Q to values $0, \pm 4, \pm 8, \ldots$ for which $\Psi_Q^K = 0$.

Below the structural phase transition, at T = 24.7 K, the structure factor for

Thomson scattering is derived from,

$$\Psi_Q^K(\mathrm{a}) = 2\{\langle T_Q^K\rangle_{c,1} + \langle T_{-Q}^K\rangle_{c,1}\} = \Psi_{-Q}^K(\mathrm{a}) = 4\,\mathrm{Re}\langle T_Q^K\rangle_{c,1}\ , \tag{10}$$

and,

$$\Psi_Q^K(\mathrm{b}) = 2\{\langle T_Q^K\rangle_{c,1} - \langle T_{-Q}^K\rangle_{c,1}\} = -\Psi_{-Q}^K(\mathrm{b}) = 4\mathrm{i}\,\mathrm{Im}\langle T_Q^K\rangle_{c,1}\ . \tag{11}$$

To express Ψ_Q^K in terms of the real or imaginary parts of $\langle T_Q^K\rangle_{c,1}$, we have used a result for $\langle T_{-Q}^K\rangle$ that is valid in the general case, namely, $\langle T_{-Q}^K\rangle = (-1)^Q\langle T_Q^K\rangle^*$, together with the fact that Q is an even integer.

The Thomson structure factors are,

$$\begin{aligned}(\mathrm{a})\quad F_c(\mathbf{k}) &= (4\pi)^{1/2}\sum_{K=2,4,6}\mathrm{i}^K\sum_{Q=2,6}[Y_{-Q}^K(\hat{\mathbf{k}}) + Y_Q^K(\hat{\mathbf{k}})]\langle j_K\rangle\Psi_Q^K(\mathrm{a})\\ &= -4\sqrt{\frac{15}{2}}\langle j_2\rangle(\hat{k}_a^2 - \hat{k}_b^2)\,\mathrm{Re}\langle T_2^2\rangle_{c,1} + \dots\ ,\end{aligned} \tag{12}$$

and,

$$\begin{aligned}(\mathrm{b})\quad F_c(\mathbf{k}) &= (4\pi)^{1/2}\sum_{K=2,4,6}\mathrm{i}^K\sum_{Q=2,6}[Y_{-Q}^K(\hat{\mathbf{k}}) - Y_Q^K(\hat{\mathbf{k}})]\langle j_K\rangle\Psi_Q^K(\mathrm{b})\\ &= -4\sqrt{30}\langle j_2\rangle\hat{k}_a\hat{k}_b\,\mathrm{Im}\langle T_2^2\rangle_{c,1} + \dots\ .\end{aligned} \tag{13}$$

Dots in these expressions denote terms with tensors of rank 4 and rank 6. A spherical tensor of rank 2 has a unique representation in terms of a symmetric traceless Cartesian tensor of rank 2 which we denote by $Q_{\alpha\beta}$. In other words, $\langle T_Q^2\rangle_{1,c}$ can be expressed in terms of a Cartesian quadrupole tensor $Q_{\alpha\beta}$. For our immediate purpose we need only [18],

$$\langle T_2^2\rangle_{1,c} = \sqrt{\frac{1}{6}}(Q_{aa} - Q_{bb} + 2\mathrm{i}Q_{ab})\ , \tag{14}$$

and components of the Cartesian quadrupole tensor are purely real. Combining (12) and (14), the leading term in $F_c(\mathbf{k})$ for reflections of type (a) is proportional to $(h^2 - k^2)(Q_{aa} - Q_{bb})$ where we have replaced $\hat{k}_a$ and $\hat{k}_b$ by the appropriate Miller indices. Reflections of type (b) are described by a structure factor whose leading term is proportional to hkQ_{ab}. Our findings are in complete agreement with experimental data reported by Adachi et al.(2002) [22] which we display in Figure 2.

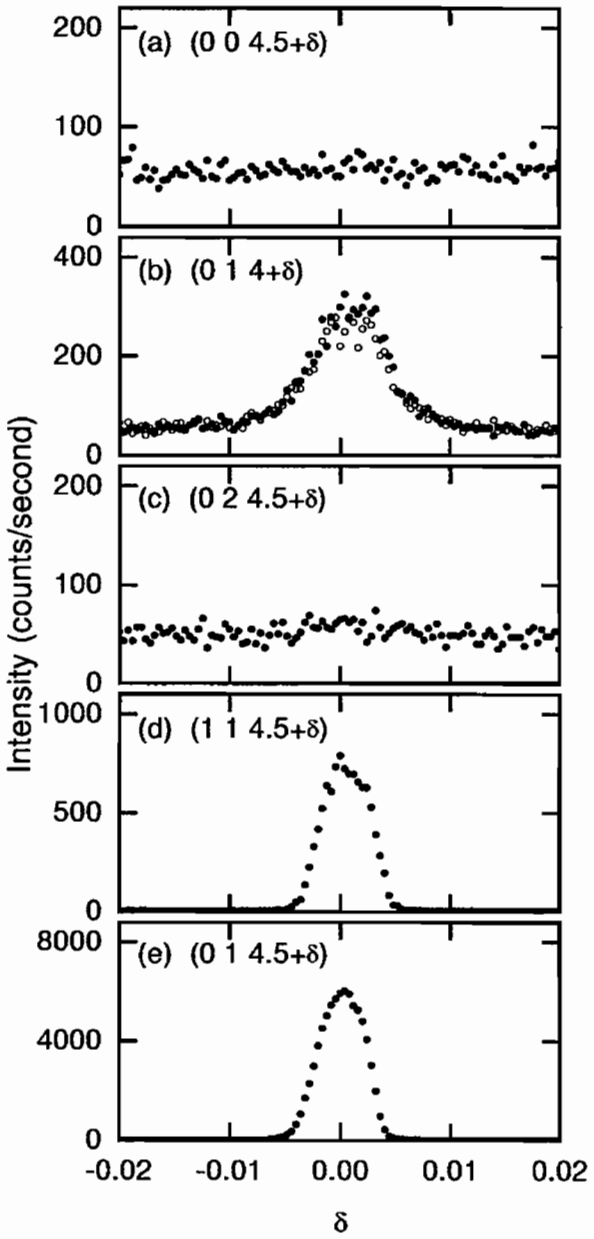

Fig. 2. Thomson scattering by DyB_2C_2. Raw data of the l-scan measurements are displayed for various types of reflections. The crystal was held at a temperature of 18 K except for data gathered in scans about (014). Intensities reported in panel (b) were taken at 18 K (solid circles) and 30 K (open circles) and they are attributed to multiple scattering. ¿From Adachi et al. [22].

2.3 Sample calculation of $\langle T_Q^K \rangle_c$

Let us consider a calculation of $\langle T_Q^K \rangle_c$ that is appropriate for DyB_2C_2. In the ground state, the Dy 4f shell is described by a wavefunction $|\Psi\rangle$ which is a linear combination of states $|JM\rangle$ where $J = 15/2$. Because there are an odd number of electrons in the 4f shell the states are two-fold degenerate (Kramers

degeneracy), in the absence of magnetic interactions [23]. The ground-state doublet can be formed by $|\Psi\rangle$ and its time-reversed version $|\bar{\Psi}\rangle = \vartheta|\Psi\rangle$. Information about the time-reversal operator ϑ is in appendix C. Thomson scattering by equivalent electrons in a single atomic-shell is a parity-even process.

Associated atomic tensors with an even rank are time-even and they possess the properties $\langle\Psi|T^K_Q|\bar{\Psi}\rangle = 0$ and $\langle\Psi|T^K_Q|\Psi\rangle = \langle\bar{\Psi}|T^K_Q|\bar{\Psi}\rangle$. Turning to the actual form of $|\Psi\rangle$, the diad symmetry element requires $|\Psi\rangle$ to be some linear combination of the states $|JJ\rangle$, $|JJ-2\rangle$, $|JJ-4\rangle$, etc.

The saturation value of $\langle T^K_Q\rangle = \langle\Psi|(T^K_Q)_c|\Psi\rangle$ is a linear combination of matrix elements of the form $\langle JM|(T^K_Q)_c|JM'\rangle$. Because $(T^K_Q)_c$ is a spherical tensor a matrix element obeys the Wigner–Eckart theorem which we write in the form [16,17],

$$\langle JM|(T^K_Q)_c|J'M'\rangle = (-1)^{J-M}\begin{pmatrix} J & K & J' \\ -M & Q & M' \end{pmatrix}(J\|T^K_Q(c)\|J') \ , \qquad (15)$$

and the reduced matrix-element for equivalent electrons in an atomic shell with angular momentum l is easily found to be

$$(J\|T^K_Q(c)\|J') = \sqrt{8\pi}(l\|Y^K\|l)W^{(0K)K} \ . \qquad (16)$$

Here,

$$(l\|Y^K\|l) = (-1)^l(2l+1)\left[\frac{(2K+1)}{4\pi}\right]^{1/2}\begin{pmatrix} l & K & l \\ 0 & 0 & 0 \end{pmatrix} \ , \qquad (17)$$

where the $3j$-symbol can be different from zero when $2l+K$ is an even integer, which means even K in this case. The unit tensor $W^{(0K)K}$ depends on the quantum numbers SLJ, $S'L'J'$ and it is tabulated for a large number of 3d and 4f ions. Some details about $W^{(0K)K}$ are in appendix D, including references to tabulated values.

A more general case is when the valence electrons are not equivalent but occupy states of the form $(a|lm\rangle + b|l'm'\rangle)$ where $l \neq l'$. In this case, the mean value of T^K_Q has off-diagonal matrix elements like $a^*b\langle lm|T^K_Q|l'm'\rangle$ that are different from zero for even $l+K+l'$ which can include odd values of K. The off-diagonal terms in question may occur when an ion is not at a centre of inversion symmetry, and the crystal potential it experiences mixes states from different atomic-shells.

The interaction operator (2) for Thomson scattering is unchanged by the reversal of time. Explicitly, time reversal applied to (2) changes the signs of $\mathbf{q}$, $\mathbf{q}'$

and $\mathbf{k} = \mathbf{q} - \mathbf{q}'$, and it takes i to $-$i. The exchange $\mathbf{q} \longleftrightarrow \mathbf{q}'$ changes the sign of $\mathbf{k}$ and $Y_Q^K(\hat{\mathbf{k}})$ in (5) is changed to $(-1)^K Y_Q^K(\hat{\mathbf{k}})$. A contribution to (5) with even K is unchanged (symmetric) by $\mathbf{q} \longleftrightarrow \mathbf{q}'$, and a contribution with odd K changes its sign (antisymmetric). Clearly, a symmetric contribution to (5) is accompanied by an atomic tensor that is both time-even and parity-even, while an antisymmetric contribution is accompanied by an atomic tensor which is time-even and parity-odd. Atomic tensors encountered in Thomson scattering change to $(-1)^K \langle T_Q^K \rangle_c$ from $\langle T_Q^K \rangle_c$ under inversion of the coordinate system of the electrons, which is also referred to as the parity transformation, and a tensor with this transformation property is called a true (or polar) tensor. (If the parity transformation introduces a phase factor $(-1)^{K+1}$ the tensor in question is called a pseudotensor, or an axial tensor. By way of an example of a pseudotensor we cite the mean helicity of an x-ray beam P_2 which is a scalar quantity that changes sign under inversion of the coordinate system.)

3 Magnetic x-ray scattering

The first correction, in an expansion in $E/m_e c^2$, to the Thomson contribution of the x-ray scattering length includes magnetic terms [14,15]. These magnetic terms appear also in the amplitude for the magnetic scattering of neutrons [24], which is the subject of the next section. However, there is one important difference between the amplitudes for magnetic neutron and magnetic x-ray scattering. In the neutron case, the spin ($\mathbf{S}$) and orbital ($\mathbf{L}$) magnetic moments of the unpaired electrons in the crystal are linked together and the amplitude is proportional to the total magnetic moment $\mathbf{L}+2\mathbf{S}$, to a good approximation. By contrast, the magnetic x-ray amplitude is such that the spin and orbital moments can be separately measured [25–27]. We note that the spin moment is also obtainable from magnetic x-ray Compton scattering [28–30] which is both incoherent and inelastic and, thus, fundamentally different from the Bragg diffraction under discussion.

3.1 Magnetic scattering length

Let us introduce a structure factor for spin moments and a structure factor for orbital moments, in analogy with the Thomson structure factor $F_c(\mathbf{k})$. To a first approximation, that is often perfectly adequate for the analysis of observations, our new structure factors are,

$$\mathbf{F}_S(\mathbf{k}) \simeq \sum_{\mathbf{d}} f_S(\mathbf{k};\mathbf{d}) \langle \mathbf{S} \rangle_{\mathbf{d}} \mathrm{e}^{\mathrm{i}\mathbf{k}\cdot\mathbf{d}} \ , \tag{18}$$

and,

$$\mathbf{F}_L(\mathbf{k}) \simeq \frac{1}{2}\sum_{\mathbf{d}} f_L(\mathbf{k};\mathbf{d})\langle \mathbf{L}\rangle_{\mathbf{d}} \mathrm{e}^{\mathrm{i}\mathbf{k}\cdot\mathbf{d}} \ . \tag{19}$$

Here, $f_S(\mathbf{k};\mathbf{d})$ and $f_L(\mathbf{k};\mathbf{d})$ are atomic form factors for the spin and orbital moment distributions, respectively, and $f_S(0;\mathbf{d}) = f_L(0;\mathbf{d}) = 1$. The general expressions for the magnetic structure factors can include octupole, and higher-order, multipole moments and the expressions are given at the end of this section.

The magnetic x-ray scattering length has a non-trivial dependence on the polarization in the primary and secondary beams. It is normal practice to label by σ polarization perpendicular to the plane of scattering, which is defined by $\mathbf{q}$ and $\mathbf{q}'$. Polarization in the plane is labelled by π. Our choice of Cartesian axes (xyz) for the geometry of the experiment is illustrated in Fig. 3, where σ and the z-axis are parallel and $\mathbf{k} = \boldsymbol{\tau}(hkl)$ is directed along $-x$ [13,26]. The x-ray scattering length is expressed as $-r_{\mathrm{e}}\mathbf{G}$ where $\mathbf{G}$ is a 2×2 matrix with components $G_{\sigma'\sigma}$, $G_{\pi'\pi}$, $G_{\sigma'\pi}$, and $G_{\pi'\sigma}$. The Thomson structure factor appears in channels where the polarization in the primary beam is not rotated on deflection by the crystal, namely, $G_{\sigma'\sigma}$ and $G_{\pi'\pi}$. These two channels also contain magnetic components $F_S^z(\mathbf{k})$ and $F_L^z(\mathbf{k})$ normal to the plane of scattering. The rotated channels, with amplitudes $G_{\pi'\sigma}$ and $G_{\sigma'\pi}$, are purely magnetic and the components of $\mathbf{F}_S(\mathbf{k})$ and $\mathbf{F}_L(\mathbf{k})$ lie in the plane.

It is convenient to express the components of $\mathbf{G}$ in terms of four other quantities specified below;

$$\beta = -\frac{1}{2}(1+\cos 2\theta)F_c(\mathbf{k}) - \mathrm{i}\delta\sin(2\theta)\{F_S^z(\mathbf{k}) + (1-\cos 2\theta)F_L^z(\mathbf{k})\} \ , \tag{20}$$

$$\alpha_3 = -\frac{1}{2}(1-\cos 2\theta)F_c(\mathbf{k}) + \mathrm{i}\delta(1-\cos 2\theta)\sin(2\theta)F_L^z(\mathbf{k}) \ , \tag{21}$$

$$\alpha_2 = \delta\cos\theta(1-\cos 2\theta)\{2F_L^y(\mathbf{k}) + F_S^y(\mathbf{k})\} \ , \tag{22}$$

$$\alpha_1 = -\mathrm{i}\delta\sin\theta(1-\cos 2\theta)F_S^x(\mathbf{k}) \ . \tag{23}$$

In these expressions, $\delta = E/m_{\mathrm{e}}c^2 = \hbar q/m_{\mathrm{e}}c$ and θ is the Bragg angle illustrated in Fig. 3. The virtue in using (20) - (23), instead of $\mathbf{G}$, lies in the ease of handling polarization. If $\mathbf{P} = (P_1, P_2, P_3)$ is the Stokes vector, the x-ray cross-section is simply,

$$\frac{\mathrm{d}\sigma}{\mathrm{d}\Omega} = r_{\mathrm{e}}^2\{\boldsymbol{\alpha}^*\cdot\boldsymbol{\alpha} + |\beta|^2 + \beta^*(\mathbf{P}\cdot\boldsymbol{\alpha}) + (\mathbf{P}\cdot\boldsymbol{\alpha}^*)\beta + \mathrm{i}\mathbf{P}\cdot(\boldsymbol{\alpha}^*\times\boldsymbol{\alpha})\} \ . \tag{24}$$

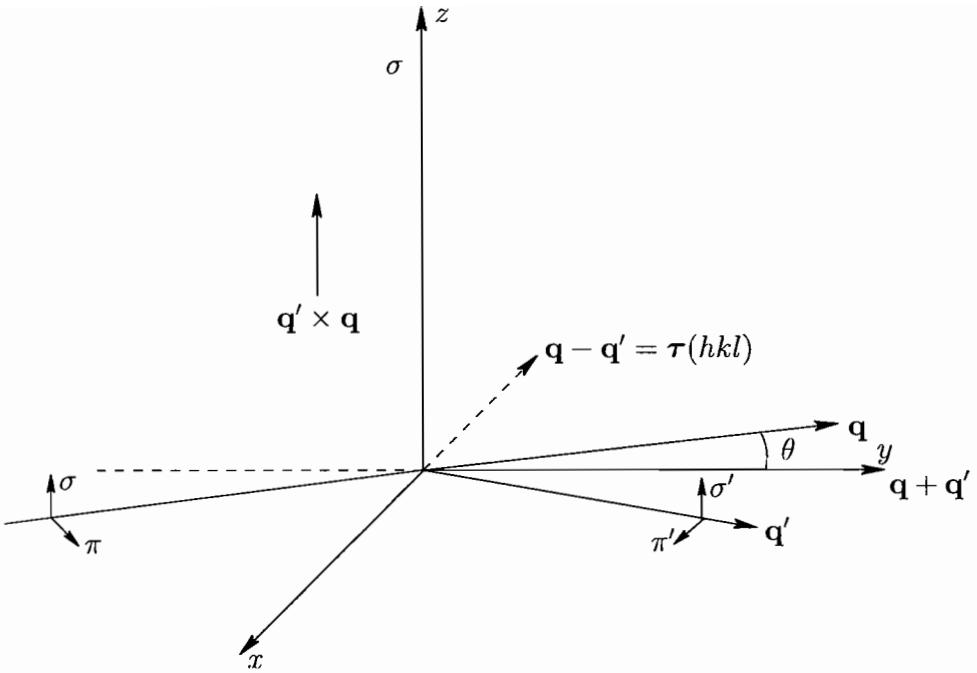

Fig. 3. The diagram illustrates the Cartesian coordinate system (xyz) adopted for Bragg diffraction and the relation to states of polarization, σ and π, in the primary and secondary beams of x-rays.

Table 2
Vectors in Figure 3

Quantities depicted in Fig. 3 and evaluated for elastic scattering $|\mathbf{q}| = |\mathbf{q}'|$.

$\hat{\mathbf{q}} = (-\sin\theta, \cos\theta, 0)$, $\hat{\mathbf{q}}' = (\sin\theta, \cos\theta, 0)$

$\hat{\mathbf{q}}' \times \hat{\mathbf{q}} = (0, 0, \sin 2\theta)$

$\hat{\mathbf{q}} - \hat{\mathbf{q}}' = (-2\sin\theta, 0, 0)$, $\hat{\mathbf{q}} + \hat{\mathbf{q}}' = (0, 2\cos\theta, 0)$

$\boldsymbol{\sigma} = \boldsymbol{\sigma'} = (0, 0, 1)$

$\boldsymbol{\pi} = (\cos\theta, \sin\theta, 0)$, $\boldsymbol{\pi'} = (\cos\theta, -\sin\theta, 0)$

$\pi'_{+1} = -\pi_{-1} = -\frac{1}{\sqrt{2}}\mathrm{e}^{-\mathrm{i}\theta}$, $\hat{q}_{+1} = \hat{q}'_{-1} = \frac{-\mathrm{i}}{\sqrt{2}}\mathrm{e}^{\mathrm{i}\theta}$

By way of illustration of (24) let us consider pure charge scattering, i.e. set $\mathbf{F}_S(\mathbf{k}) = \mathbf{F}_L(\mathbf{k}) = 0$ in (20) - (23). The expression (24) reduces to,

$$\frac{\mathrm{d}\sigma}{\mathrm{d}\Omega} = \frac{1}{2} r_\mathrm{e}^2 |F_c(\mathbf{k})|^2 (1 + \cos^2(2\theta) + P_3 \sin^2(2\theta)) \ . \tag{25}$$

The cross-section for x-rays polarized perpendicular to the plane $P_3 = +1$ (σ polarization) is larger than the cross-section for x-rays polarized in the plane $P_3 = -1$ (π polarization) [31].

When the polarization is nearly perfect, as it is with x-rays from a synchrotron source, the components of $\mathbf{G}$ provide the corresponding cross-sections. For

example, with pure σ-polarization the unrotated cross-section is $r_e^2|G_{\sigma'\sigma}|^2$. The four components of $\mathbf{G}$ are,

$$G_{\sigma'\sigma} = \beta + \alpha_3 = -F_c(\mathbf{k}) - \mathrm{i}\delta\sin(2\theta)F_S^z(\mathbf{k}) \ ,$$
$$G_{\pi'\pi} = \beta - \alpha_3, G_{\sigma'\pi} = \alpha_1 - \mathrm{i}\alpha_2, G_{\pi'\sigma} = \alpha_1 + \mathrm{i}\alpha_2 \ . \qquad (26)$$

The component $G_{\sigma'\sigma}$ is written out in full to emphasise that it depends on the spin and not on the orbital magnetization [32,33].

The spin moment is the dominant magnetic contribution in the limit of very hard x-rays, and the appropriate cross-section has a very simple form. For Bragg diffraction from planes of reflection separated by a distance d and x-rays with a wavelength $\ll d$ the cross-section is [34],

$$\frac{\mathrm{d}\sigma}{\mathrm{d}\Omega} = r_e^2|F_c(\mathbf{k}) + \mathrm{i}(\lambda_0/d)F_S^z(\mathbf{k})|^2 \ . \qquad (27)$$

Here $\lambda_0 = (2\pi\alpha a_0) = (2\pi r_e/\alpha) \simeq 0.0243$Å is the Compton wavelength.

3.2 Unit-cell structure factors

Let us now address the calculation of $\mathbf{F}_S(\mathbf{k})$ and $\mathbf{F}_L(\mathbf{k})$. Results (18) and (19) are not adequate if the wavevector is large enough for $\langle j_2(k)\rangle$ to be larger than $\langle j_0(k)\rangle$, where $\langle j_K(k)\rangle$ is the Bessel function transform of order K of the radial component of the valence wavefunction introduced in the previous section. In fact, (18) and (19) become exact in the limit $k \longrightarrow 0$ at which the atomic form factors are unity.

The definition of $\mathbf{F}_S(\mathbf{k})$ is similar to the definition of the Thomson (charge) structure factor (1), except that $\mathbf{F}_S(\mathbf{k})$ is related to the spatial Fourier transform of the spin density and it is a vector quantity. We have,

$$\mathbf{F}_S(\mathbf{k}) = \sum_{\mathbf{d}} \mathrm{e}^{\mathrm{i}\mathbf{k}\cdot\mathbf{d}} \langle \sum_j \mathrm{e}^{\mathrm{i}\mathbf{k}\cdot\mathbf{R}_j}\mathbf{s}_j\rangle_{\mathbf{d}} \ , \qquad (28)$$

where $\mathbf{R}_j$ and $\mathbf{s}_j$ are position and spin operators of the j^{th} electron associated with the site $\mathbf{d}$ in the unit cell. Matrix elements to be calculated are mixed orbit and spin, i.e. they contain the unit tensor $W^{(1K)K'}$, whereas both the Thomson (16) and orbital magnetic interactions contain $W^{(0K)K}$.

A matrix element of the spatial Fourier transform of the spin density in (28) is,

$$\langle JM|\sum_j \mathrm{e}^{\mathrm{i}\mathbf{k}\cdot\mathbf{R}_j}(\mathbf{s}_j)_p|J'M'\rangle =$$

$$= \sum_{KQ}\sum_{K'Q'} \mathrm{i}^K(4\pi)^{1/2}Y_Q^K(\hat{\mathbf{k}})\{\frac{1}{3}(2K'+1)\}^{1/2}D(K,K')$$

$$\times \quad (KQK'Q'|1p)(-1)^{J-M}\begin{pmatrix} J & K' & J' \\ -M & Q' & M' \end{pmatrix} \ . \tag{29}$$

The content of this expression is a classical spherical-tensor $Y_Q^K(\hat{\mathbf{k}})$ of rank K coupled to another spherical tensor of rank K', which is based on $W^{(1K)K'}$, to give a vector quantity of rank 1 and projection p. Our definition of the Clebsch–Gordan coefficient that effects the coupling is,

$$(KQK'Q'|jm) = (2j+1)^{1/2}(-1)^{-K+K'-m}\begin{pmatrix} K & K' & j \\ Q & Q' & -m \end{pmatrix} \ , \tag{30}$$

and in (29) one has $j = 1$ and $m = p$. The positive integer K is even and its maximum value is $2l$ where l is the angular momentum of the valence shell. The positive integer K' can only take the three values $K' = K$ or $K' = K \pm 1$. If states used to construct the mean value of the spin density all come from one manifold and $J = J'$, $L = L'$, $S = S'$ then $K' = K \pm 1$ and $D(K', K') = 0$. The definition of $D(K, K')$ is [12,35],

$$D(K,K') = (4\pi)^{1/2}\langle j_K(k)\rangle(\frac{1}{2}\|s\|\frac{1}{2})(l\|Y^K\|l)W^{(1K)K'} \ , \tag{31}$$

where $(1/2\|s\|1/2) = \sqrt{3/2}$. The appearance in (31) of reduced matrix elements of spin and a spherical harmonic confirm the mixed spin and space character of the matrix element. Numerical values for $D(K, K')$ can be obtained from (31), using tabulated values for $W^{(1K)K'}$ or by using extensive tabulations for a related quantity $C(K, K')$ where

$$D(K,K') = \mathrm{i}^K(-1)^{K'+J'-J}\left\{\frac{3(2J+1)}{(2K'+1)}\right\}^{1/2} C(K,K') \ . \tag{32}$$

Note that the unit tensor, $D(K, K')$ and $C(K, K')$ depend on the full range of quantum numbers that are required to specify a valence shell. The approximate expression (18) is recovered by keeping in (29) only the term $K = 0$, for which,

$$D(0,1) = \langle j_0(k)\rangle g_S(J\|J\|J) \ , \tag{33}$$

where $g_S = (g - 1)$ is the spin part of the Landé factor g. At this level of

approximation in (29) the latter becomes,

$$\langle JM|\sum_j e^{i\mathbf{k}\cdot\mathbf{R}_j}(\mathbf{s}_j)_p|J'M'\rangle \simeq \delta_{J,J'}\langle j_0(k)\rangle g_S\langle JM|J_p|JM'\rangle \ . \tag{34}$$

The contribution in (29) with $K' = 3$ is an octupole moment built from spin and an orbital contribution. For a single J-manifold K' has a maximum value $(2l+1)$. However, values of J and J' in $W^{(1K)K'}$ may restrict K' to a smaller value, because K', J' and J satisfy the triangular condition $|J - J'| \leq K' \leq J + J'$ in the Wigner–Eckart theorem.

The orbital structure factor $\mathbf{F}_L(\mathbf{k})$ is constructed from an operator built from $e^{i\mathbf{k}\cdot\mathbf{R}_j}$ and the linear momentum $\mathbf{p}_j$. One finds,

$$\mathbf{F}_L(\mathbf{k}) = \sum_{\mathbf{d}} e^{i\mathbf{k}\cdot\mathbf{d}}\langle\left(\frac{1}{ik^2}\right)\sum_j e^{i\mathbf{k}\cdot\mathbf{R}_j}(\mathbf{k}\times\mathbf{p}_j)\rangle_{\mathbf{d}} \ . \tag{35}$$

In working out the matrix element of the operator in (35) one can usefully take advantage that $\mathbf{F}_L(\mathbf{k})$ appears in $\mathbf{G}$ in a scalar product with vectors that are perpendicular to $\mathbf{k}$, namely, $\mathbf{q}+\mathbf{q}'$ and $\mathbf{q}\times\mathbf{q}'$. We find [12,35],

$$\begin{aligned}
&\langle JM|\left(\frac{1}{ik^2}\right)\sum_j e^{i\mathbf{k}\cdot\mathbf{R}_j}(\mathbf{k}\times\mathbf{p}_j)_p|J'M'\rangle = \\
&= \sum_Q \sum_{K'Q'} (4\pi)^{1/2} Y_Q^{K'-1}(\hat{\mathbf{k}}) \left(\frac{2K'+1}{K'+1}\right) Z_L^{K'}(K'-1) \\
&\quad \times \ (K'-1QK'Q'|1p)(-1)^{J-M}\begin{pmatrix} J & K' & J' \\ -M & Q' & M' \end{pmatrix} \ ,
\end{aligned} \tag{36}$$

and $K' = 1, 3, \ldots, (2l-1)$. The quantity $Z_L^{K'}(K'-1)$ is proportional to $W^{(0K')K'}$, a finding that is expected because the operator on the left-hand side in (36) does not include the spin operator. One finds,

$$\begin{aligned}
Z_L^{K'}(K'-1) &= -i^{K'+1}\delta_{S,S'}\{\langle j_{K'-1}(k)\rangle + \langle j_{K'+1}(k)\rangle\} \\
&\quad \times \ [\frac{2}{3}(K'+1)]^{1/2}(2l+1)^2 A(K',K',l) W^{(0K')K'} \\
&= (-1)^{K'+J'-J}(2J+1)^{1/2} A(K'-1,K') \ .
\end{aligned} \tag{37}$$

The second equality relates $Z_L^{K'}(K'-1)$ to a quantity $A(K'-1,K')$ which is used in calculations of the magnetic neutron scattering amplitude, and here we will not pause to give the actual expression for $A(K',K',l)$ that is contained in $A(K'-1,K')$.

For $K' = 1$,

$$Z_L^1(0) = \frac{1}{3}\{\langle j_0(k)\rangle + \langle j_2(k)\rangle\} g_L(J\|J\|J) \ , \tag{38}$$

where $g_L = (2 - g)$ is the orbital part of g. This result enables us to recover the approximate expression (19). Note that (33) and (38) show that the spin and orbital atomic form factors are not the same with $f_S(k) = \langle j_0(k)\rangle$ and $f_L(k) = \langle j_0(k)\rangle + \langle j_2(k)\rangle$, in the limit in question.

The value of $Z_L^{K'}(K'-1)$ for $K' = 3$ is directly related to the orbital octupole operator,

$$\Lambda = \frac{1}{2}\sum_j \{l_0(5l_0^2 - 3l(l+1) + 1)\}_j \ , \tag{39}$$

where l_0 ($\equiv l_z$) is the diagonal component of the orbital operator. The reduced matrix element of Λ is found to be,

$$(J\|\Lambda\|J') = (l\|l\|l)\left\{\frac{1}{2}(l-1)(2l-1)(l+2)(2l+3)\right\}^{1/2} W^{(03)3} \ , \tag{40}$$

and the matrix element is, of course,

$$\langle JM|\Lambda_q|J'M'\rangle = (-1)^{J-M}\begin{pmatrix} J & 3 & J' \\ -M & q & M' \end{pmatrix}(J\|\Lambda\|J') \ . \tag{41}$$

Our two main results, (29) and (36) show that the structure factors for the magnetic scattering of x-rays by spin and orbital moments are,

$$(\mathbf{F}_S(\mathbf{k}))_p = \sum_{KQ}\sum_{K'Q'}(4\pi)^{1/2} Y_Q^K(\hat{\mathbf{k}})\Psi_{Q'}^{K'}(S)(KQK'Q'|1p) \ , \tag{42}$$

and,

$$(\mathbf{F}_L(\mathbf{k}))_p = \sum_{Q}\sum_{K'Q'}(4\pi)^{1/2} Y_Q^{K'-1}(\hat{\mathbf{k}})\Psi_{Q'}^{K'}(L)(K'-1QK'Q'|1p) \ , \tag{43}$$

where,

$$\Psi_{Q'}^{K'}(S) = \sum_{\mathbf{d}} e^{i\mathbf{k}\cdot\mathbf{d}}\langle T_{Q'}^{K'}\rangle_{S,\mathbf{d}} \ , \tag{44}$$

$$\Psi_{Q'}^{K'}(L) = \sum_{\mathbf{d}} e^{i\mathbf{k}\cdot\mathbf{d}}\langle T_{Q'}^{K'}\rangle_{L,\mathbf{d}} \ , \tag{45}$$

and the reduced matrix elements are,

$$(J\|T^{K'}(S)\|J') = \mathrm{i}^K \{\frac{1}{3}(2K'+1)\}^{1/2} D(K,K') \ , \tag{46}$$

$$(J\|T^{K'}(L)\|J') = \left(\frac{2K'+1}{K'+1}\right) Z_L^{K'}(K'-1) \ . \tag{47}$$

In the spin matrix element K and K' satisfy the triangular condition imposed by a Clebsch–Gordan coefficient. The reduced matrix element for both the spin and the orbital moments depend on the magnitude of the scattering wavevector, through the Bessel function transform $\langle j_K(k)\rangle$. When k is relatively small, all but $\langle j_0(k)\rangle$ can be neglected and the structure factors $\mathbf{F}_S(\mathbf{k})$ and $\mathbf{F}_L(\mathbf{k})$ are adequately represented by (18) and (19).

When it comes to calculating $\Psi_{Q'}^{K'}$, tensors at different sites in the cell are generated by application of the symmetry operators in the space group. In the previous section, which deals with Thomson scattering, we gave an example calculation that involved both proper rotations and a mirror plane of symmetry. To these operations we need to add the influence caused by reversing the polarity of the local magnetic field. For example, a fully compensating antiferromagnet has equal numbers of ions with opposite local fields. The general rule for parity-even tensors is,

$$\langle T_Q^K\rangle_{\mathbf{H}} = (-1)^K \langle T_Q^K\rangle_{-\mathbf{H}} \ , \tag{48}$$

where $\mathbf{H}$ denotes an applied field or the direction of the spontaneous moment at the site in question.

3.3 Application to V_2O_3

We conclude this section by calculating the structure factor for vanadium ions in antiferromagnetic V_2O_3. This material is of great interest as an example of a Mott-Hubbard insulator. At room temperature the material possesses the corundum structure in the space group R$\bar{3}$c. On reducing the temperature of the material to $150-160$ K, it changes from a metal to an insulator and from a paramagnet to a fully compensating antiferromagnet depicted in Fig. 4. The long-range magnetic order coexists with a monoclinic crystal structure with space group I2/a [36] in which vanadium ions occupy sites 8(f) that possess no symmetry and, in particular, they are not centres of inversion symmetry.

The monoclinic space-group I2/a is a body-centred cell and Bragg wavevectors $\tau_m(hkl)$ for charge-allowed reflections satisfy the necessary condition

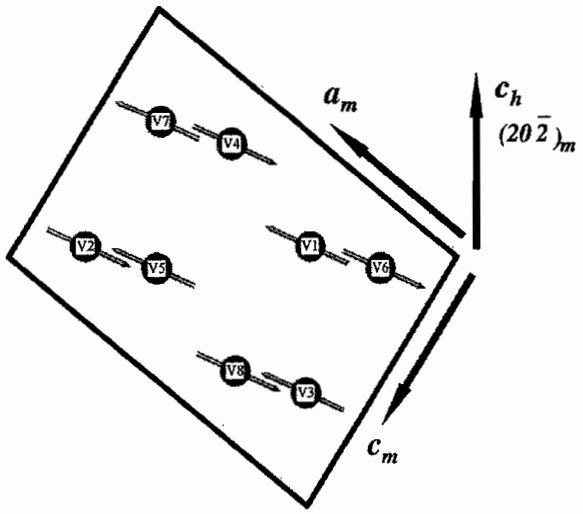

Fig. 4. Positions of the eight vanadium ions in the monoclinic cell adopted by V_2O_3 below the Néel temperature, together with the configuration of their moments in the plane spanned by $\mathbf{a}_m$ and $\mathbf{c}_m$. The monoclinic Bragg wavevector $\tau_m = (20\bar{2})_m$ is parallel to the trigonal axis $\mathbf{c}_h$, and $\mathbf{b}_m$ is normal to the plane of the diagram and parallel to $\mathbf{a}_h$ [37].

$h + k + l = 2n$ (Miller indices h, k, l are all integers). The motif of vanadium magnetic moments consists of sheets of moments with ferromagnetic alignment within $(010)_m$ layers, or hexagonal (110) layers, and moment reversal between adjacent layers. The moments align along some easy-axis in these layers [38].

The trigonal basis vectors are $\mathbf{a}_h = a(1,0,0)$, $\mathbf{b}_h = a(-1/2,(1/2)\sqrt{3},0)$ and $\mathbf{c}_h = c(0,0,1)$ and the volume of the unit cell$= a^2c\sqrt{3}/2$. Following Dernier and Marezio [36,37] in the use of an I-centred cell, from these vectors we generate monoclinic basis vectors $\mathbf{a}_m = (0,(1/\sqrt{3})2a,(1/3)c)$, $\mathbf{b}_m = \mathbf{a}_h$, and $\mathbf{c}_m = (0,(1/\sqrt{3})a,-(1/3)c)$, and the volume of the cell$= a^2c/\sqrt{3}$. The corresponding Bragg wavevector $\tau_m(hkl) \equiv (hkl)_m$ is

$$\tau_m(hkl) = \frac{1}{a}\left(k, \frac{1}{\sqrt{3}}(h+l), \frac{a}{c}(h-2l)\right) . \tag{49}$$

We note that $(l0\bar{l})_m$ is parallel to $\mathbf{c}_h$, and $(2lkl)_m$ is normal to $\mathbf{c}_h$.

Referring to figure 4, the position coordinates of vanadium ions labelled (1) and (5) are (x,y,z) and $(-x,-y,-z)$, respectively, with $x = 0.3439$, $y = 0.0012$ and $z = 0.2993$ [36]. The positions of the pair (2) and (6) are related by a body-centred translation to the pair (1) and (5). The position coordinates of (3) and (7) are $(1/2-x,y,-z)$ and $(1/2+x,-y,z)$, respectively, and the pairs (4), (8) and (3), (7) are related by the body-centre translation. The body-centre translation $(1/2,1/2,1/2)_m = a/2(1,\sqrt{3},0)$ and $(1/2,1/2,1/2)_m \cdot \tau_m(hkl) =$

$\frac{1}{2}(h+k+l)$. It is convenient to define an angle $\nu = 2\pi(x,y,z)_m \cdot \boldsymbol{\tau}_m(hkl) = 2\pi(xh+zl)$ where the second equality is correct for $y=0$.

Four pairs of vanadium ions at sites 8(f) in I2/a possess the same chemical environment, and the pairs are, (1) and (2), (3) and (4), (5) and (6), and (7) and (8). Sites (1) and (5), and (3) and (7) are related by inversion, which is an operator that does not change a parity-even atomic tensor. Referring to Fig. 4, moments on even and odd numbered sites are in opposite directions, so the odd numbered sites in $\Psi^{K'}_{Q'}$, say, acquire a factor $(-1)^{K'}$ by application of (48). Lastly, sites occupied by ions (1) and (7) are related by an a-glide which corresponds at site (7) to changing the sign of the coordinate normal to the $\mathbf{a}_m - \mathbf{c}_m$ plane, i.e. our Cartesian $x = \mathbf{a}_h$ goes to $-x$ (this corresponds to $y \rightarrow -y$ in the standard monoclinic basis). As remarked earlier, in section 2, with a parity-even tensor the mirror operation is equivalent to rotation by π about a normal to the plane, and the normal is $\mathbf{a}_h$. The relation $\langle T^{K'}_{Q'}\rangle_7 = \langle T^{K'}_{-Q'}\rangle_1$ is a result of the rotation and (48).

For the model of V_2O_3 that we have described, in the previous paragraphs, $\Psi^{K'}$ can be different from zero for even values of $K'+(h+k+l)$, so here there is a selection rule in the structure factor that links the rank of atomic tensors and the sum of Miller indices [39]. Neutron magnetic diffraction is observed at reflections with $h+k+l$ an odd integer, i.e. space-group-forbidden reflections, and the scattering amplitude is composed of tensors of rank $K' = 1, 3$ and 5. One finds,

$$\Psi^{K'}_{Q'} = 4\cos(\nu)\{\langle T^{K'}_{Q'}\rangle + (-1)^h \langle T^{K'}_{-Q'}\rangle\} \ , \tag{50}$$

and this result applies for the spin and orbital structure factors (44) and (45), and magnetic neutron diffraction discussed in the next section. The saturation moment of a vanadium ion is $1.2\mu_B$, and most of the moment aligned against the pure spin moment of $2\mu_B$ is thought to be orbital moment created by the spin-orbit interaction. This sizeable orbital moment should be visible in magnetic x-ray and magnetic neutron diffraction.

Note that for odd h we have $\Psi^{K'}_{Q'} = -\Psi^{K'}_{-Q'}$ and there is no contribution to scattering from diagonal elements of the atomic tensors $\langle T^{K'}_{Q'}\rangle_S$ and $\langle T^{K'}_{Q'}\rangle_L$. Reflections with odd h have another selection rule that stems from the motif of vanadium ions. Observe that with odd h $\Psi^{K'}_{Q'} \sim \{\langle T^{K'}_{Q'}\rangle - \langle T^{K'}_{-Q'}\rangle\}$ and evaluated for $K' = Q' = 1$ one has $\Psi^1_{+1}(L)$ proportional to $\langle L_x\rangle$ which is normal to the $\mathbf{a}_m - \mathbf{c}_m$ plane, and it is equal to zero if the orbital moment lies in this plane. A similar result applies to $\Psi^1_{+1}(S)$. Hence, in magnetic diffraction by V_2O_3, with odd h and even $k+l$, one will observe octupoles and higher-order magnetic multipoles.

4 Magnetic neutron scattering

Even though the diffraction of x-rays is the main topic it is fitting to include a brief account of neutron scattering. We will find that, a structure factor $\Psi_{Q'}^{K'}$, like (6), (44) or (45), generates the unit cell structure factor for the magnetic Bragg diffraction of neutrons.

4.1 Scattering length for neutrons

Neutrons are scattered by the magnetization in a material which is created by the spin and orbital moments of unpaired electrons [12,24]. The orbital interaction is identical to the one encountered in the magnetic scattering of x-rays, and the actual operator is displayed in (35). The spin interaction for neutron scattering is also very similar to the spin interaction in x-ray scattering. The one difference between the two cases is that in neutron scattering the spin of an electron is linked with the deflection of the beam in a double vector product $\mathbf{k} \times (\mathbf{s}_j \times \mathbf{k})/k^2$. We denote by $\mathbf{Q}_\perp$ the sum of the spin and orbital interactions,

$$\mathbf{Q}_\perp = \sum_j \mathrm{e}^{\mathrm{i}\mathbf{k}\cdot\mathbf{R}_j} \left(\frac{1}{k^2}\right) \{\mathbf{k} \times (\mathbf{s}_j \times \mathbf{k}) - \mathrm{i}(\mathbf{k} \times \mathbf{p}_j)\} \ . \tag{51}$$

A neutron with spin $\mathbf{s}_n$ has a scattering length $\gamma r_\mathrm{e} \mathbf{s}_n \cdot \mathbf{Q}_\perp$ where $\gamma = -1.9130$ is the gyromagnetic ratio.

The amplitude for Bragg diffraction is related to the mean value of $\mathbf{Q}_\perp$ for which we find,

$$\langle \mathbf{Q}_{\perp,p} \rangle = \sum_{KQ} \sum_{K'Q'} (4\pi)^{1/2} Y_Q^K(\hat{\mathbf{k}}) \Psi_{Q'}^{K'}(n) (KQK'Q'|1p) \ . \tag{52}$$

Here,

$$\Psi_{Q'}^{K'}(n) = \sum_{\mathbf{d}} \mathrm{e}^{\mathrm{i}\mathbf{k}\cdot\mathbf{d}} \langle T_{Q'}^{K'}(K) \rangle_{n,\mathbf{d}} \ , \tag{53}$$

and for relatively small wavevectors $\langle \mathbf{T}^1 \rangle_n$ is proportional to the magnetic moment, with $\langle \mathbf{T}^1 \rangle_n \to \langle \mathbf{L} + 2\mathbf{S} \rangle/3$ as k tends to zero. The result for $\langle \mathbf{T}^1 \rangle_n$ which corresponds to (33) and (38) is often called its dipole limit, because the result is obtained by neglecting all tensors other than the two with $K' = 1$,

and it is,

$$\langle \mathbf{T}^1 \rangle_n \simeq \frac{1}{3}\{2\langle \mathbf{S} \rangle \langle j_0(k) \rangle + \langle \mathbf{L} \rangle (\langle j_0(k) \rangle + \langle j_2(k) \rangle)\} \ . \tag{54}$$

The upper limit on K' is set by the angular momentum of the valence shell; for a 3d transition ion $l = 2$ and the maximum value of $K' = (2l + 1) = 5$ and for a lanthanide ion the corresponding value is $K' = 7$. If K' is an odd integer, then $K = K' \pm 1$ and,

$$\langle T^{K'}_{Q'}(K' + 1) \rangle_n = \left(\frac{K'}{K' + 1} \right)^{1/2} \langle T^{K'}_{Q'}(K' - 1) \rangle_n \ . \tag{55}$$

If K' is even, the only non-zero tensor occurs when $K = K'$ and it is entirely due to the spin operator in $\mathbf{Q}_\perp$.

Physical properties of the sample can impose restrictions on K' , and there are two possible sources. First, a property of states used to describe the valence shell can impose restrictions on K'. If a 4f shell is described by states with the same values of J, L and S (a J-manifold), then K' is odd and it can not exceed $2J$. Secondly, the actual configuration of moments in the unit cell can make $\Psi^{K'}_{Q'} = 0$ for certain K'. Such a case is V_2O_3 considered at the end of the previous section, where a fully compensating motif of vanadium ions causes $\Psi^{K'}_{Q'}$ to vanish unless K' is an odd integer.

The reduced matrix element of $\langle T^{K'}_{Q'}(K) \rangle_n$ is [12,35],

$$(J \| T^{K'}(K) \| J') = (-1)^{K'+J'-J}(2J + 1)^{1/2}\{A(K, K') + B(K, K')\} \ . \tag{56}$$

Here the orbital contribution $A(K, K')$ is exactly the quantity defined by (37), K' is an odd integer, $A(K', K')$ is zero, and,

$$A(K' + 1, K') = \left(\frac{K'}{K' + 1} \right)^{1/2} A(K' - 1, K') \ . \tag{57}$$

The spin contribution to the reduced matrix element $B(K, K')$ has more awkward properties because it is built from both spin and spatial degrees of freedom. If K' is even, the only non-zero value of $B(K, K')$ occurs when $K = K'$, in which case,

$$(-1)^{K'+J'-J}(2J + 1)^{1/2} B(K', K') = \mathrm{i}^{K'} [\frac{1}{3}(2K' + 1)]^{1/2} D(K', K') \ , \tag{58}$$

where $D(K,K')$ is defined by (31), and expression (32) relates it to a quantity for which there are extensive tables. If K' is odd, then $K = K' \pm 1$ and $B(K' \pm 1, K')$ satisfy a relation like (57). For $K = K' - 1$,

$$\begin{aligned}(-1)^{K'+J'-J}(2J+1)^{1/2}B(K'-1,K') = \\ = \mathrm{i}^{K'-1}\left\{\frac{1}{3(2K'+1)}\right\}^{1/2}\{(K'+1)D(K'-1,K') \\ -[K'(K'+1)]^{1/2}D(K'+1,K')\} \ . \end{aligned} \tag{59}$$

The quantities $A(K,K')$ and $B(K,K')$ contain Bessel function transforms of the radial density in the valence shell. $A(K'-1,K')$ is proportional to $\{\langle j_{K'-1}\rangle + \langle j_{K'+1}\rangle\}$ while $D(K,K')$ is proportional to $\langle j_K\rangle$.

4.2 Principal axes

It is often the case in crystal physics that calculations are simpler, or more convenient, in a set of Cartesian axes that are not the crystal axes, nor the axes used to define the diffraction geometry. Let us label another set of axes by Cartesian coordinates $(\xi\eta\zeta)$. We use Euler angles α, β, γ to define $(\xi\eta\zeta)$ with respect to our reference frame, and in the latter [16,18],

$$\langle T_Q^K\rangle = \sum_r \langle T_r^K\rangle_{(\xi\eta\zeta)} D_{rQ}^K(-\gamma,-\beta,-\alpha) \ , \tag{60}$$

where $D_{rQ}^K(-\gamma,-\beta,-\alpha) = \{D_{Qr}^K(\alpha,\beta,\gamma)\}^*$ is an element of the rotation matrix, or Wigner D-function, and $\langle T_r^K\rangle_{(\xi\eta\zeta)}$ is the value of the tensor $\langle T_r^K\rangle$ with respect to the axes $(\xi\eta\zeta)$. The orthogonality property of Wigner D-functions yields, $\langle T_r^K\rangle_{(\xi\eta\zeta)} = \sum_Q \langle T_Q^K\rangle D_{Qr}^K(\alpha,\beta,\gamma)$. Various other properties of coordinate rotations are gathered in appendix A.

For the moment, let us assume that $\langle T_r^K\rangle_{(\xi\eta\zeta)}$ vanishes unless $r = 0$. Axes $(\xi\eta\zeta)$ with this property for $\langle T_r^K\rangle$ might be called the principal axes for $\langle T_r^K\rangle$, in which it is diagonal and, the ζ-axis is the axis of quantization. If in $\langle \mathbf{Q}_\perp\rangle$ we represent the spherical harmonic $Y_Q^K(\hat{\mathbf{k}})$ in the principal axes, then it is straightforward to show that,

$$\begin{aligned}\hat{\boldsymbol{\zeta}}\cdot\langle\mathbf{Q}_\perp\rangle \ &= \ \sum_{K'}\left(\frac{3K'}{2K'+1}\right)^{1/2}\langle T_0^{K'}(K'-1)\rangle_{(\xi\eta\zeta)} \\ &\times \ \{P_{K'-1}(k_\zeta) - P_{K'+1}(k_\zeta)\} \ , \end{aligned} \tag{61}$$

where K' is odd, and $k_\zeta = \hat{\mathbf{k}} \cdot \hat{\boldsymbol{\zeta}}$ is the projection of $\mathbf{k}$ on to the axis of quantization. In arriving at the result (61), which must also apply to $\Psi_0^{K'}$, the term with $K = K'$ is found to cancel, and the two terms $K = K' \pm 1$ combine with the aid of (55) to give the very simple expression reported in (61). The Legendre polynomial $P_n(x)$ satisfies $P_0(x) = 1$ and $P_n(1) = 1$ for all n. We conclude that when $\mathbf{k}$ is parallel to the principal axis $\boldsymbol{\zeta}$, and $k_\zeta = 1$, the magnetic amplitude $\langle \mathbf{Q}_\perp \rangle$ is normal to $\boldsymbol{\zeta}$. This might be viewed as an extension of a well-known result for $\langle \mathbf{Q}_\perp \rangle$ in the limit of small k, where $\langle \mathbf{Q}_\perp \rangle$ tends to the value $\{\boldsymbol{\mu} - \mathbf{k}(\mathbf{k} \cdot \boldsymbol{\mu})/k^2\}/2$ in which $\boldsymbol{\mu} = \langle \mathbf{L} + 2\mathbf{S} \rangle$ is the total magnetic moment.

5 Resonant x-ray scattering: parity-even events

Fig. 5 shows data collected in x-ray Bragg diffraction by V_2O_3 with the sample held at a temperature below its Néel temperature, at which it becomes a fully compensating antiferromagnet [40,41]. The crystal structure is a body-centred cell and all the data in Fig. 5 are collected at space-group forbidden reflections, for which the sum of the Miller indices is an odd integer. The panels on the left-hand side of Fig. 5 show the intensity as a function of x-ray energy collected near the vanadium K-edge, and in the unrotated ($\sigma'\sigma$) and rotated ($\pi'\sigma$) channels of scattering. There is a strong resonance enhancement of the Bragg intensities, and the same phenomenon has been observed with many different resonant ions and many crystal structures. In the case of V_2O_3, the diffraction is due to magnetic multipoles that disorder above the Néel temperature and the Bragg intensities disappear. The strong feature in panel (a) of Fig. 5 that sits around 5.475 KeV is due to an E1 event from the vanadium K-edge, at which an electron in the 1s core is photo-ejected in a process that changes orbital angular momentum by one unit. In panel (a) there is a second, weaker feature at an energy= 5.465 eV that is due to an E2 event at the vanadium K-edge. With this process the photo-ejected electron visits a 3d valence state which is the state occupied by the unpaired electrons that form the vanadium magnetic moment. Looking at panel (c) in Fig. 5, the E1 event is absent. This observation is one consequence of a selection rule that, for odd h and even $k + l$, forbids resonance events caused by vector-like interactions, i.e. tensors with rank $K = 1$.

Panels (b) and (d) in Fig. 5 show Bragg intensities as a function of rotation of the V_2O_3 domain about the Bragg wavevector. If the scattering was from electronic states with no angular anisotropy the intensity in such scans would be constant. As it is, Bragg intensities depend strongly on the angle of rotation and, also, states of polarization in the diffracted beam.

The data in Fig. 5, collected on V_2O_3, nicely illustrates the wealth of informa-

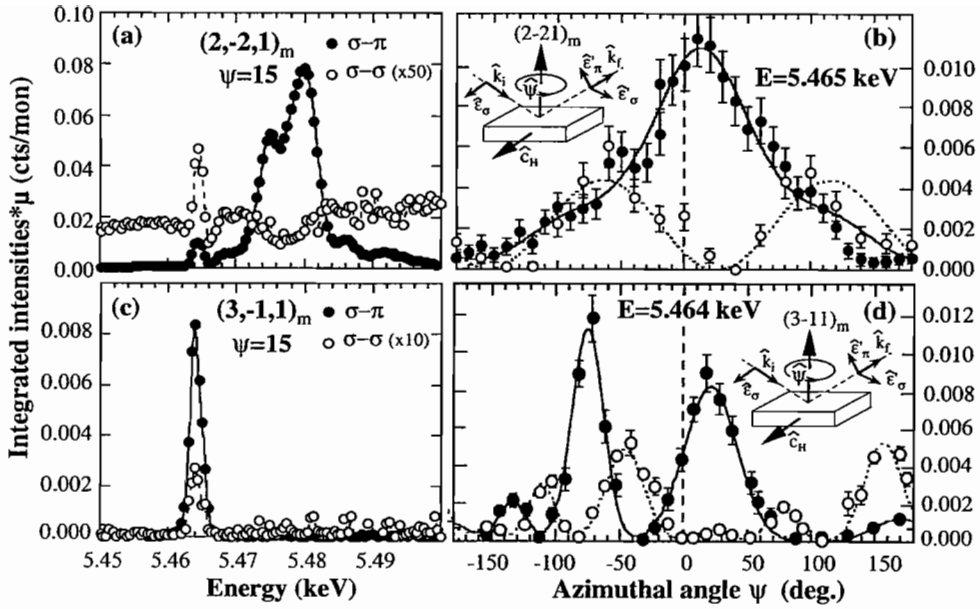

Fig. 5. Energy profiles (panels a and c) and azimuthal-angle scans (panels b and d) for resonant Bragg diffraction by a domain within antiferromagnetic V_2O_3. The observations are at space-group forbidden reflections and in channels with unrotated and rotated polarization. ¿From Paolasini et al.[40,41].

tion in x-ray resonance-enhanced Bragg diffraction. In this section we outline a framework for the interpretation of the observations. Applied to V_2O_3 it shows that, the observations reported in Fig. 5 are in complete accord with the established chemical and magnetic structures illustrated in Fig. 4 and parity-odd contributions to scattering, which are allowed because the resonant vanadium ions occupy sites that are not centres of inversion symmetry, are not visible in available diffraction data. In particular, data collected in reflections with odd h and even $k + l$ are a direct observation of the vanadium octupole moment created by orbital magnetization in the vanadium 3d valence shell [37,39].

Resonance-enhanced Bragg diffraction has most to offer when the intermediate state, visited by the photo-ejected core electron, is the valence state of the resonant ion occupied by unpaired electrons, namely, 3d, 4f and 5f states of 3d-transition, lanthanide and actinide ions [40–46]. In these experiments, the observations are directly related to states that participate in magnetic, magneto-electronic and charge-ordering effects. Observations on other states of a resonant ion, e.g. an E1 event at the K-edge of a 3d transition metal ion, can provide insight to the valence state of interest but it is less credible because there are more assumptions in the interpretation [47–50].

The x-ray scattering length expanded to the first order in $E/m_e c^2$ has two contributions with denominators that depend explicity on the x-ray energy [14,15]. These terms arise in the scattering length from inclusion at the second level of application of the radiation-matter interaction that is linear in the vector potential. To be more specific, the two energy-dependent terms are second-order in the current operator $\mathbf{J}(\mathbf{q}) = \sum(\mathbf{p}_j + \mathrm{i}\mathbf{s}_j \times \mathbf{q})\mathrm{e}^{\mathrm{i}\mathbf{q}\cdot\mathbf{R}_j}$ where $\mathbf{p}_j$, $\mathbf{R}_j$ and $\mathbf{s}_j$ are, respectively, the electron linear momentum, position and spin operators. We have already encountered these two terms in the limit of large E where they are the source of the contribution to scattering by orbital angular momentum $\mathbf{L} = (\mathbf{R} \times \mathbf{p})$ [26]. Taken together with the Thomson contribution to the scattering length and the limit of small E, the terms in question produce the Rayleigh limit of the cross-section, while the one term that admits an energy resonance gives in this condition the Kramers-Heisenberg dispersion formula. Here we are interested in the energy resonance and its influence on Bragg diffraction, which is a strictly elastic scattering process.

Let us label the virtual intermediate states by the quantum number η. Unlike the initial and final states of the crystal, intermediate states are not from the equilibrium configuration of the crystal and they decay on a timescale $\sim \hbar/\Gamma$ where Γ is the total width of the resonance. The resonant contribution to the scattering length for Bragg diffraction is,

$$f = -\left(\frac{r_e}{m_e}\right) \sum_{\eta(\Delta)} \frac{\langle\{\boldsymbol{\varepsilon}' \cdot \mathbf{J}(-\mathbf{q}')|\eta\rangle\langle\eta|\boldsymbol{\varepsilon} \cdot \mathbf{J}(\mathbf{q})\}\rangle}{E - \Delta + \mathrm{i}\Gamma/2} \quad , \tag{62}$$

where the sum of intermediate states is limited to those that contribute at the resonance energy Δ. Of course, Δ and Γ have a dependence on the intermediate states but this dependence is weak in some cases and the energy profile is observed to be that expected for a single oscillator like (62). Notice that one required the mean value of the operators in the numerator of f to describe Bragg diffraction.

To proceed with an atomic-model calculation of the scattering length, in the current operators $\mathbf{J}(\mathbf{q})$ and $\mathbf{J}(\mathbf{q}')$ sums over the electrons are partitioned into sums over unit cells, and sums over the ions in the cells that participate in resonance scattering. The corresponding wavefunctions for the electrons are defined only to within an arbitrary phase factor that is different for each ion. Moreover, the mean value denoted in (62) by angular brackets $\langle \ldots \rangle$ must incorporate an average over these phases, and all other degenerate variables associated with the equilibrium state of the crystal. The average of an individual phase factor is zero and thus cross-terms in the product of $\mathbf{J}(-\mathbf{q}')$ and $\mathbf{J}(\mathbf{q})$ are zero after the averaging. In consequence, the numerator in (62) is a

single sum over ions in unit cells, the electrons associated with the ions, and the spatial phase factors from the current operators are $e^{-i\mathbf{d}\cdot\mathbf{q}'}e^{i\mathbf{d}\cdot\mathbf{q}} = e^{i\mathbf{d}\cdot\mathbf{k}}$.

With the reduction of the numerator to a single sum over resonant ions we can focus on the matrix elements of $\mathbf{J}(\mathbf{q})$ and $\mathbf{J}(\mathbf{q}')$. For example, after expanding $\mathbf{J}(\mathbf{q})$ to the first order in $\mathbf{q}$ [51],

$$\langle\eta|\boldsymbol{\varepsilon}\cdot\mathbf{J}(\mathbf{q})|\mu\rangle = (im_e\Delta)\sum_j\langle\eta|\boldsymbol{\varepsilon}\cdot\mathbf{R}_j(1+\frac{i}{2}\mathbf{q}\cdot\mathbf{R}_j)|\mu\rangle$$
$$+ \quad \left(\frac{i}{2}\right)\langle\eta|(\mathbf{q}\times\boldsymbol{\varepsilon})\cdot(\mathbf{L}+2\mathbf{S})|\mu\rangle \ , \tag{63}$$

where $\Delta = E_\eta - E_\mu$ is the energy of the resonance. The first contribution on the right-hand side is the sum of E1 and E2 processes, and the second contribution is magnetic and it includes a matrix element of the magnetic moment $\mathbf{L}+2\mathbf{S}$. The relative magnitudes of the magnetic and E1 contributions is of the order μ_B/ea_0, where μ_B and a_0 are the Bohr magneton and the Bohr radius, and the ratio $\mu_B/ea_0 = \alpha/2$ which leads us to expect that the E1 process is the dominant one. On the other hand, the magnitudes of E2 and magnetic processes can be similar although evidence in the x-ray region is that the E2 process is the most significant. Similarly, in the x-ray region E1-E2 interference is more significant than the E1-magnetic interference process. Our calculation of resonant x-ray Bragg diffraction will therefore be based on the E1 and E2 processes in (63), and this section deals with parity-even events that are pure E1 or pure E2.

An additional assumption is to neglect in the numerator of (62) its dependence on the projection $\bar{M}$ of the angular momentum of the core state, $\bar{J}$ [52,53]. The assumption is valid in the absence of an interaction between the core state and the photo-ejected electron, and the absence of a significant exchange coupling of the core and valence states. An energy profile that is very different from a single Lorentzian shape, which is expected for a single oscillator, would suggest that the assumed degeneracy with respect to $\bar{M}$ is not good [54–56]. The assumption that we make is equivalent to the fast-collision approximation used by Hannon et al.(1988) and Luo et al.(1993) [57]; see also Carra and Thole [58].

We start with a calculation that is appropriate for the E1-E1 event, and we write the resonant x-ray scattering length as,

$$f = -\left(\frac{2\pi e}{\lambda}\right)^2 \frac{Z(\mathrm{E1})}{E - \Delta_1 + \mathrm{i}\Gamma_1/2} \ , \tag{64}$$

with,

$$Z(\mathrm{E1}) = \sum_{\mathbf{d}} \mathrm{e}^{\mathbf{ik}\cdot\mathbf{d}} \sum_{\eta(\Delta)} \langle \sum_{j(\mathbf{d})} \{\boldsymbol{\varepsilon}' \cdot \mathbf{R}_j|\eta\rangle\langle\eta|\boldsymbol{\varepsilon} \cdot \mathbf{R}_j\}\rangle \ . \tag{65}$$

The prefactor in (64) is obtained by equating Δ with the x-ray energy $E = \hbar cq = 2\pi\hbar c/\lambda$. Since $Z(\mathrm{E1})$ is a scalar quantity, the right-hand side of (65) can be written as a scalar product of a spherical tensor,

$$X^K_Q = \sum_{qq'} \varepsilon'_q \varepsilon_{q'} (1q1q'|KQ) \ , \tag{66}$$

and an atomic tensor $\langle T^K_Q\rangle_{\mathrm{E1}}$. The structure factor is [59],

$$F(\mathrm{E1}) = \sum_{KQ} (-1)^Q X^K_{-Q} \Psi^K_Q \ , \tag{67}$$

where, as in previous cases,

$$\Psi^K_Q = \sum_{\mathbf{d}} \mathrm{e}^{\mathbf{ik}\cdot\mathbf{d}} \langle T^K_Q\rangle_{\mathrm{E1},\mathbf{d}} \ , \tag{68}$$

and the sum on $\mathbf{d}$ is over all resonant ions in the unit cell. Because X^K_Q is constructed from two vector quantities the triangular condition gives $K = 0$, 1 and 2, and Table 3 contains specific values of X^K_Q that are required in calculations of dichroic signals and Bragg scattering amplitudes.

We will not include in $\langle T^K_Q\rangle_{\mathrm{E1}}$ some reduced matrix elements and, also, the E1 radial integral $\langle l|R|\bar{l}\rangle$ that will depend on the orbitals of the valence and core states labelled here by their angular momentum l and $\bar{l}$, respectively. Our choice gives,

$$\sum_{\eta(\Delta)} \langle \sum_{j(\mathbf{d})} \{\boldsymbol{\varepsilon}' \cdot \mathbf{R}_j|\eta\rangle\langle\eta|\boldsymbol{\varepsilon} \cdot \mathbf{R}_j\}\rangle = (l\|C(1)\|\bar{l})(\bar{l}\|C(1)\|l)\langle l|R|\bar{l}\rangle^2 \times \sum_{KQ} (-1)^Q X^K_{-Q} \langle T^K_Q\rangle_{\mathrm{E1},\mathbf{d}} \ , \tag{69}$$

Table 3
Properties of X^K_Q

The tensor X^K_Q is defined in (66).
$X^K_{-Q} = (-1)^{K+Q}(X^K_Q)^*$
$\mathbf{X}^1 = \frac{\mathrm{i}}{\sqrt{2}}(\boldsymbol{\epsilon}' \times \boldsymbol{\epsilon})$, $X^2_{+2} = \varepsilon'_{+1}\varepsilon_{+1}$

$\begin{bmatrix} (\mathbf{X}^1)_{\mathrm{av}} = -\hat{\mathbf{q}}P_2/\sqrt{2} \\ (X^2_{+2})_{\mathrm{av}} = \frac{(P_3+\mathrm{i}P_1)}{4} \end{bmatrix}$ $\mathbf{q} = \mathbf{q}'$ and averages over polarization described by a Stokes vector (P_1, P_2, P_3).

For the scattering geometry depicted in Fig. 3 the non-zero elements are:

$$(\sigma'\sigma)$$
$X^0_0 = -\frac{1}{\sqrt{3}}$, $X^2_0 = \left(\frac{2}{3}\right)^{1/2}$

$$(\pi'\pi)$$
$X^0_0 = -\frac{1}{\sqrt{3}}\cos(2\theta)$, $X^1_0 = \frac{\mathrm{i}}{\sqrt{2}}\sin(2\theta)$
$X^2_0 = -\frac{1}{\sqrt{6}}\cos(2\theta)$, $X^2_{+2} = \frac{1}{2}$

$$(\pi'\sigma)$$
$X^1_{+1} = -\frac{1}{2}\mathrm{e}^{-\mathrm{i}\theta}$, $X^2_{+1} = -\frac{1}{2}\mathrm{e}^{-\mathrm{i}\theta}$

$$(\sigma'\pi)$$
$X^1_{+1} = \frac{1}{2}\mathrm{e}^{\mathrm{i}\theta}$, $X^2_{+1} = -\frac{1}{2}\mathrm{e}^{\mathrm{i}\theta}$

and,

$$Z(\mathrm{E1}) = (l\|C(1)\|\bar{l})(\bar{l}\|C(1)\|l)\langle l|R|\bar{l}\rangle^2 F(\mathrm{E1}) \ . \tag{70}$$

Here the reduced matrix element of the normalized spherical harmonic is [16,17],

$$(l\|C(t)\|\bar{l}) = (-1)^l\{(2l+1)(2\bar{l}+1)\}^{1/2}\begin{pmatrix} l & t & \bar{l} \\ 0 & 0 & 0 \end{pmatrix} \ , \tag{71}$$

and it is different from zero when $l+t+\bar{l}$ is an even integer, and t satisfies the triangular condition $|l-\bar{l}| \le t \le l+\bar{l}$. The mean value $\langle T^K_Q\rangle_{\mathrm{E1}}$ is constructed from matrix elements,

$$\langle JM|(T^K_Q)_{\mathrm{E1}}|J'M'\rangle = (-1)^{J-M}\begin{pmatrix} J & K & J' \\ -M & Q & M' \end{pmatrix}(J\|T^K(\mathrm{E1})\|J') \ , \tag{72}$$

in which the reduced matrix element is related to the unit tensor $W^{(ab)K}$ [17]. A general expression is [59],

$$(J\|T^K(\mathrm{Et})\|J') = \mp(2\bar{J}+1)\sum_{ab}(-1)^b(2a+1)(2b+1)W^{(ab)K}$$
$$\times \quad \left\{\begin{matrix} \frac{1}{2} & \bar{l} & \bar{J} \\ \bar{l} & \frac{1}{2} & a \end{matrix}\right\} \left\{\begin{matrix} t & \bar{l} & l \\ t & \bar{l} & l \\ K & a & b \end{matrix}\right\} \ , \tag{73}$$

and the reduced matrix element in (72) is obtained from (73) by setting $t = 1$. The sign in the front of (73) relates to the total angular momentum of the core state $\bar{J} = \bar{l} \pm 1/2$ and the factor is $(-1)^{1/2+\bar{l}+\bar{J}}$. In the double sum a takes two values, $a = 0$ and 1. Since the $9j$-symbol contains two identical rows it vanishes if $K + a + b$ is an odd integer [16,17]. The reduced matrix element defined by (73) clearly depends on $\bar{J}$, and through $W^{(ab)K}$ it depends on all the quantum numbers for the valence states $|JM\rangle = |\nu SLJM\rangle$ and $|J'M'\rangle = |\nu' S'L'J'M'\rangle$ except the projections M and M' that are factored out in the Wigner–Eckart theorem (72). A derivation of (73) is discussed in appendix E.

A pure E2 event might be visible in the energy profile at an energy Δ_2 that is usually less than Δ_1. At this juncture, the reader can usefully visit Fig. 5. With the assumption that we make, the contribution to the scattering length has the form shown in (64) with a resonance energy and total width Δ_2 and Γ_2, respectively. The numerator $Z(\mathrm{E2})$ is found to be,

$$Z(\mathrm{E2}) = \frac{1}{6}\{q(l\|C(2)\|\bar{l})\langle l|R^2|\bar{l}\rangle\}^2 F(\mathrm{E2}) \ , \tag{74}$$

in which the structure factor is a scalar product of H^K_Q that describes the polarization and directions of the primary and secondary x-ray beams, and Ψ^K_Q modelled on (68) but with an atomic tensor $\langle T^K_Q\rangle_{\mathrm{E2}}$. We find,

$$F(\mathrm{E2}) = \sum_{KQ}(-1)^{K+Q} H^K_{-Q}\Psi^K_Q \ , \tag{75}$$

$$\Psi^K_Q = \sum_{\mathbf{d}} \mathrm{e}^{\mathbf{i}\mathbf{k}\cdot\mathbf{d}}\langle T^K_Q\rangle_{\mathrm{E2},\mathbf{d}} \ , \tag{76}$$

and the mean value $\langle T^K_Q\rangle_{\mathrm{E2}}$ is obtained with matrix elements that satisfy the Wigner–Eckart theorem and a reduced matrix element (73) evaluated with $t = 2$. The definition of H^K_Q is [60–62],

$$H^K_Q = \sum_{qq'} h(q)h'(q')(2q2q'|KQ) \ , \tag{77}$$

Table 4
Properties of H_Q^K

The tensor H_Q^K is defined in (77) and (78).

$H_{-Q}^K = (-1)^{K+Q}(H_Q^K)^*$

$\mathbf{H}^1 = \left(\frac{\mathrm{i}}{2\sqrt{10}}\right)\{(\boldsymbol{\varepsilon}'\cdot\boldsymbol{\varepsilon})(\hat{\mathbf{q}}'\times\hat{\mathbf{q}}) + (\hat{\mathbf{q}}'\cdot\hat{\mathbf{q}})(\boldsymbol{\varepsilon}'\times\boldsymbol{\varepsilon})$
$+(\boldsymbol{\varepsilon}'\cdot\hat{\mathbf{q}})(\hat{\mathbf{q}}'\times\boldsymbol{\varepsilon}) + (\boldsymbol{\varepsilon}\cdot\hat{\mathbf{q}}')(\boldsymbol{\varepsilon}'\times\hat{\mathbf{q}}')\}$

For $\mathbf{q}=\mathbf{q}'$, $\mathbf{H}^1 = \left(\frac{\mathrm{i}}{2\sqrt{10}}\right)(\boldsymbol{\varepsilon}'\times\boldsymbol{\varepsilon}) = \left(\frac{1}{2\sqrt{5}}\right)\mathbf{X}^1$

For the scattering geometry depicted in Fig. 3 the non-zero elements are:

$$(\sigma'\sigma)$$

$H_0^0 = \frac{1}{2\sqrt{5}}\cos(2\theta)$, $H_0^1 = \frac{\mathrm{i}}{2\sqrt{10}}\sin(2\theta)$

$H_0^2 = -\frac{1}{2\sqrt{14}}\cos(2\theta)$, $H_{+2}^2 = \frac{1}{4}\left(\frac{3}{7}\right)^{1/2}$

$H_0^3 = \frac{-\mathrm{i}}{\sqrt{10}}\sin(2\theta)$, $H_0^4 = -\left(\frac{2}{35}\right)^{1/2}\cos(2\theta)$

$H_{+2}^4 = -\frac{1}{2\sqrt{7}}$.

$$(\pi'\sigma)$$

$H_{+1}^1 = -\frac{1}{4\sqrt{5}}\mathrm{e}^{-3\mathrm{i}\theta}$, $H_{+1}^2 = \frac{1}{4}\left(\frac{3}{7}\right)^{1/2}\mathrm{e}^{-3\mathrm{i}\theta}$

$H_{+1}^3 = -\frac{1}{4}\left(\frac{3}{10}\right)^{1/2}\mathrm{e}^{-3\mathrm{i}\theta}$, $H_{+3}^3 = \frac{-1}{4\sqrt{2}}\mathrm{e}^{-\mathrm{i}\theta}$

$H_{+1}^4 = \frac{1}{4\sqrt{14}}\mathrm{e}^{-3\mathrm{i}\theta}$, $H_{+3}^4 = \frac{1}{4\sqrt{2}}\mathrm{e}^{-\mathrm{i}\theta}$

$$(\sigma'\pi)$$

$H_Q^K(\sigma'\pi) = (-1)^K(H_Q^K(\pi'\sigma))^*$

$$(\pi'\pi)$$

$H_0^0 = \frac{1}{2\sqrt{5}}\cos(4\theta)$, $H_0^1 = \frac{\mathrm{i}}{\sqrt{10}}\sin(4\theta)$

$H_0^2 = \frac{1}{\sqrt{14}}\cos(4\theta)$, $H_0^3 = \frac{\mathrm{i}}{2\sqrt{10}}\sin(4\theta)$

$H_0^4 = \frac{1}{2\sqrt{70}}\cos(4\theta)$, $H_{+4}^4 = -\frac{1}{4}$

Note: the rule to obtain $H_Q^K(\sigma'\pi)$ from $H_Q^K(\pi'\sigma)$ is also obeyed by $X_Q^K(\sigma'\pi)$ and $X_Q^K(\pi'\sigma)$.

where $h(q)$ and $h'(q)$ are, respectively, $\boldsymbol{\varepsilon}$ and $\hat{\mathbf{q}}$, and $\boldsymbol{\varepsilon}'$ and $\hat{\mathbf{q}}'$ coupled to give tensors of rank 2, namely,

$$h(q) = \sum_{pp'} \varepsilon_p \hat{q}_{p'}(1p1p'|2q) \ , \tag{78}$$

and the corresponding expression for $h'(q)$. Various properties of H_Q^K are gathered in Table 4.

Here we can note an alternative expression for H_Q^K in terms of X_Q^K defined by (66) and Π_Q^K also defined by (66) but with $\hat{\mathbf{q}}$ and $\hat{\mathbf{q}}'$ replacing $\boldsymbol{\varepsilon}$ and $\boldsymbol{\varepsilon}'$.

The expression is,

$$H_Q^K = 5(-1)^K \sum_{lm} \Pi_m^l \sum_{K'Q'} X_{Q'}^{K'} \{(2l+1)(2K'+1)\}^{1/2}$$
$$\times \quad (lmK'Q'|KQ) \begin{Bmatrix} l & K' & K \\ 1 & 1 & 2 \\ 1 & 1 & 2 \end{Bmatrix} , \tag{79}$$

in which the $9j$-symbol can only be different from zero when $l + K' + K$ is an even integer [16,17]. One use of (79) is to identify contributions to the E2 channel that are sensitive to time-odd (magnetic) properties of electrons in the crystal. Contributions with this property are antisymmetric with respect to the crossing transformation [51] which includes the exchanges $\boldsymbol{\varepsilon}' \longleftrightarrow \boldsymbol{\varepsilon}$ and $\mathbf{q} \longleftrightarrow \mathbf{q}'$. Terms in (79) with $l = 0, 2$ or $K' = 0, 2$ are unchanged by crossing while terms with $l = 1$ or $K' = 1$ change their sign. We conclude that parts of H_Q^K that have odd integer values of $l + K'$ are time-odd and thus sensitive to magnetism. Since $l + K' + K$ must be an even integer one finally concludes that contributions in question have odd K, i.e. time-odd contributions to the scattering in the pure E2 channel can appear with H_Q^1 and H_Q^3 only. In general, parity-even events, such as pure E1 and pure E2, possess a one to one correspondence between the rank of a tensor and its magnetic character, which is that odd (even) rank tensors are time-odd (even). This correspondence is embodied in the relation (48) for parity-even tensors, and it says that odd rank tensors change sign when the polarity of the local magnetic field is reversed, whereas even rank tensors do not change sign when the field is reversed. (The one to one correspondence we discuss here does not hold in parity-odd events, examples of which are found in section 7.) In conclusion, for the pure E1 and pure E2 channels tensors of odd rank are absent in the unit-cell structure factor when there is no magnetic order in the material, i.e. no applied magnetic field nor a spontaneous long-range magnetic order.

5.3 Reduced matrix-elements

Prior to considering examples of the framework for parity-even resonant Bragg diffraction, just described, we pause to make some comments about the reduced matrix element defined by (73). First, let us note that it reproduces the familiar sum-rules which are used to analyse dichroic signals [63–66]. Actual expressions for the sum rules are derived from (73) by taking $\bar{J} = \bar{l} - 1/2$ or $\bar{J} = \bar{l} + 1/2$, and $t = 1$ and $t = 2$ for E1 and E2, respectively. Sum rules for linear and circular dichroism in an E1 event are found in (97) and (99). For specific values of a, b and K the unit tensor $W^{(ab)K}$ can be correlated with particular operators built from $\mathbf{R}$, $\mathbf{S}$ and $\mathbf{L}$. Here, we mention a few cases for illustration using a tilde to denote the identification; $\langle \mathbf{S} \rangle \sim W^{(10)1}$,

$\langle \mathbf{L} \rangle \sim W^{(01)1}$, $\langle 3\mathbf{R}(\mathbf{R}\cdot\mathbf{S}) - \mathbf{S} \rangle \sim W^{(12)1}$, $\langle 3L_z^2 - L(L+1) \rangle \sim W^{(02)2}$, and $W^{(03)3}$ is identified in (40) with an orbital octupole. Additional information about $W^{(ab)K}$ is found in appendix D.

The next point we make about (73) is its value when summed over the two absorption edges labelled by $\bar{J} = \bar{l} - 1/2$ and $\bar{J} = \bar{l} + 1/2$. One finds that the sum enforces $a = 0$ so there is no information to be obtained about spin angular momentum in the valence state of the resonant ion. The actual result is,

$$\sum_{\bar{J}} (J\|T^K(\mathrm{Et})\|J') = [2(2K+1)]^{1/2} W^{(0K)K} \begin{Bmatrix} t & K & t \\ l & \bar{l} & l \end{Bmatrix} . \tag{80}$$

This may be viewed as a concise statement of the sum rules for dichroic signals that were derived by Thole et al. [63].

An example of (80) which is of importance for resonant Bragg diffraction is obtained with $\bar{l} = 0$ which describes the K edge of the resonant ion. One finds for $\bar{l} = 0$, $\bar{J} = 1/2$ and $t = l$ the result [62],

$$(J\|T^K(\mathrm{Et})\|J') = (-1)^K \frac{\{2(2K+1)\}^{1/2}}{(2l+1)} W^{(0K)K} . \tag{81}$$

With applications of this result to 3d transition metal ions in mind, let us record the expression for a matrix element of T^K_Q between uncoupled states,

$$|SM_S LM_L\rangle = \sum_{JM} (SM_S LM_L|JM)|JM\rangle . \tag{82}$$

The Wigner–Eckart theorem applies separately to the spin, S, and orbital, L, states. However, with K-edge events only orbital angular momentum in the valence state is observed and a matrix element of T^K_Q is diagonal with respect to spin quantum numbers. For $\bar{l} = 0$ and $t = l$,

$$\begin{aligned} &\langle SM_S LM_L|(T^K_Q)_{\mathrm{Et}}|S'M'_S L'M'_L\rangle = \delta_{M_S,M'_S}\delta_{S,S'} \\ &\times \frac{(-1)^K}{(2l+1)} \left\{\frac{2}{2S+1}\right\}^{1/2} W^{(0K)} (-1)^{L-M_L} \begin{pmatrix} L & K & L' \\ -M & Q & M'_L \end{pmatrix} . \end{aligned} \tag{83}$$

Here, $W^{(0K)}$ is a unit tensor that is defined by the orbital properties of the valence shell with angular momentum l. The result (83) applied for $K = 1, 2$ and 3 leads to expressions for $\langle T^K_Q \rangle_{\mathrm{Et}}$ in terms of $\langle \mathbf{L} \rangle$, $\langle \mathbf{Q} \rangle$ and $\langle \mathbf{\Lambda} \rangle$ where the quadrupole is defined in terms of the operator $\{3l_0^2 - l(l+1)\}/2$ and the octupole operator is defined by (39). Straightforward calculations show that,

$$\langle T^1_q\rangle_{\rm Et} = \frac{-\sqrt{3}}{(2l+1)(l\|l\|l)}\langle L_q\rangle \ , \tag{84}$$

$$\langle T^2_q\rangle_{\rm Et} = \frac{2\sqrt{5}\langle Q_q\rangle}{(2l+1)(l\|l\|l)\{(2l-1)(2l+3)\}^{1/2}} \ , \tag{85}$$

$$\langle T^3_q\rangle_{\rm Et} = \frac{-2\sqrt{7}\langle \Lambda_q\rangle}{(2l+1)(l\|l\|l)\{(l-1)(2l-1)(l+2)(2l+3)\}^{1/2}} \ . \tag{86}$$

Recall that with absorption at the K-edge of the resonant ion, which is under discussion at the moment, $t = l$ and for a 3d ion the process is an E2 event. Data for V_2O_3 displayed in Fig. 5 provides one example of (resonant) Bragg diffraction enhanced in an E2 event, and an analysis of the observations evidently yields direct information on the orbital angular momentum in the vanadium 3d valence shell [37].

6 Azimuthal-angle scans

We see in Fig. 5 that the Bragg intensity can vary as the crystal is rotated about the Bragg wavevector $\boldsymbol{\tau}(hkl)$ in an azimuthal-angle scan. The variation is directly related to the angular anisotropy in the valence shell that accommodates the photo-ejected electron, provided the x-ray beam illuminates a single domain within the crystal. Observations, like the ones reported in Fig. 5, thus provide valuable insight to the ordering of the charge and orbital degrees of freedom in the valence shell [9,10,37,58,67,68]. In this section we illustrate how the intensity as a function of the azimuthal angle can be calculated, using an atomic model.

In every case, the first task is to calculate Ψ^K_Q which is the sum over all resonant ions in an unit cell of the atomic tensors multiplied by spatial phase factors $e^{i\mathbf{k}\cdot\mathbf{d}}$. Results for Ψ^K_Q that are appropriate for Dy ions in DyB_2C_2 and vanadium ions in V_2O_3 can be found in sections 2 and 3, respectively. We consider three more examples of the calculation to obtain Ψ^K_Q and the selection rules on K and Q, and in each example go on to calculate the dependence of the structure factor on the azimuthal angle.

6.1 Tetragonal structure

The tetragonal space-group P4/mbm with ions at sites 4(g) is an appropriate description of lanthanide ions in tetraborides [45,69]. Figure 6 illustrates the positions of the four ions in a unit cell which we label 1 to 4; $\mathbf{d}_1 = (x, \frac{1}{2}+x, 0)$, $\mathbf{d}_2 = (-x, \frac{1}{2}-x, 0)$, $\mathbf{d}_3 = (\frac{1}{2}-x, x, 0)$ and $\mathbf{d}_4 = (\frac{1}{2}+x, -x, 0)$ where in GdB_4 $x = 0.31746(2)$. Let $\varphi = 2\pi x$. For a Bragg wavevector $\boldsymbol{\tau} = (h00)$ one finds,

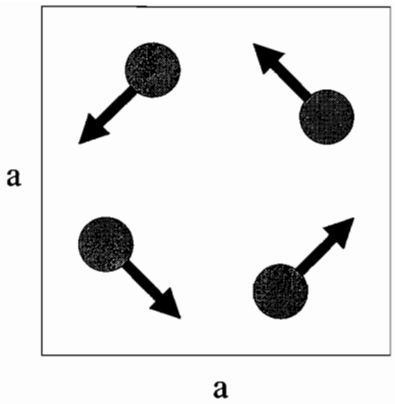

Fig. 6. Projection in the *ab*-plane of the tetragonal unit cell of the material GdB_4 showing the positions of the Gd atoms and their moments in the magnetic space group P4/m′b′m′ [45,69].

$$\Psi_Q^K = \sum_{\mathbf{d}} \mathrm{e}^{\mathrm{i}\boldsymbol{\tau}\cdot\mathbf{d}} \langle T_Q^K \rangle_{\mathbf{d}} = \\ = \mathrm{e}^{\mathrm{i}\varphi h} \langle T_Q^K \rangle_1 + \mathrm{e}^{-\mathrm{i}\varphi h} \langle T_Q^K \rangle_2 + (-1)^h \{ \mathrm{e}^{-\mathrm{i}\varphi h} \langle T_Q^K \rangle_3 + \mathrm{e}^{\mathrm{i}\varphi h} \langle T_Q^K \rangle_4 \} \ . \quad (87)$$

In this expression, $\langle T_Q^K \rangle$ is an atomic tensor that is appropriate for an E1 or an E2 event. (Alternatively, it could be a tensor that describes Thomson scattering (section 2), magnetic x-ray scattering (section 3), or magnetic neutron scattering (section 4) by ions at sites 4(g).)

The environments centred on sites 2, 3 and 4 are related to the environment at site 1 by rotations about the *c*-axis. Such a rotation applied to $\langle T_Q^K \rangle$ multiplies it by the phase factor $\mathrm{e}^{\mathrm{i}Q\beta}$ where β is the angle of rotation. From the symmetry operations of the space group one finds, $\langle T_Q^K \rangle_2 = \mathrm{e}^{\mathrm{i}Q\pi} \langle T_Q^K \rangle_1$, $\langle T_Q^K \rangle_3 = \mathrm{e}^{\mathrm{i}Q\pi/2} \langle T_Q^K \rangle_1$, and $\langle T_Q^K \rangle_4 = \mathrm{e}^{-\mathrm{i}Q\pi/2} \langle T_Q^K \rangle_1$ Using this information in (87) one gets,

$$\Psi_Q^K = \langle T_Q^K \rangle_1 \{ \mathrm{e}^{\mathrm{i}\varphi h} + (-1)^Q \mathrm{e}^{-\mathrm{i}\varphi h} \} \{ 1 + (-1)^h \mathrm{e}^{-\mathrm{i}Q\pi/2} \} \ . \quad (88)$$

Space-group forbidden reflections $h = 2n + 1$ have the property $\Psi_0^K = 0$. A necessary condition to have Ψ_Q^K different from zero and odd h is $Q = 2(2m+1)$. The point group for sites 4(g) places an additional constraint on $\langle T_Q^K \rangle$, as we will see.

The four ions lie in a plane that is a mirror plane of symmetry normal to the *c*-axis. For parity-even tensors, such a mirror plane is equivalent to a diad parallel to the *c*-axis and this symmetry operation is satisfied by even Q. Hence, the mirror plane does not impose an additional condition on Q. The remaining symmetry operations in the point group are diads parallel to $\mathbf{a} \pm \mathbf{b}$. To understand what conditions these put on $\langle T_Q^K \rangle$ we rotate the tensor by $\pi/4$ about the *c*-axis and then apply rotations by π about the new x- and y-axes. These operations should leave $\langle T_Q^K \rangle$ unchanged. Rotation by π about the x-

axis (y-axis) changes Q to $-Q$ and multiplies the tensor by $(-1)^K((-1)^{K+Q})$. The phase factors are unity because Q is even, as we have already established, and K is even for pure charge scattering on account of the identity (48). Hence, diads parallel to $\mathbf{a} \pm \mathbf{b}$ are satisfied provided that,

$$e^{iQ\pi/4}\langle T_Q^K\rangle = e^{-iQ\pi/4}\langle T_{-Q}^K\rangle \ , \tag{89}$$

and this can be written in the form,

$$\langle T_{-Q}^K\rangle = e^{iQ\pi/2}\langle T_Q^K\rangle = \langle T_Q^K\rangle^* \ , \tag{90}$$

where the second equality arises from the general relation $\langle T_Q^K\rangle^* = (-1)^Q\langle T_{-Q}^K\rangle$. Since for odd h Ψ_Q^K is different from zero for $Q = 2(2m+1)$ we conclude that diads along $\mathbf{a} \pm \mathbf{b}$ are satisfied by $\langle T_Q^K\rangle^* = -\langle T_Q^K\rangle$, i.e. $\langle T_Q^K\rangle$ is purely imaginary.

Let us assume that the ion at site 1 possesses a magnetic moment that lies in the **a**-**b** plane, and the moment direction is $(1, 1, 0)$. The symmetry operations that relate environments at sites 2, 3 and 4 to the environment at site 1 generate a non-collinear motif of moments in which $\boldsymbol{\mu}_2 = -\boldsymbol{\mu}_1$ and $\boldsymbol{\mu}_4 = -\boldsymbol{\mu}_3$. The motif depicted in Fig. 6 is described by the magnetic space-group P4/m′b′m′ and it allows the magnetoelectric effect.

Let us address the calculation of the structure factor F for resonant Bragg diffraction. Our labelling of axes and polarization is set out in Fig. 3. We require $\boldsymbol{\tau}(hkl)$ parallel with $-x$. In the present example, a tetragonal crystal, the basis vectors for $\boldsymbol{\tau}$ are parallel to the crystal axes (abc), and the chosen $\boldsymbol{\tau}$ is parallel to the a-axis. Thus, $\boldsymbol{\tau}(h00)$ is parallel with $-x$ after rotating the crystal by π about the c-axis, and this rotation takes Ψ_Q^K to $(-1)^Q\Psi_Q^K$.

An azimuthal-angle scan is the rotation of the crystal about $\boldsymbol{\tau}$. We define the rotation by ψ about the x-axis in terms of the rotation matrix, introduced in (60) and also discussed in appendix A. The rotation described changes $(-1)^Q\Psi_Q^K$ to,

$$e^{iQ\pi/2}\sum_{Q'} e^{-iQ'\pi/2} d_{Q'Q}^K(-\psi)\{(-1)^{Q'}\Psi_{Q'}^K\} \ , \tag{91}$$

where $d_{Q'Q}^K(-\psi)$ is a real function. These functions satisfy many symmetries, and two are $d_{Q'Q}^K(-\psi) = d_{QQ'}^K(\psi) = (-1)^{Q+Q'}d_{Q'Q}^K(\psi)$. Also, $d_{Q'Q}^K(0) = \delta_{Q',Q}$ so the operation (91) satisfies the obvious requirement that for $\psi = 0$ the crystal is at its original orientation, with the c-axis parallel to σ-polarization and normal to the plane of scattering.

Structure factors for E1 and E2 events are defined by (67) and (75). Let us consider an E1 event, and we refer to Table 3 for elements of X^K_Q. For pure charge scattering and parity-even atomic tensors, the rank K must be an even integer and for an E1 event the possibilities are $K = 0$ and $K = 2$. The projection Q satisfies $-K \leq Q \leq K$, and $Q = 0$ for $K = 0$. With odd h $\Psi^K_0 = 0$ and we find for an E1 event that charge scattering arises from $K = 2$ for which the allowed projections are $Q = \pm 2$. Using this information in (91) it becomes,

$$-4\cos(\varphi h)\mathrm{e}^{\mathrm{i}Q\pi/2}\langle T^2_{+2}\rangle_{\mathrm{E1}}\{d^2_{2,Q}(-\psi) - d^2_{-2,Q}(-\psi)\} \ , \tag{92}$$

where we have also used $\langle T^2_{+2}\rangle_{\mathrm{E1}} = -\langle T^2_{-2}\rangle_{\mathrm{E1}}$. To obtain F we multiply (92) by $(-1)^Q X^2_{-Q}$ and sum over Q. In the $(\sigma'\sigma)$ channel there is one X^2_Q different from zero and it has $Q = 0$. Because $d^K_{Q'Q}(\psi) = (-1)^{Q+Q'} d^K_{-Q'-Q}(\psi)$ the expression (92) is zero for $Q = 0$, and thus we have the result $F_{\sigma'\sigma}(\mathrm{E1}) = 0$.

In the $(\pi'\sigma)$ channel the non-zero X^2_Q have $Q = \pm 1$. The structure factor is,

$$\begin{aligned} F_{\pi'\sigma}(\mathrm{E1}) &= -4\cos(\varphi h)\langle T^2_{+2}\rangle_{\mathrm{E1}} \sum_Q (-1)^Q X^2_{-Q}\mathrm{e}^{\mathrm{i}Q\pi/2}\{d^2_{2,Q}(-\psi) - d^2_{-2,Q}(-\psi)\} \\ &= 4\mathrm{i}\cos\theta\cos(\varphi h)\sin\psi\langle T^2_{+2}\rangle_{\mathrm{E1}} \ , \end{aligned} \tag{93}$$

and the structure factor is purely real because $\langle T^2_{+2}\rangle_{\mathrm{E1}}$ is purely imaginary. Using (14) to relate the atomic tensor to a Cartesian tensor, one can replace the atomic tensor in $F_{\pi'\sigma}(\mathrm{E1})$ by the xy component of a Cartesian tensor of rank 2.

Furthermore, we can use (73) to calculate $\langle T^2_Q\rangle_{\mathrm{E1}}$, and to express it in terms of more familiar operators that contain the unit tensors $W^{(02)2}$, $W^{(11)2}$ and $W^{(13)2}$. In fact, let us define the diagonal components of three operators of rank 2 which correspond to these unit tensors, namely [70],

$$Q = \frac{1}{2}\sum_j \{3l_0^2 - l(l+1)\}_j \ , \tag{94}$$

$$P = \frac{1}{2}\sum_j \{3s_0 l_0 - \mathbf{s}\cdot\mathbf{l}\}_j \ , \tag{95}$$

$$R = -\frac{1}{2}\sum_j \{(2l(l+1)+1)s_0 l_0 + (l(l+1)-2)\mathbf{s}\cdot\mathbf{l} - 5l_0(\mathbf{s}\cdot\mathbf{l})l_0\}_j \ . \tag{96}$$

Here, l_0 is the spherical component l_q of the angular momentum operator that has $q = 0$, and similarly for the spin s_0. The result (73) shows us that,

$$\langle \mathbf{T}^2\rangle_{\mathrm{E1}} \propto (2\bar{J}+1)\langle \mathbf{Q}\rangle \pm \frac{4}{5}[(l-1)(2l-1)\langle \mathbf{P}\rangle + 3\langle \mathbf{R}\rangle] \ , \tag{97}$$

where the signs are related to the total angular momentum of the core level $\bar{J} = \bar{l} \pm \frac{1}{2}$, and the coefficient of proportionality depends on the angular momentum of the valence shell, l.

We move next to the contribution to diffraction by the magnetic moments depicted in Fig. 6 and described by the magnetic space group (Shubnikov group) P4/m'b'm'. In an E1 event magnetic diffraction involves tensors of rank $K = 1$. Looking at Table 3, the channels $(\pi'\pi)$ and $(\pi'\sigma)$ allow this diffraction and it is forbidden in $(\sigma'\sigma)$. Because the magnetic moments lie in the **a**-**b** plane the projection $Q = \pm 1$, since $\langle T^1_0 \rangle$ is the component parallel to the c-axis. The contribution to $F_{\pi'\sigma}(\mathrm{E1})$ made by the magnetic moments is proportional, to $\langle T^1_{-1} - T^1_{+1} \rangle_1 = \sqrt{2}\langle T^1_x \rangle_1 = \sqrt{2}\langle T^1_y \rangle_1$. The complete expression, including (93), is

$$\begin{aligned} F_{\pi'\sigma}(\mathrm{E1}) = & -2\sqrt{2}\cos\theta \sin(\varphi h)\cos\psi \langle T^1_x \rangle_{\mathrm{E1}} \\ & + \quad 4\mathrm{i}\cos\theta\cos(\varphi h)\sin\psi \langle T^2_{+2} \rangle_{\mathrm{E2}} \ . \end{aligned} \tag{98}$$

This expression is purely real, and the charge and magnetic contributions are not 90^o out of phase as is often the case. The absence of the phase shift is related to the possibility of a magnetoelectric effect from the material [71]. Bragg intensities are proportional to $|F_{\pi'\sigma}(\mathrm{E1})|^2$ and the dependence on ψ is non-trivial in the magnetically ordered phase. This finding has been confirmed for GdB_4 [45]. In addition, in (98) there is a non-trivial dependence on the Miller index h [45], although the charge and magnetic contribution share a $\cos\theta$ dependence on the Bragg angle θ.

The physical content of $\langle T^1_Q \rangle_{\mathrm{E1}}$ is derived from (73), just as we reported for $\langle T^2_Q \rangle_{\mathrm{E1}}$. For $\langle T^1_Q \rangle_{\mathrm{E1}}$ the analogue of (97) is,

$$\langle \mathbf{T}^1 \rangle_{\mathrm{E1}} \propto (2\bar{J}+1)\langle \mathbf{L} \rangle \pm \frac{4}{3}(l-1)[l\langle \mathbf{S} \rangle + (2l+3)\langle \mathbf{T} \rangle] \ . \tag{99}$$

Here, $\langle \mathbf{L} \rangle$ and $\langle \mathbf{S} \rangle$ are the orbital and spin moments in the valence shell, and $\langle \mathbf{T} \rangle$ is related to the unit tensor $W^{(12)1}$, and it is defined by,

$$T = -\sum_j \{3\hat{R}_0(\hat{\mathbf{R}} \cdot \mathbf{s} - s_0)\}_j \ , \tag{100}$$

where $\mathbf{R} = R\hat{\mathbf{R}}$.

It should be noted that (97) and (99) express sum rules for linear and circular dichroism in an E1 event [63,64]. The polarization factors associated with the absorption events are $(X^2_{\pm 2})_{\mathrm{av}}$ and $(\hat{\mathbf{q}} \cdot \mathbf{X}^1)_{\mathrm{av}}$, and those factors are found in Table 3. Further information about dichroic signals is found in section 8.

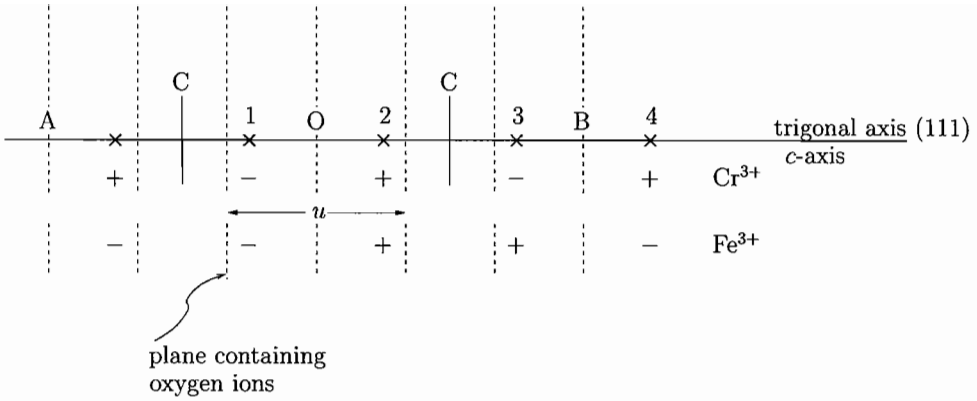

Fig. 7. A sketch of the rhombohedral cell for Cr_2O_3 and α-Fe_2O_3 [5]. Specific features are described in section 6.2

6.2 Corundum structure

The rhombohedral corundum structure, described by the space group $R\bar{3}c$, is appropriate for some 3d ion sesquioxides [41,43,71]. In hexagonal axes four ions occupy sites 12(c) that have point-group symmetry C_3 and lie on the c-axis, which is the trigonal (111). O in Fig. 7 [5] marks the centre of a rhombohedral cell and the distance AC=AB/4. Elements of symmetry in the cell include a diad at O parallel to $\mathbf{a}_h$ and normal to a mirror plane that contains the triad axis (c-axis), while the position C marks a centre of inversion symmetry. A 3d ion is octahedrally coordinated by oxygen ions that are contained in planes normal to the c-axis, and in Fig. 7 the planes are denoted by vertical lines. In Cr_2O_3 and α-Fe_2O_3 (haematite) the 3d ions are displaced from the oxygen planes, and their sites are not centres of inversion symmetry. Octahedra are joined in pairs and the triangular face which is common in a pair contains the position O and a diad axis.

Cr_2O_3 [71,72] undergoes a transition from a paramagnetic to an antiferromagnetic structure at 310 K. The Cr^{3+} moments align parallel to the c-axis. Ions with opposite moments are related by centres of inversion symmetry and by diad axes. In such a structure the charge and magnetic scattering are superimposed. Also, the two contributions are in phase in the structure factor, which is a situation encountered in the previous example of GdB_4 based on the magnetic space group P4/m′b′m′. The magnetic class of Cr_2O_3 is the same as the crystal class and it does not contain the element of time reversal. The motif of Cr moments breaks the time reversal symmetry and the inversion symmetry that are present in the paramagnetic phase, however, the product of the two symmetries is not changed by the onset of magnetic order. For the magnetoelectric effect to exist, the inversion can occur only paired with time reversal.

The motifs of magnetic moments in haematite and Cr_2O_3 are different [5,71].

In particular, signatures in the motifs are $++--$ (haematite) and $+-+-$ (Cr_2O_3) and they are illustrated in Fig. 7. In consequence, the crystals have very different properties. Haematite is not magnetoelectric and it displays weak ferromagnetism in a temperature interval from $T_N = 950$ K down to the Morin temperature $T_M = 260$ K, below which the Fe moments are parallel to the c-axis. Between T_N and T_M Fe moments are perpendicular to the triad axis and the magnetic symmetry is reduced to 2/m. Hence, unlike Cr_2O_3, the magnetic class of haematite is not the same as the crystal class and it contains time reversal as a separate symmetry. Weak ferromagnetism (pyromagnetism) caused by an antisymmetric exchange interaction of Dzyaloshinsky-Moriya [73], is prohibited in Cr_2O_3, and haematite taken below T_M. For, any departure of the magnetic moments from the c-axis lowers the symmetry of the crystal, since the c-axis is then no longer a triad axis. The ferromagnetic moment in haematite is parallel to a diad axis and normal to a mirror plane of symmetry, yielding a magnetic symmetry 2/m already mentioned. The ferromagnetic component along $\mathbf{a}_h$, say, is the same for every Fe ion and it is not changed by a rotation about $\mathbf{a}_h$, which is an operation applied in the calculation of Ψ_Q^K that we next describe.

The four 3d ions in a cell are numbered 1 to 4. Their positions are defined in Fig. 7, and we will use O as the origin. Let $\varphi = -\pi u$, where $u = 2z - \frac{1}{2} = 0.1952$ for Cr_2O_3. The distance OB=AB/2, and for $\boldsymbol{\tau}(hkl)$,

$$\Psi_Q^K = \sum_{\mathbf{d}} \mathrm{e}^{\mathrm{i}\boldsymbol{\tau}\cdot\mathbf{d}} \langle T_Q^K \rangle_{\mathbf{d}} =$$
$$= \mathrm{e}^{\mathrm{i}\varphi l} \langle T_Q^K \rangle_1 + \mathrm{e}^{-\mathrm{i}\varphi l} \langle T_Q^K \rangle_2 + (-1)^l \{ \mathrm{e}^{\mathrm{i}\varphi l} \langle T_Q^K \rangle_3 + \mathrm{e}^{-\mathrm{i}\varphi l} \langle T_Q^K \rangle_4 \} \ . \qquad (101)$$

The environments in the pair 1 and 2, and the pair 3 and 4, are related by a rotation of π about $\mathbf{a}_h$. Hence, $\langle T_Q^K \rangle_2 = (-1)^K \langle T_{-Q}^K \rangle_1$ with a similar relation between atomic tensors for the pair at sites 3 and 4. Environments at sites 1 and 4 are related by the inversion operator, while environments at sites 1 and 3 are related by the product of a diad along $\mathbf{a}_h$ and inversion and this product is equivalent to a mirror plane of symmetry normal to $\mathbf{a}_h$. Rotation about $\mathbf{a}_h$ reverses the polarity of moments normal to it, so moments in the pair 1 and 2, and in the pair 3 and 4, have the correct relative orientation. The centre of inversion symmetry at C does not change a parity-even tensor, and it implies that $\langle T_Q^K \rangle_2 = \langle T_Q^K \rangle_3$. This is correct for the signature of moments in haematite and it leads to,

$$\Psi_Q^K(\alpha - Fe_2O_3) = \mathrm{e}^{\mathrm{i}\varphi l} \langle T_Q^K \rangle_1 + \mathrm{e}^{-\mathrm{i}\varphi l} (-1)^K \langle T_{-Q}^K \rangle_1$$
$$+ (-1)^l \{ \mathrm{e}^{\mathrm{i}\varphi l} (-1)^K \langle T_{-Q}^K \rangle_1 + \mathrm{e}^{-\mathrm{i}\varphi l} \langle T_Q^K \rangle_1 \}$$
$$= \{ \mathrm{e}^{\mathrm{i}\varphi l} + (-1)^l \mathrm{e}^{-\mathrm{i}\varphi l} \} \{ \langle T_Q^K \rangle_1 + (-1)^{K+l} \langle T_{-Q}^K \rangle_1 \} \ . \qquad (102)$$

The signature of moments appropriate for Cr_2O_3 requires an additional oper-

ation that reverses the polarity between the sites 2 and 3, so that $\langle T^K_Q\rangle_2 = (-1)^K\langle T^K_Q\rangle_3$. One arrives at,

$$\begin{aligned}\Psi^K_Q(Cr_2O_3) &= e^{i\varphi l}\langle T^K_Q\rangle_1 + e^{-i\varphi l}(-1)^K\langle T^K_{-Q}\rangle_1 \\ &\quad +(-1)^{K+l}\{e^{i\varphi l}(-1)^K\langle T^K_{-Q}\rangle_1 + e^{-i\varphi l}\langle T^K_Q\rangle_1\} \\ &= \{e^{i\varphi l} + (-1)^{K+l}e^{-i\varphi l}\}\{\langle T^K_Q\rangle_1 + (-1)^l\langle T^K_{-Q}\rangle_1\} \ . \qquad (103)\end{aligned}$$

For even K, which describes scattering by electron charge distributions, the structure factors for α-Fe_2O_3 and Cr_2O_3 are the same. Resonant Bragg diffraction from haematite by Finkelstein et al. [43] was a seminal contribution to the development of the technique, and an appreciation of what the technique has to offer in crystal physics.

We continue the discussion of diffraction by Cr_2O_3 which is based on (103). With odd l $\Psi^K_0 = 0$ as expected for space group forbidden reflections. The triad axis imposes the condition $Q = 0, \pm 3$, so we reach the conclusion that with odd l Bragg diffraction is described by tensors with rank $K > 2$ and this excludes all E1 events. As we demonstrate in section 5.3, magnetic scattering enhanced by resonance of an E2 event at the K edge is purely orbital and this is expected to be quite small for Cr_2O_3, in contrast to vanadium ions in V_2O_3 (I/2a) which possess a relatively large orbital magnetic moment. However, neutron diffraction data on Cr_2O_3 has recently been interpreted to give a Cr moment of $2.5\mu_B$ [71]. The 17% reduction of the pure spin moment could mean a significant Cr orbital moment $\sim -0.5\mu_B$, although there are other equally feasible interpretations of the moment reduction.

The ferric ion ($3d^5$) has no orbital angular momentum. Thus, diffraction by haematite with enhancement from an E2 event at the Fe K edge has no magnetic contribution, to a good approximation. In particular, this type of diffraction from haematite is not expected to change on account of the reorientation of Fe moments on passing through the Morin transition [43].

We conclude the discussion of the corundum structure with a calculation of the E2 structure factor based on the result (103) which is appropriate for Cr_2O_3. The calculation is made for odd l, and a reflection of the type $(00l)$ for which the Bragg wavevector is parallel with the triad axis, or the trigonal axis (111). To this end, we apply to Ψ^K_Q a rotation that brings the triad axis parallel to $-x$ in Fig. 3, and rotates by ψ about this axis. In the previous example the two contributions, a rotation of the crystal to align $\boldsymbol{\tau}$ with $-x$ and rotation by ψ about $\boldsymbol{\tau}$, are explicitly shown in (91). Here, we combine the two contributions, by use of the addition theorem for Wigner D-functions (A.5), and the result

is to transform Ψ_Q^K to,

$$(-1)^Q \sum_{Q'} \mathrm{e}^{\mathrm{i}Q'\psi} d^K_{QQ'}\left(\frac{\pi}{2}\right) \Psi^K_{Q'} \ . \tag{104}$$

For $\psi = 0$, $\mathbf{a}_h$ is normal to the plane of scattering and pointing along $-z$, while the c-axis (triad) is pointing along $-x$. Note that periodicity in Ψ_Q^K is transmitted to the azimuthal angle ψ. In the present case, the triad axis imposes on Ψ_Q^K the condition $Q = \pm 3$ and the structure factor will be 3-fold periodic in ψ.

The E2 structure factor (75) is,

$$F(\mathrm{E2}) = \sum_{KQ} (-1)^K H^K_{-Q} \Psi^K_{+3} \{\mathrm{e}^{3\mathrm{i}\psi} d^K_{Q3}\left(\frac{\pi}{2}\right) - \mathrm{e}^{-3\mathrm{i}\psi} d^K_{Q-3}\left(\frac{\pi}{2}\right)\} \ , \tag{105}$$

where we have used $\Psi_Q^K = -\Psi^K_{-Q}$. Values of H_Q^K are taken from Table 4, and we find,

$$F_{\sigma'\sigma}(\mathrm{E2}) = \mathrm{i}\sqrt{2}\sin(2\theta)\cos(\varphi l)\cos(3\psi)\langle T^3_3\rangle' \ , \tag{106}$$

and,

$$\begin{aligned} F_{\pi'\sigma}(\mathrm{E2}) = \frac{\mathrm{i}}{2\sqrt{2}}\{&(\cos\theta + 3\cos 3\theta)\cos(\varphi l)\sin(3\psi)\ \langle T^3_3\rangle' \\ &+ \ (3\cos\theta + \cos 3\theta)\sin(\varphi l)\cos(3\psi)\ \langle T^4_3\rangle'\} \ . \end{aligned} \tag{107}$$

These expressions for Cr_2O_3 also apply to the charge (even K) scattering by haematite for which the magnetic (odd K) scattering at the Fe K edge is zero, to a good approximation, because the ferric ion is in an S-state. Diffraction in the unrotated channel of polarization described by (106) is purely magnetic and due to an octupole moment $\langle T^3_3\rangle' = \mathrm{Re}\langle T^3_3\rangle$ of the orbital magnetization in the Cr 3d valence shell. Scattering in the $(\pi'\sigma)$ channel is a combination of charge and magnetic scattering which are not shifted in phase by 90^o, as is often the case. Because the two contributions have different dependences on ψ and l the magnetic contribution could be distinguished by comparing data collected above and below the Néel temperature. The result (107) is the basis of an analysis of observations on haematite made by Finkelstein et al. [39,43,58].

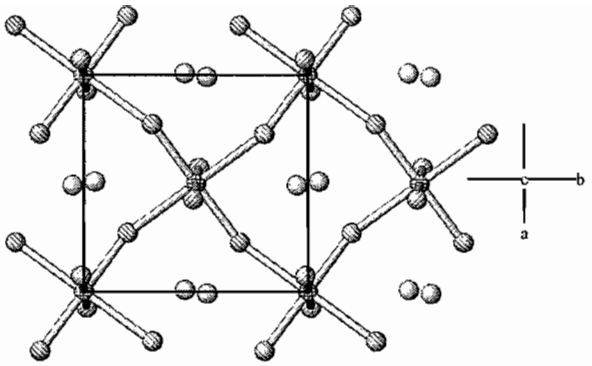

Fig. 8. $LaMnO_3$ (space group Pbnm), with the origin Mn on (000) and viewed down the c-axis.

6.3 Orthorhombic structure

Next we examine diffraction by ions in an orthorhombic crystal described by the space group Pbnm. Perovskite-type manganites possess this structure and $LaMnO_3$ is illustrated Fig. 8. These manganites are of great interest because they display a rich variety of magnetic and magneto-electronic properties, including negative colossal magnetoresistance [8]. The orthorhombic Pbnm crystal structure can be viewed as a cubic perovskite with two types of distortion. One distortion is a tilting of the MnO_6 octahedra which makes the Mn-O-Mn angle less than 180^o. Added to this is a distortion, driven by a Jahn-Teller interaction [23,73], that shortens four Mn-O bonds and lengthens the remaining two bonds. An orthorhombic structure has orthonormal basis vectors, $a \neq b \neq c$, and three mutually perpendicular diad axes but no axes of higher order [4,6].

Resonant ions are at the four sites $\mathbf{d}_1 = (000)$, $\mathbf{d}_2 = (00\frac{1}{2})$, $\mathbf{d}_3 = (\frac{1}{2}\frac{1}{2}0)$ and $\mathbf{d}_4 = (\frac{1}{2}\frac{1}{2}\frac{1}{2})$. The sites have no symmetry apart from being centres of inversion symmetry, which forbids parity-odd contributions in scattering. Point-group symmetry here places no restrictions on an atomic tensor $\langle T^K_Q \rangle$, and in this respect the present example of a crystal structure differs from the previous two examples in which axes of rotation symmetry in the point-group place limits on Q. The magnetic structure in the orthorhombic crystal is taken to be A-type canted antiferromagnetism with moments confined to the **b**-**c** plane. Each ion has a ferromagnetic component along the c-axis. The component of the moment along the b-axis alternates in direction on moving along the c-axis, so moments at even and odd numbered sites in the unit cell differ by rotation by π about the c-axis.

Let us construct Ψ^K_Q for the magnetic crystal specified in the previous paragraph. The environment at $\mathbf{d}_2$ is related to the environment at our origin $\mathbf{d}_1$ by a rotation by π about the c-axis, and $\langle T^K_Q \rangle_2 = (-1)^Q \langle T^K_Q \rangle_1$. The magnetic moments at $\mathbf{d}_1$ and $\mathbf{d}_2$ are in the required relative orientation. Environments

at $\mathbf{d}_3$ and $\mathbf{d}_4$ are related to $\mathbf{d}_1$ by rotations of π about the a- and b-axes, respectively. In addition to their chemical environments, which are related by the symmetry operations described, the sites $\mathbf{d}_3$ and $\mathbf{d}_4$ are required to have magnetic moments that are identical to the moments at $\mathbf{d}_1$ and $\mathbf{d}_2$. This is achieved by reversing the polarity at sites $\mathbf{d}_3$ and $\mathbf{d}_4$ by the use of (48), to give $\langle T^K_Q\rangle_3 = \langle T^K_{-Q}\rangle_1$ and $\langle T^K_Q\rangle_4 = (-1)^Q\langle T^K_{-Q}\rangle_1$. Note that $\langle T^K_Q\rangle_3$ and $\langle T^K_Q\rangle_4$ are related by a rotation of π about the c-axis, as expected. Assembling all this information in Ψ^K_Q we find,

$$\Psi^K_Q = \sum_{\mathbf{d}} \mathrm{e}^{\mathrm{i}\boldsymbol{\tau}\cdot\mathbf{d}}\langle T^K_Q\rangle_{\mathbf{d}} = \\ = \{1+(-1)^{l+Q}\}\{\langle T^K_Q\rangle_1 + (-1)^{h+k}\langle T^K_{-Q}\rangle_1\} \ . \tag{108}$$

It is seen that for all K, Ψ^K_0 vanishes for space-group forbidden reflections with Miller indices $l = 2n+1$ or $h+k = 2n+1$. A necessary condition for diffraction is even $l+Q$, which can be viewed as a selection rule on Q that is imposed by the space group.

We will consider an azimuthal angle scan at the reflection $(0kl)$ with odd k and odd l. In general, the Bragg wavevector $\boldsymbol{\tau}(0kl)$ does not lie along a cell edge or an axis of symmetry. For this choice of Miller indices, $\Psi^K_Q = 4\langle T^K_Q\rangle'_1$ where $\langle T^K_Q\rangle'_1$ is the real part of the atomic tensor associated with the resonant ion at site $\mathbf{d}_1$. Also, $|Q|$ is an odd integer and $\Psi^K_Q = -\Psi^K_{-Q}$. Notice that $\langle T^1_{+1}\rangle'_1$ is related to magnetization that lies along the a-axis and this component is zero with the A-type antiferromagnetic in question. In the case of an E1 event, the components of $\langle \mathbf{T}^1\rangle$ are found in (99), and the corresponding expression for an E2 event is a similar linear combination of $\langle \mathbf{L}\rangle$, $\langle \mathbf{S}\rangle$ and $\langle \mathbf{T}\rangle$.

In calculating a structure factor, the first task is to obtain the Euler angles for the rotation that takes $\boldsymbol{\tau}(0kl)$ to $-x$ in Fig. 3. The rotation in question is defined by (60) and we choose Euler angles α, β, γ such that $\boldsymbol{\tau}(0kl)$ lies along $-x$, and the crystal a-axis lies along the y-axis that is parallel to $\mathbf{q}+\mathbf{q}'$. Writing $\boldsymbol{\tau} = |\boldsymbol{\tau}|(t_1, t_2, t_3)$ one finds, $\alpha = 0$, $\gamma = \pi/2$ and β is specified by $\cos\beta = t_2$ and $\sin\beta = -t_3$. Next, apply a rotation ψ about the new direction for $\boldsymbol{\tau}$. The rotation matrix for this is defined in (91). The new Ψ^K_Q, for an azimuthal angle scan about $\boldsymbol{\tau}(0kl)$, is derived by application of the two coordinate rotations just described and it is,

$$\mathrm{e}^{\mathrm{i}Q\pi/2}\sum_{Q'}\mathrm{e}^{-\mathrm{i}Q'\pi/2}d^K_{Q'Q}(-\psi)\sum_q \mathrm{e}^{\mathrm{i}q\pi/2}d^K_{qQ'}(-\beta)\Psi^K_q = \\ = \mathrm{e}^{\mathrm{i}Q\pi/2}\sum_q \mathrm{e}^{\mathrm{i}q\pi/2}\Psi^K_q \sum_{Q'}\mathrm{e}^{-\mathrm{i}Q'\pi/2}d^K_{QQ'}(\psi)d^K_{Q'q}(\beta) \ .$$

The sum over Q' can be expressed as one Wigner D-function by application

of the addition theorem for the functions [18] and found in (A.5). This step brings our expression for the new Ψ_Q^K to,

$$e^{iQ\left(\frac{\pi}{2}-\alpha_0\right)} \sum_q e^{iq\left(\frac{\pi}{2}-\gamma_0\right)} d^K_{Qq}(\beta_0) \Psi^K_q \ , \tag{109}$$

where Euler angles $\alpha_0, \beta_0, \gamma_0$ satisfy,

$$\begin{aligned} \cot\alpha_0 &= \cot\beta \sin\psi \ , \\ \cos\beta_0 &= t_2 \cos\psi \ , \\ \cot\gamma_0 &= -t_3 \cot\psi \ , \end{aligned}$$

with $\cot\beta = -t_2/t_3$. At the origin of the azimuthal angle scan $\alpha_0 = \pi/2$, $\beta_0 = \beta$ and $\gamma_0 = 0$. Lastly, the structure factor $F(\mathrm{E1})$ for Bragg diffraction enhanced by an E1 event is,

$$F(\mathrm{E1}) = \sum_{KQ} (-1)^Q X^K_{-Q} e^{iQ\left(\frac{\pi}{2}-\alpha_0\right)} \sum_q e^{iq\left(\frac{\pi}{2}-\gamma_0\right)} d^K_{Qq}(\beta_0) \Psi^K_q \ . \tag{110}$$

Since an E1 event involves tensors up to rank $K = 2$ and $|q|$ is an odd integer, terms in (110) have $K = 1$ and 2, and $q = \pm 1$. In addition, $\Psi^1_{\pm 1}$ are zero because the magnetic moment on a resonant ion lies in the **b**-**c** plane. We find,

$$F_{\sigma'\sigma}(\mathrm{E1}) = 4\langle T^2_{+1}\rangle'_{\mathrm{E1}} \sin(2\beta_0) \sin\gamma_0 \ , \tag{111}$$

and

$$\begin{aligned} F_{\pi'\sigma}(\mathrm{E1}) = \langle T^2_{+1}\rangle'_{\mathrm{E1}} \{ &\cos(\alpha_0+\theta)\cos\beta_0\cos\gamma_0 \\ - \ &\sin(\alpha_0+\theta)\cos(2\beta_0)\sin\gamma_0\} \ . \end{aligned} \tag{112}$$

Expressed as a Cartesian tensor of rank 2, $\langle T^2_{+1}\rangle'_{\mathrm{E1}}$ is proportional to the xz, or ac, component of (97). Because t_2 and t_3 are not zero, since both k and l are odd, and t_2/t_3 for an orthorhombic crystal is not a rational number, the ψ-dependence of the structure factors (111) and (112) is non-trivial.

A simple dependence of the structure factor on ψ is obtained for $\boldsymbol{\tau}(hkl)$ that lie along a cell edge, that are axes of symmetry. With odd h and $\boldsymbol{\tau} = (h00)$ one obtains $F_{\sigma'\sigma}(\mathrm{E1}) = 0$ and $F_{\pi'\sigma}(\mathrm{E1}) = -4\langle T^2_{+2}\rangle''_{\mathrm{E1}} \sin\psi\cos\theta$ [47–50]. The imaginary part of $\langle T^2_{+2}\rangle_{\mathrm{E1}}$ is proportional to the xy, or ab, component of the equivalent Cartesian tensor. (The origin $\psi = 0$ finds the c-axis normal to the plane of scattering). Magnetic scattering contributes at odd l and $\boldsymbol{\tau} = (00l)$, for which $F_{\sigma'\sigma}(\mathrm{E1}) = 0$ and $F_{\pi'\sigma}(\mathrm{E1}) = 4\cos\theta\{-i\langle T^1_{+1}\rangle''_{\mathrm{E1}} \cos\psi + \langle T^2_{+1}\rangle''_{E1} \sin\psi\}$.

Here, $\langle T^1_{+1}\rangle''_{\rm E1}$ is proportional to magnetization along the b-axis, and $\langle T^2_{+1}\rangle''_{\rm E1}$ is proportional to the bc component of a Cartesian tensor formed with (97).

We conclude the section by mentioning, once again, that resonance-enhanced Bragg diffraction is a direct observation of electrons in the valence shell of the resonant ion in specific cases. E1 events, just discussed, can provide direct observations on the 3d valence shell when absorption takes place at 2p states of the cation [46]. The corresponding x-ray wavelength is large and the condition for Bragg diffraction can be fulfilled only with materials (crystals and fabricated structures) that have a very large cell dimension. In the case of single crystals, enhancement with an E1 event has a larger scope when applied to lanthanide or actinide cations because relevant absorption edges, the M_4 and M_5 edges, are at energies in excess of 1 keV $\equiv$ 12.4 Å. At M-edges in the actinides resonant enhancements can reach many orders of magnitude, leading to magnetic satellite intensities of order 0.1% of the charge Bragg peaks [42].

7 Resonant x-ray scattering: parity-odd events

If the resonant ion occupies a site in the crystal that is not a centre of inversion symmetry parity-odd events are allowed, which include a contribution to scattering through the mixed E1-E2 channel [74]. The electric crystal-field potential experienced by a cation is a possible mechanism. The potential can be represented by even-rank spherical harmonics when the cation site is a centre of symmetry. Odd-rank components to the potential are present in the absence of inversion symmetry, and these components may mix the valence state of the cation with states from a different atomic shell and a different angular momentum [23,73]. For example, the d-state of a cation and the p-state of an anion might have a significant overlap and hybridization. A state of an electron is then $|\psi\rangle = a|ljm\rangle + b|l'j'm'\rangle$, where $l \neq l'$, $j = l \pm 1/2$, and $j' = l' \pm 1/2$.

Turning back to (63), the E1-E2 amplitude is found to be,

$$Z(\text{E1-E2}) = \frac{\mathrm{i}}{2} \sum_{\eta(\Delta)} \langle \{ (\boldsymbol{\varepsilon}' \cdot \mathbf{R})|\eta\rangle\langle\eta|(\boldsymbol{\varepsilon} \cdot \mathbf{R})(\mathbf{q} \cdot \mathbf{R}) - (\boldsymbol{\varepsilon}' \cdot \mathbf{R})(\mathbf{q}' \cdot \mathbf{R})|\eta\rangle\langle\eta|(\boldsymbol{\varepsilon} \cdot \mathbf{R})\} \rangle \ . \tag{113}$$

Angular brackets denote the mean value of enclosed operators calculated with states like $|\psi\rangle$. Since the operator in (113) for electrons changes sign when their coordinates are inverted, i.e. $\mathbf{R} \rightarrow -\mathbf{R}$, the mean value can be different from zero for off-diagonal and parity-odd matrix elements, and all parity-even contributions vanish. The core state labelled η has quantum numbers $\bar{J}$, $\bar{M}$ and

the sum in (113) is interpreted as a sum over projections $\bar{M}$ [52,53]. In taking this step we exactly follow the calculation of the reduced matrix element for parity-even processes, and in the present case it leads to,

$$Z(\text{E1-E2}) = (l\|C(1)\|\bar{l})(\bar{l}\|C(2)\|l')q\langle l|R|\bar{l}\rangle\langle\bar{l}|R^2|l'\rangle \times \sum_{KQ}(-1)^Q\{\tilde{N}_Q^K\langle\Upsilon_{-Q}^K\rangle + (N_Q^K)^*\langle\Upsilon_{-Q}^K\rangle^*\} \ . \tag{114}$$

The quantities $\tilde{N}_Q^K$ and N_Q^K depend on the polarization vectors of the primary and secondary x-ray beams. They are defined using $h(p)$ which is built from $\boldsymbol{\varepsilon}$ and $\hat{\mathbf{q}}$ and defined in (78), and $h'(p)$ (which is similarly built from $\boldsymbol{\varepsilon}'$ and $\hat{\mathbf{q}}'$), namely,

$$\tilde{N}_Q^K = \frac{\mathrm{i}}{\sqrt{5}}\sum_{pp'} h(p)\varepsilon'_{p'}(2p1p'|KQ) \tag{115}$$

and

$$N_Q^K = \frac{\mathrm{i}}{\sqrt{5}}\sum_{pp'} h'(p)\varepsilon_{p'}(2p1p'|KQ) \ . \tag{116}$$

By their construction, $\tilde{N}_Q^K$ and N_Q^K are related to each other by the exchange of the pairs of variables $\boldsymbol{\varepsilon}, \hat{\mathbf{q}}$ and $\boldsymbol{\varepsilon}', \hat{\mathbf{q}}'$. Some properties of $\tilde{N}_Q^K$ and N_Q^K are provided in Table 5. Because $\tilde{N}_Q^K$, N_Q^K and Υ_Q^K are all products of tensors of rank 1 and rank 2 the triangular condition gives $K = 1, 2$ and 3.

Calculations of the mixing parameter ab^* can not be made with great confidence it seems. Ab initio calculations are good for pure E1 events, and confidence in results diminishes on moving to E1-E2 and pure E2 events. One anticipates that $|ab^*|$ is relatively small. After accounting for the radial integrals, the E1-E2 contribution to scattering and absorption is found to be several orders of magnitude down on the pure E1 contribution [75,76]. We do not consider the parity-odd process that arises from thermally induced relative displacements of the resonant ion [77,78]. Observations made on ZnO of a complex energy-profile that changes with temperature are attributed to this scattering process [79].

The reduced matrix element of Υ_Q^K is nicely written in terms of a reduced matrix element $(t\bar{J}j\|V^K\|t'\bar{J}j')$ where V^K works only on the part t in the coupled scheme $t\bar{J}j$. By this we mean that $(t\bar{J}j\|V^K\|t'\bar{J}j')$ is proportional to $(t\|V^K\|t')$ and the coefficient of proportionality contains the dependence on $\bar{J}, j$ and j'. The actual formula in question is standard and it can be found in Edmonds' book (7.1.7) [16], for example. With these definitions one finds,

Table 5
Properties of $\tilde{N}^K_Q$ and N^K_Q

$\tilde{N}^K_Q$ and N^K_Q are defined by (115) and (116), or (120).

$\tilde{N}^K_{-Q} = (-1)^{K+Q}(\tilde{N}^K_Q)^*$, $N^K_{-Q} = (-1)^{K+Q}(N^K_Q)^*$

$\tilde{\mathbf{N}}^1 = -\frac{i\sqrt{3}}{10}\{\hat{\mathbf{q}}(\boldsymbol{\varepsilon}' \cdot \boldsymbol{\varepsilon}) + (\boldsymbol{\varepsilon}' \times \boldsymbol{\varepsilon}) \times \hat{\mathbf{q}}\}$

$\mathbf{N}^1 = -\frac{i\sqrt{3}}{10}\{\hat{\mathbf{q}}'(\boldsymbol{\varepsilon}' \cdot \boldsymbol{\varepsilon}) + \hat{\mathbf{q}}' \times (\boldsymbol{\varepsilon}' \times \boldsymbol{\varepsilon})\}$

$(\tilde{\mathbf{N}}^1)_{\rm av} = (\mathbf{N}^1)_{\rm av} = -\frac{i\sqrt{3}}{10}\hat{\mathbf{q}}$,
with $\mathbf{q} = \mathbf{q}'$ and an average over polarization.

For the scattering geometry depicted in Figure 3 the nonzero elements are:

$(\sigma'\sigma)$

$\tilde{N}^1_{+1} = -\frac{1}{10}\left(\frac{3}{2}\right)^{1/2} e^{i\theta}$, $\tilde{N}^2_{+1} = \frac{1}{2}\left(\frac{1}{30}\right)^{1/2} e^{i\theta}$
$\tilde{N}^3_{+1} = \frac{1}{5}\left(\frac{2}{3}\right)^{1/2} e^{i\theta}$
Values of N^K_Q and $\tilde{N}^K_Q$ are the same except for the sign of θ.

$(\pi'\sigma)$

$\tilde{N}^1_0 = \frac{i}{10}\sqrt{3}\sin(2\theta)$, $\tilde{N}^2_0 = \frac{1}{2}\left(\frac{1}{5}\right)^{1/2}\cos(2\theta)$
$\tilde{N}^2_{+2} = \frac{1}{2}\left(\frac{1}{30}\right)^{1/2}$, $\tilde{N}^3_0 = \frac{i}{5}\left(\frac{1}{2}\right)^{1/2}\sin(2\theta)$
$\tilde{N}^3_{+2} = -\frac{1}{2}\left(\frac{1}{15}\right)^{1/2}$, $N^2_{+2} = -\left(\frac{1}{30}\right)^{1/2} e^{-2i\theta}$
$N^3_{+2} = -\frac{1}{2}\left(\frac{1}{15}\right)^{1/2} e^{-2i\theta}$

$(\pi'\pi)$

$\tilde{N}^1_{+1} = -\frac{1}{10}\left(\frac{3}{2}\right)^{1/2} e^{3i\theta}$, $\tilde{N}^2_{+1} = -\frac{1}{2}\left(\frac{1}{30}\right)^{1/2} e^{3i\theta}$
$\tilde{N}^3_{+1} = -\frac{1}{10}\left(\frac{1}{6}\right)^{1/2} e^{3i\theta}$, $\tilde{N}^3_{+3} = \frac{1}{2}\left(\frac{1}{10}\right)^{1/2} e^{i\theta}$
Values of N^K_Q and $\tilde{N}^K_Q$ are the same except for the sign of θ.
This relation holds for the unrotated polarizations $(\sigma'\sigma)$ and $(\pi'\pi)$ only.

$$(lj\|\Upsilon^K\|l'j') = \left(\frac{5}{6}\right)^{1/2}(2\bar{J}+1)\begin{Bmatrix} j & t & \bar{J} \\ \bar{l} & 1/2 & l \end{Bmatrix} \times \begin{Bmatrix} j' & t' & \bar{J} \\ \bar{l} & 1/2 & l' \end{Bmatrix}(t\bar{J}j\|V^K\|t'\bar{J}j') \ , \qquad (117)$$

where $t = 1$ and $t' = 2$. The spin of the electron $s = 1/2$ appears in the coefficient on the right hand side of (117). By using the algebraic methods employed in [70] for parity-even processes, it is quite easy to develop the reduced matrix element of Υ as a linear combination of atomic quantities that depend on both the spin and orbital variables associated with the resonant ion. Just as in parity-even processes, one finds that spin variables are absent in the reduced matrix element at the K-edge where $\bar{l} = 0$. Since this situation

is of particular practical interest, in the subsequent discussion, we look only at the orbital properties, by developing a discussion of V^K. Marri and Carra (2004) [80] develop both the spin and the orbital properties.

A perspicacious rendering of expression (114) is derived by partitioning it into contributions that are symmetric and antisymmetric with respect to the crossing transformation [51]. Readers not completely familiar with this line of reasoning could find it useful to consider properties of the axial vector $(\boldsymbol{\varepsilon}' \times \boldsymbol{\varepsilon}) = -\mathrm{i}\sqrt{2}\mathbf{X}^1$ which has featured in previous sections. After averaging over states of polarization one finds [13],

$$2(\boldsymbol{\varepsilon}' \times \boldsymbol{\varepsilon})_{\mathrm{av}} = (\hat{\mathbf{q}} - \hat{\mathbf{q}}')P_1 + \mathrm{i}(\hat{\mathbf{q}} + \hat{\mathbf{q}}')P_2 + (\hat{\mathbf{q}} \times \hat{\mathbf{q}}')(P_3 - 1) \ . \tag{118}$$

Recall that, the three Stokes parameters are purely real and time-even. Moreover, P_1 and P_3 are (true) scalars while the mean helicity P_2 is a pseudoscalar that changes sign with the inversion transformation (inversion-odd). The right-hand side of (118) has two contributions that are not explicitly axial. It is not clear how the entire right-hand side changes sign on exchanging $\boldsymbol{\varepsilon}'$ with $\boldsymbol{\varepsilon}$, at first sight. This property is revealed by the crossing transformation that includes an exchange of the variables $\boldsymbol{\varepsilon}$, $\boldsymbol{\varepsilon}'$, $\mathbf{q}$, $\mathbf{q}'$, P_1, P_2, P_3, with $\boldsymbol{\varepsilon}'$, $\boldsymbol{\varepsilon}$, $\mathbf{q}'$, $\mathbf{q}$, P_1, $-P_2$, P_3, and (118) is antisymmetric with respect to the transformation. The transformation that is conjugate to the crossing transformation includes the operations of time reversal and spatial inversion. A contribution to the scattering amplitude that is symmetric (antisymmetric) with respect to the crossing transformation must be accompanied in the amplitude by an atomic tensor that is symmetric (antisymmetric) with respect to the product of time reversal and inversion operations. Pure E1 and pure E2 channels are inversion-even, and parity-even is an alternative label that we have adopted. In the E1 and E2 channels all atomic tensors are inversion-even, of course. Thus, a contribution symmetric with respect to crossing is accompanied by a time-even atomic tensor, and an antisymmetric contribution is accompanied by a time-odd atomic tensor. Specifically, in the E1 channel $\mathbf{X}^1$ is accompanied by a time-odd atomic tensor. In section 5 we demonstrate, by using the crossing transformation, that in the pure E2 channel also time-odd (magnetic) contributions to scattering are tensors with an odd rank, namely, $K = 1$ and $K = 3$.

Turning to the mixed, inversion-odd E1-E2 channel, all the atomic tensors therein are inversion-odd. A contribution to the E1-E2 amplitude which is symmetric with respect to the crossing transformation must be accompanied by an atomic tensor which is also time-odd and thus symmetric with respect to the product of inversion and time-reversal operations. We denote by G^K_Q atomic tensors that are both inversion-odd and time-odd. They are referred to as magnetoelectric tensors to mark an analogy with the magnetoelectric effect which is allowed when the elements of symmetry in a magnetic crystal

contain inversion and time-reversal as a product, i.e. inversion is not a separate symmetry. Evidently, $\langle G_Q^K \rangle$ vanishes in crystals which are not magnetically ordered. Atomic tensors that are both inversion-odd and time-even are denoted by U_Q^K, and in the E1-E2 channel $\langle U_Q^K \rangle$ is accompanied by an antisymmetric x-ray factor. For example, $\mathbf{X}^1 \cdot (\mathbf{q} + \mathbf{q}')$ can be accompanied by $\langle U_Q^K \rangle$, while $\mathbf{X}^1 \cdot (\mathbf{q} - \mathbf{q}')$ can be accompanied by $\langle G_Q^K \rangle$.

In the light of the foregoing discussion, we re-express the x-ray factors $\tilde{N}_Q^K$ and N_Q^K in the E1-E2 amplitude as linear combinations $\tilde{N}_Q^K + N_Q^K$ and $\tilde{N}_Q^K - N_Q^K$, which, respectively, are symmetric and antisymmetric with respect to the crossing transformation. The E1-E2 amplitude (113) is purely real for $\boldsymbol{\varepsilon}' = \boldsymbol{\varepsilon}$ and $\mathbf{q}' = \mathbf{q}$, and it is purely imaginary for $\boldsymbol{\varepsilon}' = -\boldsymbol{\varepsilon}$ and $\mathbf{q}' = -\mathbf{q}$. These two cases correspond to $\tilde{N}_Q^K = N_Q^K$ and $\tilde{N}_Q^K = -N_Q^K$, and they enable us to precisely determine the relations between Υ_Q^K and the atomic tensors G_Q^K and U_Q^K. One finds $\langle \Upsilon_Q^K \rangle = -\mathrm{i}^K \langle G_Q^K \rangle$ in the symmetric contribution, and $\langle \Upsilon_Q^K \rangle = \mathrm{i}^{K-1} \langle U_Q^K \rangle$ in the antisymmetric contribution. The phase difference of 90° in the two contributions reflects the fact that $\langle G_Q^K \rangle$ and $\langle U_Q^K \rangle$ have opposite time signatures, with $\langle G_Q^K \rangle$ time-odd and $\langle U_Q^K \rangle$ time-even. After assembling our findings we arrive at an expression for the unit-cell structure factor for the parity-odd, E1-E2 channel of scattering,

$$\begin{aligned} F(\text{E1-E2}) &= \sum_{KQ} (-1)^Q \sum_{\mathbf{d}} \{ \tilde{N}_Q^K \langle \Upsilon_{-Q}^K \rangle_{\mathbf{d}} + (N_Q^K)^* \langle \Upsilon_{-Q}^K \rangle_{\mathbf{d}}^* \} \mathrm{e}^{\mathrm{i}\mathbf{k}\cdot\mathbf{d}} \\ &= \sum_K \mathrm{i}^{K-1} \sum_Q (-1)^Q \left\{ -\mathrm{i} \Psi_Q^{K,g} (\tilde{N}_{-Q}^K + N_{-Q}^K) \right. \\ &\qquad \left. + \quad \Psi_Q^{K,u} (\tilde{N}_{-Q}^K - N_{-Q}^K) \right\} \ . \end{aligned} \tag{119}$$

where $\Psi_Q^{K,g}$ ($\Psi_Q^{K,u}$) is a linear combination of $\langle G_Q^K \rangle_{\mathbf{d}}$ ($\langle U_Q^K \rangle_{\mathbf{d}}$) multiplied by spatial phase factors $\mathrm{e}^{\mathrm{i}\mathbf{k}\cdot\mathbf{d}}$.

At this stage it is helpful to look at expressions for the x-ray factors written in terms of $\mathbf{X}_Q^K$. From the definitions (115) and (116) one obtains,

$$\begin{aligned} \tilde{N}_Q^K \pm N_Q^K = \mathrm{i} \sum_{K'Q'} & X_{Q'}^{K'} (2K'+1)^{1/2} \sum_\nu (\hat{q}_\nu \pm (-1)^{K'} \hat{q}'_\nu) \\ & \times \quad \begin{Bmatrix} 1 & 1 & 2 \\ 1 & K & K' \end{Bmatrix} (K'Q'1\nu | KQ) \ . \end{aligned} \tag{120}$$

This expression confirms that $\mathbf{X}^1$ appears with $(\hat{\mathbf{q}} - \hat{\mathbf{q}}')$ in the symmetric combination $\tilde{N}_Q^K + N_Q^K$. To be more precise, the two vector quantities $\mathbf{X}^1$ and $(\mathbf{q} - \mathbf{q}')$ in $\tilde{N}_Q^K + N_Q^K$ together appear as a tensor product which we denote by $(\mathbf{X}^1 \otimes (\hat{\mathbf{q}} - \hat{\mathbf{q}}'))^K$. In the other case, $(\mathbf{X}^1 \otimes (\hat{\mathbf{q}} + \hat{\mathbf{q}}'))^K$ occurs in the antisymmetric combination. Actual values of $\tilde{N}_Q^K \pm N_Q^K$ for unrotated

and rotated channels of scattering can be obtained from entries in Table 5. In the case of unrotated polarization one finds very simple expressions, with $\tilde{N}_Q^K + N_Q^K$ proportional to $\cos\theta$ or $\cos(3\theta)$ and $\tilde{N}_Q^K - N_Q^K$ proportional to $\mathrm{i}\sin\theta$ or $\mathrm{i}\sin(3\theta)$. The corresponding expressions for rotated polarization are slightly more complicated functions of the Bragg angle.

Marri and Carra (2004) [80] give an expression for the E1-E2 amplitude. Unlike (119), their expression does not respect the crossing transformation.

We construct operator equivalents for G_Q^K and U_Q^K in terms of the angular momentum operator, $\mathbf{L}$, the polar unit vector $\mathbf{n}$, and

$$\mathbf{\Omega} = \mathrm{i}(\mathbf{L}^2\mathbf{n} - \mathbf{n}\mathbf{L}^2) = \mathrm{i}[\mathbf{L}^2, \mathbf{n}] \ , \tag{121}$$

which is frequently called the operator for the orbital anapole.

Let us record some basic properties of these operators. First, $\mathbf{L}$ is diagonal with respect to angular momentum states and $\langle lm|L_\alpha|l'm'\rangle = \delta_{l,l'}\langle lm|L_\alpha|lm'\rangle$, while $\langle lm|n_\alpha|l'm'\rangle$ is different from zero for $l' = l \pm 1$. The basic commutation relations are,

$$\begin{aligned} [L_\alpha, L_\beta] &= \mathrm{i}\epsilon_{\alpha\beta\gamma}L_\gamma \ , \\ [L_\alpha, n_\beta] &= \mathrm{i}\epsilon_{\alpha\beta\gamma}n_\gamma \ , \\ [L_\alpha, \Omega_\beta] &= \mathrm{i}\epsilon_{\alpha\beta\gamma}\Omega_\gamma \ , \end{aligned} \tag{122}$$

where $\epsilon_{\alpha\beta\gamma}$ is the antisymmetric unit tensor of rank three (also called the unit axial tensor), and α, β, γ label Cartesian components of a vector quantity. Commutation relations for spherical components of $\mathbf{L}$, $\mathbf{n}$ and $\mathbf{\Omega}$ are readily constructed, e.g. $[L_0, n_{\pm 1}] = \pm n_{\pm 1}$, $[L_0, \Omega_{\pm 1}] = \pm\Omega_{\pm 1}$. Recall that $[\mathbf{L}^2, L_\alpha] = 0$. One finds that $\mathbf{L}\cdot\mathbf{n} = \mathbf{L}\cdot\mathbf{\Omega} = 0$, while $\mathbf{n}\cdot\mathbf{\Omega} = -\mathbf{\Omega}\cdot\mathbf{n} = 2\mathrm{i}$. The operators L_α, n_α and Ω_α are all Hermitian. With regard to time-reversal, n_α is even and L_α and Ω_α are odd, i.e. $\bar{n}_\alpha = n_\alpha$, $\bar{L}_\alpha = -L_\alpha$ and $\bar{\Omega}_\alpha = -\Omega_\alpha$. Spherical components of $\mathbf{L}$ and $\mathbf{\Omega}$ are time-odd so that $L_q^+ = -\bar{L}_q$ and $\Omega_q^+ = -\bar{\Omega}_q$, while n_q is time-even and $n_q^+ = \bar{n}_q$.

The anapole operator $\mathbf{\Omega}$ is inversion-odd and it is also time-odd. Hence, G_Q^1 can be represented by an operator equivalent which is proportional to Ω_Q. The tensor products $(\mathbf{L}\otimes\mathbf{n})_Q^2$ and $(\mathbf{L}\otimes(\mathbf{L}\otimes\mathbf{\Omega})^2)_Q^3$ are used, respectively, to represent G_Q^2 and G_Q^3. Table 6 contains the precise operator equivalents we use for G_Q^K and U_Q^K, and they are the same essentially as those chosen by Carra et al.(2003) [81], Marri and Carra (2004) [80], and Carra (2004) [82]. Various properties of the magnetoelectric and polar operators are also included in Table 6. In particular, $(G_Q^K)^+ = -\bar{G}_Q^K$ and $(U_Q^K)^+ = \bar{U}_Q^K$, and thus,

$$\langle G_Q^K\rangle_{\mathbf{H}} = -\langle G_Q^K\rangle_{-\mathbf{H}} \ , \tag{123}$$

Table 6
Representations of G_Q^K and U_Q^K

K	G_Q^K	U_Q^K
1	$\frac{1}{4}\left(\frac{3}{2}\right)^{1/2}\mathbf{\Omega}_Q$	$-\left(\frac{3}{2}\right)^{1/2}\mathbf{n}_Q$
2	$-\left(\frac{5}{3}\right)^{1/2}(\mathbf{L}\otimes\mathbf{n})^2_Q$	$-\frac{1}{4}\left(\frac{5}{3}\right)^{1/2}(\mathbf{L}\otimes\mathbf{\Omega})^2_Q$
3	$-\frac{1}{4}\left(\frac{5}{2}\right)^{1/2}(\mathbf{L}\otimes(\mathbf{L}\otimes\mathbf{\Omega})^2)^3_Q$	$\left(\frac{5}{2}\right)^{1/2}(\mathbf{L}\otimes(\mathbf{L}\otimes\mathbf{n})^2)^3_Q$

Numerical factors are calculated from
$(t\|V^K\|t') = -\mathrm{i}^K(t\|G^K\|t') = \mathrm{i}^{K-1}(t\|U^K\|t') = (2K+1)^{1/2}$
with $t = 1, t' = 2$
which is a requirement derived from the result (114).

Transformation properties of $\mathbf{L}, \mathbf{\Omega}$ and $\mathbf{n}$
Time-reversal:
$\bar{L}_q = (-1)^{1+q}L_{-q}\,, \quad \bar{\Omega}_q = (-1)^{1+q}\Omega_{-q}\,, \quad \bar{n}_q = (-1)^q n_{-q}$
$\bar{G}_Q^K = (-1)^{1+Q}G_{-Q}^K\,, \quad \bar{U}_Q^K = (-1)^Q U_{-Q}^K$

Hermitian conjugation:
$L_q^+ = (-1)^q L_{-q}\,, \quad \Omega_q^+ = (-1)^q\Omega_{-q}\,, \quad n_q^+ = (-1)^q n_{-q}$
$(G_Q^K)^+ = (-1)^Q G_{-Q}^K\,, \quad (U_Q^K)^+ = (-1)^Q U_{-Q}^K$

$$\langle U_Q^K\rangle_{\mathbf{H}} = \langle U_Q^K\rangle_{-\mathbf{H}}\,, \tag{124}$$

where $\mathbf{H}$ is a local magnetic field. The corresponding result for parity-even atomic tensors is found in (48). Concerning the influence on operator equivalents of the inversion, or parity, operator let us note first that all components of a given tensor operator have the same parity for the parity operator commutes with rotations. (For a c-number tensor the parity is equal to the rank of the tensor, e.g. a spherical harmonic Y_Q^K is transformed to $(-1)^K Y_Q^K$ by the parity operator.) Secondly, the parity of a tensor operator built from tensor products, as is the case for G_Q^K and U_Q^K with $K > 1$, is the product of the parities of the constituent tensor operators. In Table 6, odd-rank ($K = 1$ or 3) tensors are true (or polar) tensors and even-rank ($K = 2$) tensors are pseudotensors (or axial tensors).

Prior to applying the foregoing expressions in a discussion of resonant scattering by Cr_2O_3, we add a few comments about the anapole operator $\mathbf{\Omega}$. An operator with the same transformation properties was discussed by Zel'dovich [83] in 1957 and some time later the name anapole was attached to it. An anapole moment characterizes a system that does not transform into itself under space inversion [84]. A system like this generates a distribution of magnetic fields which is quite different from parity-even multipoles, such as dipole or quadrupole moments. The magnetic field distribution of an anapole looks like the mag-

netic field created by a current flowing in a toroidal winding, and the field is completely confined inside the winding.

Chromium sesquioxide is described in section 6, and Cr ions in the unit cell are depicted in Fig. 7. The centre of inversion symmetry at C between the pairs labelled 1 and 2, and 3 and 4 means that $\langle U_Q^K\rangle_3$ and $\langle U_Q^K\rangle_4$ differ in sign from $\langle U_Q^K\rangle_1$ and $\langle U_Q^K\rangle_2$. We find,

$$\Psi_Q^{K,u} = \left\{e^{i\varphi l} - (-1)^l e^{-i\varphi l}\right\}\left\{\langle U_Q^K\rangle - (-1)^{l+K}\langle U_{-Q}^K\rangle\right\} \ . \tag{125}$$

In the construction of $\Psi_Q^{K,g}$ the sign difference that we mention, due to the inversion at C, is cancelled by a change in sign of $\langle G_Q^K\rangle$ caused by the change in the polarity of the local magnetic field, i.e. the product of inversion and time-reversal is one. The corresponding structure factor is,

$$\Psi_Q^{K,g} = \left\{e^{i\varphi l} + (-1)^l e^{-i\varphi l}\right\}\left\{\langle G_Q^K\rangle + (-1)^{l+K}\langle G_{-Q}^K\rangle\right\} \ . \tag{126}$$

The structure factor for parity-even processes is found in (103), and it is used to calculate the unit-cell structure factors for pure E2 diffraction at $(00l)$ with odd l.

By following the same steps in the calculation of the structure factor reported in section 6 and applying them to (125) and (126) we obtain structure factors for E1-E2. Adding the contributions in the pure E2 channel, (106) and (107), we arrive at,

$$\begin{aligned} F_{\sigma'\sigma} = i\sqrt{2}\cos(3\psi)\Big\{ & \sin(2\theta)\cos(\varphi l)\langle T_3^3\rangle' \\ & - \frac{4}{\sqrt{5}}\cos(\theta)\sin(\varphi l)\langle G_3^3\rangle''\Big\} \ , \end{aligned} \tag{127}$$

and,

$$\begin{aligned} F_{\pi'\sigma} = \frac{i}{2\sqrt{2}}\{ & [\cos\theta + 3\cos(3\theta)]\cos(\varphi l)\sin(3\psi)\langle T_3^3\rangle' \\ & + [3\cos\theta + \cos(3\theta)]\sin(\varphi l)\cos(3\psi)\langle T_3^4\rangle'\} \\ & + i2\left(\frac{2}{5}\right)^{1/2}\sin(2\theta)\sin(\varphi l)\sin(3\psi)\langle G_3^3\rangle'' \\ & + i\frac{2}{\sqrt{5}}\cos^2\theta\cos(\varphi l)\langle U_0^2\rangle \ . \end{aligned} \tag{128}$$

Here, $\langle U_0^2\rangle$ is purely real, because U_0^2 is Hermitian, $\mathrm{Re}\langle\ldots\rangle \equiv \langle\ldots\rangle'$ and $\mathrm{Im}\langle\ldots\rangle \equiv \langle\ldots\rangle''$. In the absence of magnetic order $\langle T_3^3\rangle$ and $\langle G_Q^K\rangle$ are zero.

The corresponding structure factor also applies to paramagnetic V_2O_3 and haematite for which there is experimental evidence of a contribution in the $(\pi'\sigma)$ channel that does not depend on the azimuthal angle ψ, and here we find that such a term is due to a polar multipole of rank 2 [76]. One can, after some algebra, show that $\langle U_0^2 \rangle = 1/4(5/2)^{1/2}\langle L_0\Omega_0 \rangle$ and $L_0\Omega_0 = \Omega_0 L_0$ is a Hermitian operator. In both channels, parity-even and parity-odd contributions are in phase. Time-odd contributions have a common behaviour with respect to the azimuthal angle, ψ. Since this dependence on ψ is not shared by the two time-even contributions to $F_{\pi'\sigma}$ the intensity as a function of ψ should change on passing through the Néel temperature.

8 X-ray dichroism

Near-edge dichroism is a very useful probe of electronic states in crystals and fabricated materials. Linear and circular polarizations are employed in experiments performed with x-ray beams from a synchrotron source, leading to linear and circular dichroic signals, respectively [11,85]. A linear dichroic signal is the difference in absorption spectra with linear polarization, P_3, parallel or perpendicular to an axis of symmetry in the crystal, and it picks out angular anisotropy in the distribution of electron charge. Circular dichroism, a difference in absorption signals recorded with left- and right-handed helicity, P_2, picks out pseudotensor properties of a crystal [66]. Dichroism experiments measure a signal not seen in diffraction experiments but the two techniques have in common the x-ray scattering length as a framework for the analysis of observations. In the development employed here for the analysis of signals seen in Bragg diffraction, a dichroism experiment is a measure of the unit-cell structure factor evaluated for zero deflection, namely, $\mathbf{k} = \mathbf{q} - \mathbf{q}' = 0$. This quantity is extracted from an absorption signal by integration with respect to the x-ray energy. In favourable cases, the integrated dichroic signal is proportional to the structure factor, evaluated with $\mathbf{k} = 0$, which expresses a sum rule for integrated intensity [63,64].

8.1 Parity-even dichroic signals

Structure factors for E1 and E2 events are defined by (67) and (75), respectively. Let us choose to have the x-ray beam parallel to the z-axis in Cartesian coordinates. Polarization vectors lie in the x-y plane. For an E1 event we need to consider,

$$(F(\mathrm{E1}))_{\mathrm{av}} = \sum_{KQ} (-1)^Q \left(X^K_{-Q}\right)_{\mathrm{av}} \Psi^K_Q \ , \tag{129}$$

where the average is an average with respect to polarization in the x-ray beam, and Ψ^K_Q is evaluated with $\mathbf{k} = 0$. It is easy to show that X^0_0 and X^2_0 are proportional to $(\boldsymbol{\varepsilon}' \cdot \boldsymbol{\varepsilon})$ and $(\boldsymbol{\varepsilon}' \cdot \boldsymbol{\varepsilon})_{\rm av} = 1$. These terms cancel in a difference signal and the latter is found to be proportional to,

$$\begin{aligned}(\Delta F(\mathrm{E1}))_{\rm av} &= \left(\mathbf{X}^1\right)_{\rm av} \cdot \boldsymbol{\Psi}^1 + \sum_{Q=\pm 2} \left(X^2_{-Q}\right)_{\rm av} \Psi^2_Q \\ &= -\frac{1}{\sqrt{2}} \hat{q}_0 P_2 \Psi^1_0 + \frac{1}{4} P_3 \sum_{Q=\pm 2} \Psi^2_Q \ , \end{aligned} \tag{130}$$

where we have used results in Table 3 and $\hat{q}_0 = \hat{q}_z$. Regarding the first term in the second equality, Ψ^1_0 is a linear combination of tensors $\langle T^1_0 \rangle_{\rm E1}$ that are time-odd, and they are zero in the absence of magnetic order. The product $\hat{q}_0 \Psi^1_0$ is even with respect to the reversal of time, the product $\hat{q}_0 P_2$ is even with respect to the parity operation, and time-reversal and parity reversal leave unchanged P_2 and Ψ^1_0, respectively. Like P_2, the Stokes parameter P_3 is unchanged by the reversal of time but P_3 is a true scalar while P_2 is a pseudoscalar that changes sign with parity-reversal. Ψ^1_0 can be different from zero for a ferro- or ferri-magnet, and it is identically zero for a fully compensating antiferromagnet.

The atomic tensors in Ψ^2_Q and Ψ^1_Q are found in (97) and (99), respectively. An average over the two spin-orbit split core states, with total angular momentum $\bar{J} = \bar{l} - 1/2$ and $\bar{J} = \bar{l} + 1/2$, leaves $\langle \mathbf{T}^2 \rangle_{\rm E1}$ proportional to the quadrupole moment $\langle \mathbf{Q} \rangle$ and $\langle \mathbf{T}^1 \rangle_{\rm E1}$ proportional to the orbital angular momentum $\langle \mathbf{L} \rangle$ [63]. These expectation values, $\langle \mathbf{Q} \rangle$ and $\langle \mathbf{L} \rangle$, are ground state properties of the valence shell that accommodates the photo-ejected core-electron, and the same is true of the other atomic quantities in (97) and (99). Absorption at the K-edge with $\bar{l} = 0$ also leaves $\langle \mathbf{T}^1 \rangle_{\rm E1}$ and $\langle \mathbf{T}^2 \rangle_{\rm E1}$ proportional to $\langle \mathbf{L} \rangle$ and $\langle \mathbf{Q} \rangle$, respectively, because the $1s$ core state is not split by the spin-orbit interaction.

Dichroic signals in an E2 event are derived from (75) and appropriate average values of H^K_Q. The corresponding atomic tensors $\langle \mathbf{T}^K \rangle_{\rm E2}$ are derived from (73). Here we consider two important cases. First the linear dichroic signals for a lanthanide or actinide resonant ion, where the valence shell angular momentum $l = 3$. The signal in question is,

$$(\Delta F(\mathrm{E2}))_{\rm av} = \frac{1}{4\sqrt{7}} P_3 \sum_{q=\pm 2} \left\{ -\frac{\sqrt{3}}{2} \Psi^2_q + \Psi^4_q \right\} \ , \tag{131}$$

and

$$\langle \mathbf{T}^2 \rangle_{\rm E2} \propto (2\bar{J} + 1) \langle \mathbf{Q} \rangle \pm \frac{2}{5} [10 \langle \mathbf{P} \rangle + 3 \langle \mathbf{R} \rangle] \ . \tag{132}$$

The operators in (132) are defined in (94)-(96).

The second case we consider is the circular dichroic signal at the K-edge of a 3d transition metal ion. The signal is due to orbital magnetism in the 3d shell and we find ($l = 2$),

$$(\Delta F(\mathrm{E2}))_{\mathrm{av}} = \frac{1}{2\sqrt{10}} \hat{q}_0 P_2 \left\{ \Psi_0^1 - 2\Psi_0^3 \right\} \ . \tag{133}$$

In this expression, Ψ_0^1 is constructed from operators proportional to the orbital angular momentum $\langle \mathbf{L} \rangle_{\mathbf{d}}$ and Ψ_0^3 is constructed from operators proportional to the orbital octupole $\langle \mathbf{\Lambda} \rangle_{\mathbf{d}}$ defined in (39). If we actually use $\langle \mathbf{L} \rangle_{\mathbf{d}}$ and $\langle \mathbf{\Lambda} \rangle_{\mathbf{d}}$, so that $\Psi_0^1 = \sum_{\mathbf{d}} \langle L_0 \rangle_{\mathbf{d}}$ and $\Psi_0^3 = \sum_{\mathbf{d}} \langle \Lambda_0 \rangle_{\mathbf{d}}$, then in (133) $\{\Psi_0^1 - 2\Psi_0^3\} \rightarrow \{\Psi_0^1 - (2/3)\Psi_0^3\}/5\sqrt{10}$.

8.2 Parity-odd dichroic signals

Third-generation synchrotron radiation rings and insertion devices provide x-ray beams that are adequate for the observation of very weak signals due to parity-odd events. One example is natural circular dichroism which creates in a non-magnetic material a differential absorption of right- and left-handed circular polarization [81,86–89]. The fractional effect, which is of the order of 10^{-3}, is allowed by a mechanism that is related to optical transitions responsible for the colour intensity of some glasses and minerals. Nonreciprocal linear dichroism may also contribute in a parity-odd event [81,90–92]. A striking feature of this linear dichroic signal is its dependence on magnetoelectric tensors that are time-odd and reverse their sign when the polarity of an applied field is reversed.

Our discussion of these intriguing effects is based on material presented in section 7. With the x-ray beam defining the z-axis of Cartesian coordinates, $\tilde{N}_Q^K$ and N_Q^K are different from zero for $Q = 0, \pm 2$. One finds $\tilde{N}_0^2 = -N_0^2 = \hat{q}_0(\boldsymbol{\varepsilon}' \times \boldsymbol{\varepsilon})_0/2\sqrt{5}$, and the structure factor $(F(\mathrm{E1\text{-}E2}))_{\mathrm{av}}$ given by (119) is proportional to $P_2 \Psi_0^{2,u}$ after using $\hat{q}_0(\boldsymbol{\varepsilon}' \times \boldsymbol{\varepsilon})_{\mathrm{av}} = \mathrm{i}P_2$. Here, $\Psi_0^{2,u}$ is evaluated with $\mathbf{k} = 0$ and it is a linear combination of pseudotensors $\langle U_0^2 \rangle$. The dichroic signal $P_2 \Psi_0^{2,u}$ is natural circular dichroism. It is zero for the established model of Cr_2O_3, since from (125), calculated with a Miller index $l = 0$, $\Psi_0^{2,u} = 0$ although $\langle U_0^2 \rangle$ contributes in space-group forbidden Bragg reflections that have odd l as we see from (128).

Terms in the structure factor (119) with $Q = 0$ and $K = 1$ and 3 describe a dichroism of unpolarized x-rays that is called magnetochiral dichroism [81,93]. Magnetoelectric tensors $\langle G_0^1 \rangle$ and $\langle G_0^3 \rangle$ are probed in this signal. One finds,

$\tilde{N}_0^1 = N_0^1 = -\mathrm{i}\sqrt{3}\hat{q}_0(\boldsymbol{\varepsilon}' \cdot \boldsymbol{\varepsilon})/10$, $\tilde{N}_0^3 = N_0^3 = (2/3)^{1/2}\tilde{N}_0^1$ and $(\boldsymbol{\varepsilon}' \cdot \boldsymbol{\varepsilon})_{\mathrm{av}} = 1$, of course. The contribution to $(F(\mathrm{E1\text{-}E2}))_{\mathrm{av}}$ from these terms, $K = 1, 3$ and $Q = 0$, is proportional to $\hat{q}_0(\Psi_0^{1,g} - (2/3)^{1/2}\Psi_0^{3,g})$, and it can only be present when there is magnetic order. We see from (126) that, magnetochiral dichroism does not develop in Cr_2O_3 as it is taken through the Néel temperature.

Terms in the structure factor (119) with $Q = \pm 2$ can involve tensors with rank $K = 2$ and $K = 3$, and they are responsible for nonreciprocal linear dichroism. It is found that $\tilde{N}_2^K = N_2^K$ which leaves $F(\mathrm{E1\text{-}E2})$ to depend on magnetoelectric tensors only. In addition, $N_2^3 = -\sqrt{2}N_2^2$ and $N_2^2 \propto -\mathrm{i}\hat{q}_0 X_{+2}^2$ with $(X_{+2}^2)_{\mathrm{av}} = (X_{-2}^2)_{\mathrm{av}} = P_3/4$. The contribution to $(F(\mathrm{E1\text{-}E2}))_{\mathrm{av}}$ made by these terms is proportional to $\hat{q}_0 P_3\{\mathrm{i}(\Psi_{+2}^{2,g} - \Psi_{-2}^{2,g}) - \sqrt{2}(\Psi_{+2}^{3,g} + \Psi_{-2}^{3,g})\}$. Once more, for the established model of Cr_2O_3 this dichroic signal is zero since $\Psi_{+2}^{2,g} = \Psi_{-2}^{2,g}$ and $\Psi_{+2}^{3,g} = -\Psi_{-2}^{3,g}$ are consequences of (126) evaluated with $l = 0$. Notice that the signal in nonreciprocal linear dichroism is a linear combination of true tensors, $\langle G_Q^3 \rangle$, and pseudotensors $\langle G_Q^2 \rangle$, and the two contributions to the signal are out of phase by 90° even though all magnetoelectric tensors have the same time-signature.

A reason for using Cr_2O_3 to illustrate the calculation of parity-odd events is that the material is a paradigm magnetoelectric, which has been studied with various experimental techniques supported by detailed theoretical analysis [5,71,72]. One set of experiments, using x-ray absorption, suggests that the established model of Cr_2O_3 is not fully correct. The experiments in question provide evidence to favour magnetochiral dichroism which is forbidden in the established model of Cr_2O_3, as we have just confirmed [93,94]. Another sesquioxide, V_2O_3, is of interest for a similar reason. Nonreciprocal linear dichroism at the K-edge of the vanadium ion in the antiferromagnetic phase of V_2O_3 has been reported [90]. However, the established model of this phase of V_2O_3, in section 3, predicts a null nonreciprocal linear dichroism [92]. An explanation of the observed x-ray dichroic signal requires a reduction of the magnetic symmetry such that inversion is not a separate symmetry [81]; like the magnetoelectric effect, nonreciprocal linear dichroism is allowed when inversion symmetry occurs jointly with time-reversal symmetry in the magnetic space-group.

Appendices

A Coordinate rotations

Two Cartesian coordinate systems (x, y, z) and (ξ, η, ζ) are related through Euler angles α, β, γ and associated spherical tensors satisfy (60) which can be

written,

$$A_Q^K(xyz) = \sum_q D_{qQ}^K(-\gamma, -\beta, -\alpha) A_q^K(\xi\eta\zeta) =$$
$$= e^{iQ\alpha} \sum_q e^{iq\gamma} d_{Qq}^K(\beta) A_q^K(\xi\eta\zeta) \ . \tag{A.1}$$

Our choices of Euler angles and $d_{Qq}^K(\beta)$ agree with Edmonds (1960) [16] and Varshalovitch, Moskalev and Kheronskii (1988) [18]. Applied to a vector ($K = 1$) equation (A.1) leads to,

$$\begin{aligned} x &= \xi(\cos\alpha\cos\beta\cos\gamma - \sin\alpha\sin\gamma) \\ &\quad -\eta(\cos\alpha\cos\beta\sin\gamma + \sin\alpha\cos\gamma) \\ &\quad +\zeta\cos\alpha\sin\beta \ , \\ y &= \xi(\sin\alpha\cos\beta\cos\gamma + \cos\alpha\sin\gamma) \\ &\quad -\eta(\sin\alpha\cos\beta\sin\gamma - \cos\alpha\cos\gamma) \\ &\quad +\zeta\sin\alpha\sin\beta \ , \\ z &= -\xi\sin\beta\cos\gamma + \eta\sin\beta\sin\gamma + \zeta\cos\beta \ . \end{aligned} \tag{A.2}$$

Special cases of (A.1) used in the main text are, rotation about the ξ-axis by an angle ψ,

$$A_Q^K(xyz) = e^{iQ\pi/2} \sum_q e^{-iq\pi/2} d_{Qq}^K(\psi) A_q^K(\xi\eta\zeta) \ , \tag{A.3}$$

and, secondly, $(\xi, \eta, \zeta) \rightarrow (-\zeta, -\eta, -\xi)$ followed by rotation by ψ about the x-axis,

$$A_Q^K(xyz) = (-1)^Q \sum_q e^{iq\psi} d_{Qq}^K(\pi/2) A_q^K(\xi\eta\zeta) \ . \tag{A.4}$$

One method of deriving (A.4) is to apply the addition theorem for rotations that takes the form [18],

$$\sum_q d_{mq}^K(\beta_1) d_{qm'}^K(\beta_2) e^{-iq\varphi} = e^{-im\alpha - im'\gamma} d_{mm'}^K(\beta) \ . \tag{A.5}$$

Here,

$$\begin{aligned} \cot\alpha &= \cos\beta_1\cot\varphi + \sin\beta_1\cot\beta_2/\sin\varphi \\ \cos\beta &= \cos\beta_1\cos\beta_2 - \sin\beta_1\sin\beta_2\cos\varphi \\ \cot\gamma &= \cos\beta_2\cot\varphi + \cot\beta_1\sin\beta_2/\sin\varphi \ . \end{aligned} \tag{A.6}$$

B Tensor rotations

Three special cases of (A.1) that frequently arise in the construction of structure factors are, rotation by φ around the ζ-axis which takes $\langle T^K_Q\rangle$ to $\mathrm{e}^{\mathrm{i}Q\varphi}\langle T^K_Q\rangle$, and rotation by π about the ξ-axis or the η-axis which, respectively, take $\langle T^K_Q\rangle$ to $(-1)^K\langle T^K_{-Q}\rangle$ and $(-1)^{K+Q}\langle T^K_{-Q}\rangle$.

In making calculations for a cubic system (x, y, z) it is sometimes convenient to work with axes (ξ, η, ζ) in which ζ coincides with the body-diagonal $(1, 1, 1)$. For this case, let ξ coincide with $(1, \bar{1}, 0)$ and η coincide with $(1, 1, \bar{2})$. The rotation that takes η to $(1, 1, 0)$ and ζ to $z = (0, 0, 1)$ while leaving unchanged $\xi = (1, \bar{1}, 0)/\sqrt{2}$ is described by,

$$A^K_Q(xyz) = \mathrm{e}^{\mathrm{i}Q\pi/4}\sum_q \mathrm{e}^{-\mathrm{i}q\pi/4} d^K_{Qq}(\beta) A^K_q(\xi\eta\zeta) \ . \tag{B.1}$$

with $\sin\beta = -(2/3)^{1/2}$ and $\cos\beta = (1/3)^{1/2}$. Adding a rotation by $\pi/4$ about the z-axis to the transformation (B.1), which requires one change $\mathrm{e}^{\mathrm{i}Q\pi/4} \rightarrow \mathrm{e}^{\mathrm{i}Q\pi/2}$ only, lets the ξ and η axes coincide with $x = (1, 0, 0)$ and $y = (0, 1, 0)$, respectively, and $\zeta = (0, 0, 1)$. A triad axis parallel to $(1, 1, 1)$ limits the sum on the right-hand side to $q = 0, \pm 3, \pm 6, \ldots$

C Symmetries

Proper rotations of a spherical tensor are described by formulae in the preceding appendices. Rotations by π about x, y and z axes are frequently occurring elements of symmetry in space-groups. In a tetragonal space-group there can be diad axes parallel to $(1, \pm 1, 0)$. [6] One finds that rotation by π about $(1, \pm 1, 0)$ takes $\mathrm{e}^{\mathrm{i}Q\pi/4}\langle T^K_Q\rangle$ to $(-1)^K\mathrm{e}^{-\mathrm{i}Q\pi/4}\langle T^K_{-Q}\rangle$, and $(-1)^{K+Q}\mathrm{e}^{-\mathrm{i}Q\pi/4}\langle T^K_{-Q}\rangle$. Diad axes are satisfied when the π rotation leaves $\mathrm{e}^{\mathrm{i}Q\pi/4}\langle T^K_Q\rangle$ unchanged. For example, a diad axis along $(1, 1, 0)$ is satisfied by a spherical tensor with the property $\langle T^K_Q\rangle^* = (-1)^{K+Q}\mathrm{e}^{\mathrm{i}Q\pi/2}\langle T^K_Q\rangle = (-1)^Q\langle T^K_{-Q}\rangle$ where the second equality arises from the Hermitian property of the spherical tensor.

Reflection in a mirror plane is equivalent to inversion, $(x, y, z) \rightarrow (-x, -y, -z)$, followed by a rotation by π about a normal to the plane. Inversion leaves parity-even tensors unchanged and reflection in a plane is the same as rotation by π about a normal, for such tensors. Parity-even tensors arise in Thomson scattering, magnetic x-ray and neutron scattering, and pure E1 and pure E2 x-ray resonant diffraction. These tensors are of two types, namely, true spherical tensors with even K and an even time-reversal signature and, secondly,

pseudotensors (or axial tensors) with odd K and an odd time-reversal signature. A description of the amplitude in the mixed E1-E2 resonant channel for diffraction is accomplished with parity-odd tensors which change their sign following the inversion operation. These tensors we label G^K_Q and U^K_Q, and G^K_Q is time-odd and U^K_Q is time-even. G^1_Q, G^3_Q, U^1_Q and U^3_Q are true tensors, while G^2_Q and U^2_Q are pseudotensors. In sections 7 and 8, G^K_Q is called a magnetoelectric tensor because it is unchanged by the product of the operations of time-reversal and inversion, and U^K_Q is called a polar tensor because its sign is changed by the product of these two operations.

Let us use ϑ to denote a time-reversal operator that is antilinear and antiunitary [95], by which we mean that, first,

$$\vartheta(c\psi) = c^*(\vartheta\psi) \ , \tag{C.1}$$

where c is a classical number and ψ is a wavefunction and, secondly, a matrix element $(\psi|B|\varphi) \equiv (\psi, B\varphi)$ of an arbitrary operator B satisfies

$$(\vartheta\psi, \vartheta B\varphi) = (\psi, B\varphi)^* \ . \tag{C.2}$$

The action of ϑ on a spinor $|JM\rangle$ is taken to be

$$\vartheta(c|JM\rangle) = c^*\vartheta|JM\rangle = c^*(-1)^{J-M}|J\ -M\rangle \ . \tag{C.3}$$

Here, two features merit comment. First, the action of ϑ on the spinor is equivalent to a rotation by π about the y-axis (in an application of this rotation to a spherical tensor of rank K and projection Q the phase factor $(-1)^{K+Q} = (-1)^{K-Q}$ because K and Q are integers, while for a spinor J and M can be half-integer and the phase factor created by the rotation is $(-1)^{J-M}$ with our chosen convention). Secondly, time-reversal applied to $|JM\rangle$ reverses the polarity of the projection M on the axis of quantization. Indeed, if $\mathbf{H}$ represents a magnetic field acting on a system and $\psi(\mathbf{H})$ is a wave function of the system then $\psi^*(\mathbf{H}) = \vartheta\psi(\mathbf{H}) = \psi(-\mathbf{H})$.

We return to (C.2) and consider a system with a magnetic field. First of all,

$$\begin{aligned}(\psi, B\varphi) &= (\vartheta\psi, \vartheta B\varphi)^* = (\vartheta\psi, [\vartheta B\vartheta^{-1}]\vartheta\varphi)^* \\ &= (\vartheta\varphi, [\vartheta B\vartheta^{-1}]^+\vartheta\psi) \ ,\end{aligned} \tag{C.4}$$

where $+$ denotes Hermitian conjugation. The result (C.4) provides a relation between matrix elements in systems with fields of opposite polarity and we write it in the form,

$$(\psi, B\varphi)_{\mathbf{H}} = (\varphi, [\vartheta B \vartheta^{-1}]^{+}\psi)_{-\mathbf{H}} \ . \tag{C.5}$$

Evidently, when considering the mean value of B the operator transforms with reversal of the magnetic field to $[\vartheta B \vartheta^{-1}]^{+}$. We shall call an operator B time-odd if $\vartheta B \vartheta^{-1} = -B^{+}$ and, similarly, an operator time-even if $\vartheta B \vartheta^{-1} = +B^{+}$. If B is Hermitian, $B^{+} = B$ but spherical tensors with $Q \neq 0$ are non-Hermitian and they satisfy $(T^K_Q)^{+} = (-1)^Q T^K_{-Q}$. Thus, $(\psi, T^K_Q \psi) = \langle T^K_Q \rangle$ satisfies,

$$\langle T^K_Q \rangle_{\mathbf{H}} = (-1)^Q \langle \bar{T}^K_{-Q} \rangle_{-\mathbf{H}} \ , \tag{C.6}$$

where we have introduced a notation $\bar{B} = \vartheta B \vartheta^{-1}$. Our parity-even tensors are such that $\bar{T}^K_Q = (-1)^{K+Q} T^K_{-Q}$. Thus, parity-even tensors with even K are time-even and tensors with odd K are time-odd. For these tensors, (C.6) reduces to (48). Parity-odd tensors, on the other hand, satisfy (123) and (124). Particular examples of parity-even and parity-odd spherical tensors are the angular momentum $\mathbf{J}$ and unit (polar) vector $\mathbf{n}$. Spherical components of these variables satisfy, $\bar{J}_q = (-1)^{1+q} J_{-q}$, $J^{+}_q = (-1)^q J_{-q}$ and $\bar{n}_q = (-1)^q n_{-q} = n^{+}_q$. ¿From these results and our convention for distinguishing time-odd and time-even operators, we find J_q is time-odd and n_q is time-even and the findings coincide with properties of their Cartesian (and Hermitian) components.

D Unit tensors for equivalent particles

Our tensors $W^{(ab)}$ and $W^{(ab)K}$ for equivalent electrons and equivalent holes are based on definitions used by Judd (1963) [17]. Values of these tensors for occupied states, denoted by $|\mu\rangle$, and empty states $|\Phi_{\text{emp}}\rangle$, which can be occupied by a photo-ejected core state electron, are related in a simple way. Let $|\Phi\rangle$ be the state of electrons in a closed, full shell. The closure statement for the shell in question is,

$$\langle \Phi_{\text{emp}} | W^{(ab)K} | \Phi_{\text{emp}} \rangle = \langle \Phi | W^{(ab)K} | \Phi \rangle - \langle \mu | W^{(ab)K} | \mu \rangle \ .$$

For $a + b > 0$, $\langle \Phi | W^{(ab)K} | \Phi \rangle = 0$ while for $a + b = 0$ the matrix element is proportional to the number of states in the shell $2(2l + 1)$. Hence, matrix elements with empty states $\langle \Phi_{\text{emp}} | W^{(ab)K} | \Phi_{\text{emp}} \rangle = -\langle \mu | W^{(ab)K} | \mu \rangle$ when $a+b > 0$, and they are proportional to the number of empty states $n_h = 2(2l+1) - n_e$ when $a+b = 0$. The quantum numbers for the n_h empty states and n_e electron states are the same. Denoting the seniority quantum number by ν, the two states $|l^{n_h} \nu S L\rangle$ and $|l^{n_e} \nu S L\rangle$ are said to be conjugate state functions.

Initially, we separately consider even and odd K. For even K, a minus sign is inserted in $\langle \mu | W^{(ab)K} | \mu \rangle$ which is then the matrix element required in the

resonant scattering length. Our tabulated $W^{(ab)K}$ for even K, thus, are equal in magnitude and opposite in sign to values tabulated for electrons. For odd K, no minus is introduced in $\langle\mu|W^{(ab)K}|\mu\rangle$ and this aligns our definition with a standard definition of hole states [59,61,62].

Our hole states $|h\rangle$ are derived from $|\Phi_{\rm emp}\rangle$ by application of the time-reversal operator ϑ, introduced in appendix C. Let $|\Phi_{\rm emp}\rangle = \vartheta|h\rangle$, and apply (C.4) to the matrix element $(h, \mathbf{S}h)$, where $\mathbf{S}$ is a spin operator; we obtain,

$$(h, \mathbf{S}h) = (\vartheta h, [\vartheta \mathbf{S} \vartheta^{-1}]^{+} \vartheta h) = -(\vartheta h, \mathbf{S}\vartheta h) = -(\Phi_{\rm emp}, \mathbf{S}\Phi_{\rm emp}) = (\mu, \mathbf{S}\mu) \ .$$

Hence, with $a + b > 0$ the general case is,

$$\langle\mu|W^{(ab)K}|\mu\rangle = -\langle\Phi_{\rm emp}|W^{(ab)K}|\Phi_{\rm emp}\rangle = \pm\langle h|W^{(ab)K}|h\rangle \ ,$$

where the plus sign is for time-odd operators, that have odd K, and the negative sign applies for time-even operators, that have even K. Recall that, the resonant scattering-length, which is used to interpret dichroic signals and resonant Bragg diffraction, is calculated with the states $|\Phi_{\rm emp}\rangle$. Thomson scattering, magnetic x-ray diffraction, and magnetic neutron scattering are calculated with the states $|\mu\rangle$. With respect to the latter, holes are positive charges for time-even operators but negative charges when coupled to a magnetic field. With respect to the empty states $|\Phi_{\rm emp}\rangle$, the role of positive and negative charges for hole states is the opposite of that with respect to $|\mu\rangle$.

The reduced matrix element of an operator that is the tensor product of an operator z^a acting on the spin and y^b acting on the orbital state of an electron is $(s\|z^a\|s)(l\|y^b\|l)W^{(ab)K}$, and all electrons are in the shell with angular momentum l. If J is not a good quantum number, and uncoupled states νSL are appropriate, a matrix element can be written in terms of a unit tensor $W^{(ab)}$. The relation between the coupling scheme $\nu SLJM$ and $\nu SM_S LM_L$ applied to a tensor T^K_Q is,

$$\begin{aligned}
&(-1)^{J-M}\begin{pmatrix} J & K & J' \\ -M & Q & M' \end{pmatrix} W^{(ab)K} \Longrightarrow \\
&\Longrightarrow (-1)^{a+b+Q}\left\{\frac{(2K+1)}{(2a+1)(2b+1)}\right\}^{1/2} W^{(ab)} \sum_{mn}\begin{pmatrix} a & K & b \\ -m & Q & -n \end{pmatrix} \\
&\quad \times (-1)^{S-M_S}\begin{pmatrix} S & a & S' \\ -M_S & m & M'_S \end{pmatrix}(-1)^{L-M_L}\begin{pmatrix} L & b & L' \\ -M_L & n & M'_L \end{pmatrix} \ . \quad \text{(D.1)}
\end{aligned}$$

Here, we see that the Wigner–Eckart theorem applies separately to the spin and orbital parts of $\nu SM_S LM_L$. Equation (83) is a particular case of (D.1). The actual relation between the two unit tensors is,

$$W^{(ab)K} = \left\{ \frac{(2J+1)(2K+1)(2J'+1)}{(2a+1)(2b+1)} \right\}^{1/2} \begin{Bmatrix} S & S' & a \\ L & L' & b \\ J & J' & K \end{Bmatrix} W^{(ab)} \quad . \quad \text{(D.2)}$$

The $9j$-symbol with $S = S'$, $L = L'$ and $J = J'$ exists only for even $a+b+K$. Some values of $3j$- and $6j$-symbols are found in reference [96]. An alternative source of nj-symbols, which includes $9j$-symbols, is a computer program [97].

Let us record two particular applications of (D.1). A matrix element of S_q is derived by setting $b = 0$, $K = 1$ and $Q = q$. Now $(l\|y^0\|l) = (2l+1)^{1/2}$, and (D.1) reduces to,

$$\langle SM_S LM_L|S_q|S'M'_S L'M'_L\rangle = [3(2L+1)]^{-1/2}(s\|s\|s)(2l+1)^{1/2} \times W^{(10)}\delta_{M_L,M'_L}\delta_{L,L'}(-1)^{S-M_S} \begin{pmatrix} S & 1 & S' \\ -M_S & q & M'_S \end{pmatrix} .$$

Taking $s = 1/2$ one has $(s\|s\|s) = (3/2)^{1/2}$ and we arrive at the following expression for $W^{(10)}$,

$$W^{(10)} = \left\{ \frac{2(2L+1)}{(2l+1)} \right\}^{1/2} (S\|S\|S)\delta_{S,S'}\delta_{L,L'} \ .$$

The corresponding expression for $W^{(01)}$ is obtained by setting $a = 0$, $(s\|z^0\|s) = \sqrt{2}$, and we get,

$$W^{(01)} = \left\{ \frac{3(2S+1)}{2} \right\}^{1/2} \frac{(L\|L\|L)}{(l\|l\|l)}\delta_{S,S'}\delta_{L,L'} \ .$$

In these two expressions the reduced matrix elements of an angular momentum operator $(l\|l\|l) = [l(l+1)(2l+1)]^{1/2}$ and a similar expression is used for $s = 1/2$ and S.

The diagonal part of $W^{(ab)K}$ appears in the matrix element $\langle T^K_Q\rangle_{\rm Et}$ with $K = Q = 0$. ¿From (73) we get,

$$\langle T^K_Q\rangle_{\rm Et} = \frac{1}{2(2\bar{l}+1)(2l+1)(2t+1)^{1/2}} \times \left\{ (2\bar{J}+1)n_h \pm \frac{2[\bar{l}(\bar{l}+1) + l(l+1) - t(t+1)]}{l(l+1)}\langle \mathbf{S}\cdot\mathbf{L}\rangle \right\} \ , \quad \text{(D.3)}$$

where $\langle \mathbf{S}\cdot\mathbf{L}\rangle$ is the mean value of the spin-orbit interaction. The signs in (D.3) relate to $\bar{J} = \bar{l} \pm 1/2$, which is the total angular momentum of the core state. For the state specified by Hund's rules,

$$\langle \mathbf{S}\cdot\mathbf{L}\rangle = \pm\frac{1}{4S}[J(J+1)-S(S+1)-L(L+1)] \ , \tag{D.4}$$

where the upper sign applies to $n_h < (2l+1)$ and the lower sign applies to $n_h \geq (2l+1)$. More generally, the reduced matrix element $(SLJ\|\mathbf{S}\cdot\mathbf{L}\|S'L'J')$ of the spin-orbit interaction is proportional to the unit tensor $W^{(11)0}$. The coefficient of proportionality is the product of the reduced matrix elements of $s = 1/2$ and l, and a factor $-\sqrt{3}$ that arises in the relation between a scalar product, here $\mathbf{S}\cdot\mathbf{L}$, and the tensor product of $\mathbf{S}$ and $\mathbf{L}$ evaluated for $K = Q = 0$. One finds,

$$(SLJ\|\mathbf{S}\cdot\mathbf{L}\|S'L'J) = -\frac{3}{\sqrt{2}}(l\|l\|l)W^{(11)0} \ . \tag{D.5}$$

The result (D.3) is a sum rule for the absorption signal. This particular sum rule gives a relation between the integrated signal and the spin-orbit interaction, which is a fundamental quantity in determining various physical properties, including, itinerant magnetism and heavy-fermion behaviour [98]. Other sum rules for dichroic signals are discussed in section 8.

E The selective sum over intermediate states

The amplitudes of the channels for resonant x-ray scattering and absorption discussed in this review consist of products of many electron matrix elements. This is due to the fact that we consider a two stage process in which a core shell electron is initially excited to the valence shell and, in a second step, allowed to re-emit the absorbed x-ray photon. The initial and final states, $|\mu\rangle$ and $|\mu'\rangle$, are described by the quantum numbers $SLJM$ and $S'L'J'M'$, respectively, and refer to equivalent electrons in a shell of orbital angular momentum l. For simplicity of notation we do not indicate extra quantum numbers necessary for a complete characterization of the Russel-Saunders coupled states.

The intermediate state is a bit more complicated because it contains two active shells, where the core shell has one hole, and the valence shell harbours the additional photo-ejected electron, which has to be coupled to the SL of the electrons of the initial valence shell. If $|\eta\rangle$ is described, say, by the quantum numbers $S^\eta L^\eta J^\eta M^\eta$ one assumes implicitly a coupling of $s \oplus S^\times \Rightarrow S^\eta$ and $\bar{l} \oplus L^\times \Rightarrow L^\eta$, where $S^\times, L^\times$ are the new spin and orbital quantum numbers for the valence shell. This is, however, not the only possibility. An alternative procedure would consist in a coupling of $s \oplus \bar{l} \Rightarrow \bar{J}$ and $S^\times \oplus L^\times \Rightarrow J^\times$. In this case, the spin and orbital angular momenta of the core shell are coupled to a total angular momentum $\bar{J}$ and the total angular momentum quantum

number for the valence shell is $J^{\times}$, both coupled, $\bar{J} \oplus J^{\times} \Rightarrow J^{\eta}$, to give the total angular momentum J^{η} of the intermediate state.

In the preceding sections we have not specified the selective sum over intermediate states denoted by $\sum_{\eta(\Delta)}$ in equations (62), (65), and (113). It is our intention to perform a selective sum over the quantum numbers describing the intermediate states, thereby leaving intact the dependence of the product of matrix elements on selected quantum numbers, like for instance $\bar{J}$. Our inspiration for this step is found in work by Judd [52] and Ofelt [53].

The actual calculations are rather involved, and we attempt to sketch the general properties by looking at the E1-E1 channel. To perform the calculation properly, one would have to resort to the graphical methods for nj-symbols as developed by Yutsis et al. [99] and applied in detail by Varshalovitch et al. [18]. Due to the Wigner–Eckart theorem the product of matrix elements for the E1 transition will contain a product of two $3j$-symbols,

$$(-1)^{J-M} \begin{pmatrix} J & 1 & J^{\eta} \\ -M & q & M^{\eta} \end{pmatrix} (-1)^{J^{\eta}-M^{\eta}} \begin{pmatrix} J^{\eta} & 1 & J' \\ -M^{\eta} & q' & M' \end{pmatrix} , \tag{E.1}$$

and a product of reduced matrix elements [100],

$$(SLJM \| \sum R^1_q \| S^{\eta} L^{\eta} J^{\eta} M^{\eta}) (S^{\eta} L^{\eta} J^{\eta} M^{\eta} \| \sum R^1_q \| S' L' J' M') \ . \tag{E.2}$$

The reduced matrix elements in (E.2) do not explicitly display the fact that the core hole $s, \bar{l}$ is coupled to the valence electrons $S^{\times}, L^{\times}$ in order to arrive at S^{η}, L^{η}. It is now possible to regroup and rearrange the nj-symbols in the product of (E.1) and (E.2), and to perform the summations over S^{η}, L^{η} and also over J^{η}. The introduction of a sum over an additional quantum label K leads to the emergence of the following essential terms obtained by graphical analysis,

$$(-1)^{J-M} \begin{pmatrix} J & K & J' \\ -M & Q & M' \end{pmatrix} (-1)^{K-Q} \begin{pmatrix} K & 1 & 1 \\ -Q & q' & q \end{pmatrix} , \tag{E.3}$$

and a product of three $6j$-symbols,

$$\begin{Bmatrix} J & K & J' \\ L' & S & L \end{Bmatrix} \begin{Bmatrix} L & K & L' \\ l & L^{\times} & l \end{Bmatrix} \begin{Bmatrix} l & K & l \\ 1 & \bar{l} & 1 \end{Bmatrix} . \tag{E.4}$$

The first $3j$-symbol in (E.3) is the Wigner–Eckart signature of a matrix element for a tensor of rank K, and the first $6j$-symbol in (E.4) is the signature of a reduced matrix element for a tensor of rank K that acts only on the orbital part of the wave function. The second $6j$-symbol in (E.4) is an important

ingredient in the definition of $(SL\|V^{(K)}\|S'L')$, as defined by Judd [17], which represents the corresponding unit tensor. This unit tensor is, of course, closely related to $(SL\|W^{(0K)}\|S'L')$ in appendix D, and the relation is,

$$(SL\|W^{(0K)}\|S'L') = \left(\frac{2S+1}{2}\right)^{1/2} (SL\|V^{(K)}\|S'L') \ . \tag{E.5}$$

The method described so far has the disadvantage that the important quantum label $\bar{J}$, the total angular momentum of the spin-orbit coupled core hole, is not manifest in our expressions. To bring the angular momentum to the foreground requires a recoupling of the angular momenta of the core hole and the valence electrons. This introduces two $9j$-symbols and sums over S^η, L^η and $S^{\eta'}, L^{\eta'}$ into the product of reduced matrix elements,

$$(SLJM\|\textstyle\sum R^1_q\|\bar{J}J^\times J^\eta M^\eta)(\bar{J}J^\times J^\eta M^\eta\|\sum R^1_q\|S'L'J'M') \ , \tag{E.6}$$

while the Wigner–Eckart $3j$-symbols are the same as in (E.1). The corresponding nj-symbol can now be summed over J^η and $J^\times$. Further simplification may be achieved by the introduction of additional quantum labels, a, b, and K, and summations over these. The $3j$-symbols obtained in this way are the same as given in (E.3), and the essential remaining elements are,

$$\begin{Bmatrix} S & S' & a \\ L & L' & b \\ J & J' & K \end{Bmatrix} \begin{Bmatrix} S & a & S' \\ s & S^\times & s \end{Bmatrix} \begin{Bmatrix} L & b & L' \\ l & L^\times & l \end{Bmatrix} \times \begin{Bmatrix} 1 & \bar{l} & l \\ 1 & \bar{l} & l \\ K & a & b \end{Bmatrix} \begin{Bmatrix} \bar{l} & a & \bar{l} \\ s & \bar{J} & s \end{Bmatrix} \tag{E.7}$$

Here, the first $9j$-symbol represents the signature of a coupled tensor operator of rank K acting on both spin a and orbital b components. The following two $6j$-symbols are essential building blocks for the construction of the unit tensor $W^{(ab)}$, if summed over $S^\times, L^\times$. The second line in (E.7) displays the explicit dependence on the one electron quantum numbers $s, \bar{l}, \bar{J}$, and l. It is now easy to see, that a sum over $\bar{J}$ forces $a = 0$ and $b = K$ in our expressions and, thus, returns us to the results displayed in (E.4).

Yet another level of complication arises if we desire not only to keep the dependence on $\bar{J}$, but also on $\bar{M}$, and exclude it from the selective summation over all other quantum numbers as in [55] and an application to observations on NpO_2 [56]. In this case, the starting point is again from expressions (E.1) and (E.6) but the graphical analysis implements two more labels r, x in ad-

dition to a, b, and K and the corresponding summations. Application of the rules for the graphical method produces a group of four $3j$-symbols,

$$(-1)^{J-M}\begin{pmatrix} J & x & J' \\ -M & Q & M' \end{pmatrix}(-1)^{K-Q}\begin{pmatrix} K & 1 & 1 \\ -Q & q' & q \end{pmatrix} \times \begin{pmatrix} \bar{J} & r & \bar{J} \\ -\bar{M} & 0 & \bar{M} \end{pmatrix}\begin{pmatrix} K & r & x \\ -Q & 0 & Q \end{pmatrix}, \tag{E.8}$$

and the following nj-symbols,

$$\begin{Bmatrix} S & S' & a \\ L & L' & b \\ J & J' & x \end{Bmatrix}\begin{Bmatrix} S & a & S' \\ s & S^{\times} & s \end{Bmatrix}\begin{Bmatrix} L & b & L' \\ l & L^{\times} & l \end{Bmatrix} \times \begin{Bmatrix} K & r & x \\ a & b & y \end{Bmatrix}\begin{Bmatrix} 1 & \bar{l} & l \\ 1 & \bar{l} & l \\ K & a & b \end{Bmatrix}\begin{Bmatrix} s & \bar{l} & \bar{J} \\ s & \bar{l} & \bar{J} \\ a & y & r \end{Bmatrix} \tag{E.9}$$

Note here that, the signature of the coupled tensor operator is now for a tensor of rank x and the corresponding Wigner–Eckart $3j$-symbol in (E.8) is in accordance with this. The dependence on $\bar{M}$ is explicit. A sum over this quantum number forces $r = 0$ and at the same time, $x = K$ and $y = K$, and, once more, returns the previous result given in (E.7). The $6j$-symbols in the first line of (E.9) allow the construction of $W^{(ab)}$, which, together with the appropriate $9j$-symbol leads to $W^{(ab)x}$, in this case.

The most general result, as described in (E.9), contains a hierarchy of results, (E.7), derived by summing over $\bar{M}$, and (E.4), by summing over $\bar{J}$ successively. In all cases the many electron features of the combined, final matrix element are encapsulated in the unit tensors $W^{(0K)K}$, $W^{(ab)K}$, or $W^{(ab)x}$.

We regret that, a detailed discussion of the form of these unit tensors would take us beyond the limits of this review, and should, therefore, be sought in the literature.

Acknowledgements

We have benefited from discussions and correspondence with J.A. Blanco, A. Bombardi, P.J. Brown, P. Carra, S.P. Collins, C. Detlefs, J. Igarashi, K. Katsumata, S. Langridge, L. Paolasini, L.P. Pitaevskii, P.G. Radaelli, D.S. Sivia, U. Staub, Y. Tanaka, and G. van der Laan.

References

[1] R.W. James, The Optical Principles of the Diffraction of X-rays (Bell, East Brunswick NJ, 1967).

[2] P.J. Brown, Int. J. Mod. Phys. B7 (1993) 3029.

[3] P.J. Duke, Synchrotron Radiation (Oxford University Press, Oxford, 2000).

[4] J.F. Nye, Physical Properties of Crystals (Clarendon Press, Oxford, 1985).

[5] R.R. Birss, Symmetry and Magnetism (North-Holland, Amsterdam, 1964) and A.P. Cracknell, Magnetism in Crystalline Materials (Pergamon Press, Oxford, 1975).

[6] G. Burns and A.M. Glazer, Space Groups for Solid State Scientists (Academic Press Inc., Boston, 1990).

[7] P.M. Chaikin and T.C. Lubensky, Principles of Condensed Matter Physics (Cambridge University Press, Cambridge, 1995).

[8] R.C. O'Handley, Modern Magnetic Materials (John Wiley & Sons, New York, 2000).

[9] V.E. Dmitrienko, Acta Crystallogr. Sect. A39 (1983) 29; 40 (1984) 89.

[10] D.H. Templeton and L.K. Templeton, Acta. Crystallogr. A41 (1985) 133; 41 (1985) 365; 42 (1986) 478.

[11] Ch. Brouder, J. Phys.: Condens. Matter 2 (1990) 701, and references therein.

[12] E. Balcar and S.W. Lovesey, Theory of Magnetic Neutron and Photon Scattering (Clarendon Press, Oxford, 1989).

[13] S.W. Lovesey and S.P. Collins, X-ray Scattering and Absorption by Magnetic Materials (Clarendon Press, Oxford, 1996).

[14] H. Grotch et al., Phys. Rev. A27 (1983) 243.

[15] G. Bhatt et al., Phys. Rev. A28 (1983) 2195.

[16] A.R. Edmonds, Angular Momentum in Quantum Mechanics (Princeton University Press, Princeton, 1960).

[17] B.R. Judd, Operator Techniques in Atomic Spectroscopy (McGraw-Hill, New York, 1963).

[18] D.A. Varshalovich, A.N. Moskalev and V.K. Khersonskii, Quantum Theory of Angular Momentum (World Scientific, Singapore, 1988).

[19] Y. Tanaka et al., J. Phys.: Condens. Matter 11 (1999) L505.

[20] S.W. Lovesey and K.S. Knight, Phys. Rev. B64 (2001) 094401.

[21] Y. Tanaka et al., Phys. Rev. B69 (2004) 24417.

[22] H. Adachi et al., Phys. Rev. Lett. 89 (2002) 206401.

[23] A. Abragam and B. Bleaney, Electron Paramagnetic Resonance of Transition Ions (Clarendon Press, Oxford, 1970).

[24] V.F. Sears, Phys. Reports 141 (1986) 281.

[25] F. de Bergevin and M. Brunel, Phys. Lett. 39A (1972) 141.

[26] F. de Bergevin and M. Brunel, Acta. Crystallogr. A37 (1981) 314.

[27] M. Brunel and F. de Bergevin, Acta. Crystallogr. A37 (1981) 324.

[28] P.P. Kane, Phys. Reports 218 (1992) 67.

[29] F. Bell, J. Felsteiner and L.P. Pitaevskii, Phys. Rev. A53 (1996) R1213.

[30] M.J. Cooper et al., X-ray Compton Scattering (Oxford University Press, Oxford, 2004).

[31] D. Gibbs et al., Phys. Rev. B43 (1991) 5663.

[32] S.P. Collins, D. Laundy and G.Y. Guo, J. Phys.: Condens. Matter 5 (1993) L637.

[33] R. Caciuffo et al., Phys. Rev. B65 (2002) 174425.

[34] M. Lippert et al., Europhys. Lett. 27 (1994) 537.

[35] E. Balcar and S.W. Lovesey, J. Phys.: Condens. Matter 14 (2002) 10281.

[36] P.D. Dernier and M. Marezio, Phys. Rev. B2 (1970) 3771.

[37] S.W. Lovesey, K.S. Knight and D.S. Sivia, Phys. Rev. B65 (2002) 224402.

[38] R.M. Moon, Phys. Rev. Lett. 25 (1970) 527.

[39] S.W. Lovesey and K.S. Knight, J. Phys.: Condens. Matter 12 (2000) L367.

[40] L. Paolasini et al., Phys. Rev. Lett. 82 (1999) 4719.

[41] L. Paolasini et al., J. Electron Spectrosc. Relat. Phenom. 120/1-3 (2001) 1.

[42] D.B. McWhan et al., Phys. Rev. B42 (1990) 6007.

[43] K.D. Finkelstein, Q. Shen and S. Shastri, Phys. Rev. Lett. 69 (1992) 1612.

[44] J. Kokubun et al., J. Phys. Soc. Jpn. 67 (1998) 3114.

[45] S. Ji et al., Phys. Rev. Lett. 91 (2003) 257205.

[46] S.B. Wilkins et al., Phys. Rev. Lett. 91 (2003) 167205.

[47] Y. Murakami et al., Phys. Rev. Lett. 81 (1998) 582.

[48] I.S. Elfimov, V.I. Anisimov and G.A. Sawatzky, Phys. Rev. Lett. 82 (1999) 4264.

[49] M. Benfatto, Y. Joly and C.R. Natoli, Phys. Rev. Lett. 83 (1999) 636.

[50] M. Takahashi, J. Igarashi and P. Fulde, J. Phys. Soc. Jpn. 68 (1999) 2530; ibid. 69 (1999) 1614.

[51] L.D. Landau and E.M. Lifshitz, Vol. 4, Quantum Electrodynamics, 2^{nd} edition (Pergamon Press, Oxford, 1982).

[52] B.R. Judd, Phys. Rev. 127 (1962) 750.

[53] G.S. Ofelt, J. Chem. Phys. 37 (1962) 511.

[54] J.A. Paixao et al., Phys. Rev. Lett. 89 (2002) 187202.

[55] S.W. Lovesey, J. Phys.: Condens. Matter 9 (1997) 7501.

[56] S.W. Lovesey et al., J. Phys.: Condens. Matter 15 (2003) 4511.

[57] J.P. Hannon et al., Phys. Rev. Lett. 61 (1988) 1245; ibid. 62 (1989) 2644 (E): J. Luo, G.T. Trammell and J.P. Hannon, Phys. Rev. Lett. 71 (1993) 287.

[58] P. Carra and B.T. Thole, Rev. Mod. Phys. 66 (1994) 1509.

[59] S.W. Lovesey and E. Balcar, J. Phys.: Condens. Matter 9 (1997) 4237.

[60] S.W. Lovesey, J. Phys.: Condens. Matter 8 (1996) 11009.

[61] S.W. Lovesey, O. Fritz and E. Balcar, J. Phys.: Condens. Matter 10 (1998) 501.

[62] S.W. Lovesey, J. Phys.: Condens. Matter 10 (1998) 2505.

[63] B.T. Thole et al., Phys. Rev. Lett. 68 (1992) 1943.

[64] P. Carra et al., Phys. Rev. Lett. 70 (1993) 694.

[65] J.C. Lang et al., Phys. Rev. Lett. 74 (1995) 4935.

[66] J. Stohr, J. Mag. Mag. Materials 200 (1999) 470.

[67] E.N. Ovchinnikova and V.E. Dmitrienko, Acta Crystallogr., Sect. A: Found. Crystallogr. 56 (2000) 2.

[68] S.W. Lovesey, K.S. Knight and E. Balcar, Phys. Rev. B64 (2001) 054405.

[69] S.W. Lovesey et al., Phys. Rev. B70 (2004) 172414.

[70] S.W. Lovesey and E. Balcar, J. Phys.: Condens. Matter 9 (1997) 8679.

[71] P.J. Brown et al., J. Phys.: Condens. Matter 14 (2002) 1957.

[72] M. Muto et al., Phys. Rev. B57 (1998) 9586.

[73] K. Yoshida, Theory of Magnetism (Springer, Berlin, 1996).

[74] D.H. Templeton and L.K. Templeton, Phys. Rev. B49 (1994) 14850: Acta Crystallogr., Sect. A: Found. Crystallogr. 53 (1997) 352; ibid. 54 (1998) 158.

[75] I.S. Elfimov et al., Phys. Rev. Lett. 88 (2002) 015504; ibid. 88 (2002) 239904 (E).

[76] S. Di Matteo et al., Phys. Rev. Lett. 91 (2003) 257402.

[77] V.E. Dmitrienko, E.N. Ovchinnikova and K. Ishida, JETP Lett. 69 (1999) 938.

[78] J. Kokubun et al., Phys. Rev. B64 (2001) 073203.

[79] S.P. Collins et al., Phys. Rev. B68 (2003) 064110.

[80] I. Marri and P. Carra, Phys. Rev. B69 (2004) 113101.

[81] P. Carra, A. Jerez and I. Marri, Phys. Rev. B67 (2003) 045111.

[82] P. Carra, J. Phys. A: Math. Gen. 37 (2004) L183.

[83] Ya.B. Zel'dovich, Sov. Phys. JETP 6 (1958) 1184.

[84] I.B. Khriplovich, Uspekhi 40 (1997) 1161.

[85] D.H. Templeton and L.K. Templeton, Acta Crystallogr., Sect. A: Cryst. Phys. Diffr. Theor. Gen. Crystallogr. 36 (1980) 237.

[86] J. Goulon et al., J. Chem. Phys. 108 (1998) 6394.

[87] L. Alagna et al., Phys. Rev. Lett. 80 (1998) 4799.

[88] C.R. Natoli et al., Euro. Phys. J. B4 (1998) 1.

[89] P. Carra and R. Benoist, Phys. Rev. B62 (2000) R7703.

[90] J. Goulon et al., Phys. Rev. Lett. 85 (2000) 4385.

[91] S. Di Matteo and C.R. Natoli, J. Synchrotron Rad. 9 (2002) 9.

[92] S. Di Matteo, Y. Joly and C.R. Natoli, Phys. Rev. B67 (2003) 195105.

[93] J. Goulon et al., Phys. Rev. Lett. 88 (2002) 237401.

[94] S. Di Matteo and C.R. Natoli, Phys. Rev. B66 (2002) 212413.

[95] S.W. Lovesey, Condensed Matter Physics: Dynamic Correlations (The Benjamin/Cummings Publishing Company Inc., Menlo Park, 1986).

[96] M. Rotenberg et al., The $3j$ and $6j$ Symbols (Crosby Lockwood & Son Ltd, London, 1959).

[97] Program `winjsym`, available on demand from `balcar@ati.ac.at`.

[98] G. van der Laan et al., Phys. Rev. Lett. 93 (2004) 097401.

[99] A.P. Yutsis, I.B. Levinson and V.V. Vanagas, The Mathematical Apparatus of the Theory of Angular Momentum (Israel Program for Scientific Translation, Jerusalem, 1962).

[100] R.D. Cowan, The Theory of Atomic Structure and Spectra (University of California Press, Berkeley, 1981).